ABSTRACT

Title of Document: INTEGRATION OF VIRUS-LIKE PARTICLE MACROMOLECULAR BIORECEPTORS IN ELECTROCHEMICAL BIOSENSORS

Faheng Zang, Doctor of Philosophy, 2016

Directed By: Professor Reza Ghodssi, Department of Electrical and Computer Engineering

Rapid, sensitive and selective detection of chemical hazards and biological pathogens has shown growing importance in the fields of homeland security, public safety and personal health. In the past two decades, efforts have been focusing on performing point-of-care chemical and biological detections using miniaturized biosensors. These sensors convert target molecule binding events into measurable electrical signals for quantifying target molecule concentration. However, the low receptor density and the use of complex surface chemistry in receptors immobilization on transducers are common bottlenecks in the current biosensor development, adding to the cost, complexity and time. This dissertation presents the development of selective macromolecular *Tobacco mosaic* virus-like particle (TMV VLP) biosensing

receptor, and the microsystem integration of VLPs in microfabricated electrochemical biosensors for rapid and performance-enhanced chemical and biological sensing.

Two constructs of VLPs carrying different receptor peptides targeting at 2,4,6-trinitrotoluene (TNT) explosive or anti-FLAG antibody are successfully bioengineered. The VLP-based TNT electrochemical sensor utilizes unique diffusion modulation method enabled by biological binding between target TNT and receptor VLP. The method avoids the influence from any interfering species and environmental background signals, making it extremely suitable for directly quantifying the TNT level in a sample. It is also a rapid method that does not need any sensor surface functionalization process. For antibody sensing, the VLPs carrying both antibody binding peptides and cysteine residues are assembled onto the gold electrodes of an impedance microsensor. With two-phase immunoassays, the VLP-based impedance sensor is able to quantify antibody concentrations down to 9.1 ng/mL.

A capillary microfluidics and impedance sensor integrated microsystem is developed to further accelerate the process of VLP assembly on sensors and improve the sensitivity. Open channel capillary micropumps and stop-valves facilitate localized and evaporation-assisted VLP assembly on sensor electrodes within 6 minutes. The VLP-functionalized impedance sensor is capable of label-free sensing of antibodies with the detection limit of 8.8 ng/mL within 5 minutes after sensor functionalization, demonstrating great potential of VLP-based sensors for rapid and on-demand chemical and biological sensing.

INTEGRATION OF VIRUS-LIKE PARTICLE MACROMOLECULAR BIORECEPTORS IN ELECTROCHEMICAL BIOSENSORS

by

Faheng Zang

Dissertation submitted to the Faculty of the Graduate School of the
University of Maryland, College Park, in partial fulfillment
of the requirements for the degree of
Doctor of philosophy
2016

Advisory Committee:
Professor Reza Ghodssi, Chair
Professor Pamela Abshire
Professor James N. Culver
Professor Alireza Khaligh
Professor Ian White

Dedication

To my dear wife Zhijuan

for her unconditional love, understanding and support at any moment.

To my parent

who give endless love and care to me and lead in my life.

To my baby daughter Kezhen

who gives me happiness, hope and new purposes in life.

I love you all forever.

Acknowledgements

I would like to thank my advisor Professor Reza Ghodssi for his continuous guidance and support throughout the course of this work. I would also like to thank the members of the Ph.D. dissertation committee, Professor James N. Culver, Professor Pamela Abshire, Professor Alireza Khaligh, and Professor Ian White for their helpful suggestions and discussions leading to the completion of this work.

A huge acknowledgement is dedicated to all my collaborators through my Ph.D. research. Particularly, the professional and technical guidance and assistance from Professor James N. Culver, the help in VLP purification from Dr. Xiao Zhu Fan, the genetic modification of VLP by Mr. Adam D. Brown and Ms. Lindsay Naves, the discussion on experimental procedure and results with Dr. Konstantinos Gerasopoulos and Mr. Sangwook Chu have been invaluable. I would like to also acknowledge the support I received in the fabrication and characterization from the Maryland NanoCenter staff members (Dr. Jim O'Connor, Dr. Wen-An Chou, Mr. Thomas Loughran, Mr. John Abrahams, and Mr. Jonathan Hummel).

Last but not least, I would like to thank all the members of the MEMS Sensors and Actuators Laboratory for their indispensable discussions, suggestions, support, and camaraderie, particularly Dr. Konstantinos Gerasopoulos and Dr. Xiao Zhu Fan for their professional advice.

Table of Contents

List of Tables

List of Figures

Chapter 1: Introduction

1.1 Motivation and background

Rapid detection of hazardous chemicals and biological pathogens are growing in importance for the applications in security, safety and personal health. In security and safety domain, hazardous chemicals, such as explosives, have been widely used in both military weapons, and civilian construction and mining. In the production, transportation and utilization of these chemicals, possible contamination of natural resources and exposure to the public can cause environmental and health issues. Also, due to the dangerous nature of these chemicals, any mishandling may lead to devastating consequences for public safety. Therefore, accurate and rapid monitoring of the presence of such chemicals in the environment is crucial. In the public health domain, the spreading of contagious diseases caused by viral and bacterial infections have escalated due to rapid pathogen mutations and the convenience of global transportations [1-3]. In order to contain the spread of diseases at an early stage, diagnostic technologies need to be adapted to achieve a reduced response time and improved accuracy. In the personal health aspect, medical emergencies such as acute myocarditis and acute pancreatitis are life-threatening especially when a medical facility is not immediately available. Therefore, a quick response, selective and sensitive diagnosis of pathogens or biomarkers is an essential step in identifying the source of disease at the early stage and form the right strategy for treatment in both public and personal level. It would be ideal

to develop a universal and rapid-response sensor platform with extraordinary versatility to meet these very different needs at different levels.

During the last two decades, efforts have been focusing on performing decentralized (point-of-care) chemical and pathogen detection [4, 5] using miniaturized biosensors to achieve fast-response sensing. Biosensors are analytical devices that utilize the integration of biological sensing receptors with physical sensors. Their transduction mechanism converts biological target molecule binding events into measurable electrical signals to quantify target molecule concentration[6]. Miniaturized biosensors have been increasingly implemented in point-on-care pathogen detection due to their extraordinary portability, low cost, versatility and low cost [7, 8]. They have provided fast and reliable alternatives to central analytical facilities.

Selectivity and sensitivity are two essential aspects to characterize the performance of a biosensor. To ensure high selectivity, most biosensors utilize biological molecules to functionalize the transducers in order to show selective affinity to target molecules. Possible biological receptors such as antibodies, enzymes, cells, tissues and microorganisms have been integrated in the sensor through microfabrication processes [9, 10]. The sensing efficacy is largely determined by the density and binding affinity of the immobilized sensing receptors, which limit the amount of bound target molecules and control the change in signal of the biosensor. Currently, a major challenge associated with the most commonly used biomolecule receptors, such as antibodies and DNAs, is the uncontrollability in immobilization and randomness in receptor

distribution, which often results in low receptor density on transducer surfaces. Combining the fact of low surface area of a miniaturized sensor, this may result in an impaired sensitivity.

Recently, the exponential advances in nanotechnology have created new possibilities for integration of nanostructured materials (such as gold nanoparticles, carbon nanotubes and silicon nanowires) as sensing components in biosensors, due to their unique properties such as high surface to volume ratios as well as their highly controllable structures. These properties provide nanostructured materials the potential for improved signal to noise ratio, remarkable selectivity, and the utilization of novel transduction mechanism, making them ideal candidates as functional parts in next-generation miniaturized sensors as they offer the potential for improved signal to noise ratios, remarkable selectivity, and the utilization of novel transduction mechanisms. However, the immobilization steps that creating links between bioreceptors with nanostructures still require complex surface chemistry to create complimentary chemical functional groups on both transducers and receptors. The low receptor density and complex surface chemistry in the immobilization of receptors on transducers are common bottlenecks in the biosensor development, adding to the cost, complexity and time. For these reasons, development of new sensing receptors and sensor functionalization technologies are necessary for the next generation miniaturized biosensors, which can simultaneously simplify the sensor preparation and maximize sensor performance.

While significant research has been conducted in the surface modification, functionalization and utilization of nanostructured materials in microfluidic based sensors, several key challenges still remain. When organic nanostructures are used directly as receptor layers, process compatibility and the ability to arrange them in a highly ordered fashion in a device is often the bottleneck. On the other hand, inorganic nanomaterials are more compatible with standard device processing; however, they require special functionalization procedures so that they can be conjugated with a probe receptor. Besides, while several devices demonstrating binding events between nano-probes and analytes have been developed, very little information is available on the optimization of nanomaterial integration in immunoassay sensors.

Interestingly, biological structures such as DNA, proteins and viruses offers a tremendous library for material synthesis based on their unique variations in molecular functionalities and assembly properties. This work addresses the aforementioned challenges through the integration of nanostructured biological molecule *Tobacco mosaic* virus-like particles (TMV VLPs) as sensing elements in microfabricated devices. Compared to the conventional biosensing receptors such as DNA and antibodies, these VLPs are much larger macromolecules with well-defined one-dimensional nanostructures. Integration of VLPs as sensing receptors can simultaneously solve the challenges in both sensitivity and selectivity. Particular emphasis is placed on fundamental studies exploring the interface between the transducer and the

nanoparticles to identify optimal configurations in the VLP immobilization on surfaces. Moreover, a significant amount of effort is focused on the design and optimization sensor microsystems in order to facilitate rapid sensor functionalization using VLP sensing receptors to meet the needs of sensitive on-site and on-demand detection of chemical and biological hazard.

The detailed research goals of this dissertation are: (1) to develop TMV VLPs as versatile sensing elements, (2) to implement VLPs in microsensors for selective chemical and biological sensing, (3) to develop a microsystem solution for rapid sensor functionalization using VLPs and enhanced biosensing performance. This research utilizes experimental investigations to establish the optimized sensor functionalization protocol using VLPs. Through the integrated sensor microsystem and genetic modification of VLPs, it can be expected that VLPs being further explored as versatile and universal sensing receptors for rapid chemical and biological detections.

1.2 Thesis contributions

The research described in this dissertation constitutes an experimental investigation aimed towards the rapid integration of macromolecules - Tobacco mosaic virus-like particles (TMV VLPs) – as a highly selective and versatile bio-recognition element in microscale biosensors. The VLP-based biosensors are suitable for rapid and decentralized analysis of both chemical and biological targets. This dissertation contributes to the VLP nanoreceptor integration in biosensors in the following aspects:

1.2.1 Accelerated and enhanced VLP receptor assembly process

The current VLP self-assembly process requires the immersion of the entire microdevice in a relatively large volume of VLP solution for around 18 hours. Despite the long immobilization time and volume, the density of the assembled VLP sensing probes (VLP-FLAG) still needs significant improvement to achieve better sensitivity for antibody sensing. The time of VLP self-assembly process and the density of the assembled VLP layer are currently the bottlenecks that limit the sensor preparation and performance.

This dissertation proposes a new type of evaporation-based VLP assembly protocol to solve the aforementioned problems. This process utilizes the increased VLP concentration and van der Waals force during the evaporation of a droplet of VLP solution to achieve the high VLP density and low assembly time. Colorimetric immunoassay demonstrates that the biosensing efficacy of VLP remains after the evaporation-based process, and the evaporation can improve the localized VLP assembly. Using evaporation-based VLP assembly process in a capillary microfluidic platform, the density of VLP functional layer is significantly improved, resulting in the coverage of over 91% on impedance sensor electrodes (vs. ~60% using VLP self-assembly process). The assembly time reduced significantly from 18 hours to 6 minutes.

1.2.2 Integration of VLP receptors in chemical and biological microsensors

VLP receptors have shown tremendous potentials of being genetically engineered to become a universal and versatile vehicle to carry different types of bio-recognition peptides. In this part of the work, two different constructs of

VLPs have been successfully developed to target the explosive 2,4,6,-trinitrotoluene (TNT) molecules and anti-FLAG IgG antibodies, respectively. These are integrated in both macro- and micro-scale sensor systems.

For the detection of TNT, VLP receptors are integrated as free-floating binding agents that utilize a diffusion modulation-based differential method to selectively detect the presence of TNT in solution. This method is the first demonstration of utilizing the distinct size difference between sensing probe (VLP) and target (TNT) to selectively lower the diffusion coefficient in an electrochemical system. This change in the diffusion coefficient generates a selective differential current that only related with the biological binding between VLP and TNT. The impact of this method is that it significantly improved the selectivity of conventional voltammetric sensing without the needs for background signal subtractions. The feasibility of using microliters of liquid sample to perform TNT trace detection has been validated in a microfabricated electrochemical TNT sensor platform.

To selectively sense the presence of biological analyte, the VLP-FLAG receptors are self-assembled on to interdigitated impedimetric microsensor, forming a functional VLP receptor layer. Based on the changing complex impedance during immunoassay process, the VLP-functionalized impedance microsensors are able to selectively detect the biological target in a miniaturized platform in real-time. The impedance microsensor is utilized to study the VLP self-assembly dynamics on-chip, revealing the gradual saturation over an 18-hour self-assembly process. The impedance sensor with

self-assembled VLP layer is able to detect target antibody at the concentration down to 9.1 ng/mL using labelled method – enzyme-linked immunosorbent assay (ELISA).

1.2.3 A microsystem solution for rapid sensor functionalization and label-free antibody sensing

A microsystem platform is developed which utilizes open-channel capillary pumps and stop-valves to achieve rapid and localized VLP nanoreceptor assembly on an impedance sensor. This is the first demonstration of a large-scale open-channel microfluidic system fabricated using bottom-up processes. The localization and confinement of VLPs is realized by autonomous delivery of the VLP-containing buffer solution on the sensor electrode surface and using of the capillary stop valves. The VLP assembly process involves evaporation of the VLP solution from micropillar structures in the capillary channel. The integrated impedance sensor monitors the assembly dynamics of VLP nanoreceptor on the sensor, and performs real-time label-free antibody sensing. Sensitivity optimization is also studied by changing the receptor VLP concentrations in the sensor functionalization.

This is the first demonstration of controlled biological nanoreceptor immobilization on microsensors through capillary microfluidics. This is also the first open-channel capillary microfluidic system that is fabricated using bottom-up process using negative photoresist KMPR. It is extremely suitable for sensor integration compared to the existing silicon-based capillary microfluidics. Using BOE etching and O_2 plasma activation, hydrophilic

KMPR sidewalls and more hydrophobic substrate are generated simultaneously, creating capillary microfluidics that is controlled by the sidewall geometries. The VLP receptors, capillary microfluidics and impedance sensors combined also provided a system solution to perform on-demand sensor programing and rapid biosensing with minimum user intervention.

1.3 Literature review

1.3.1 Biosensor transduction mechanisms

Biosensors are devices that leverage the highly specific biological reactions for sensing of analytes. They combine biological recognition elements (specific to the target) with physical transducers that translate bio-recognition events into a measurable data, such as an electrical signal, an optical emission or a mechanical motion [11]. Progress in microfabrication and nanomaterials allows development of highly sensitive sensors with the additional advantage of miniaturization [12]. Micro- and nano-scale sensors are based on microelectronics and the related micro-electromechanical system (MEMS) technologies. These sensor components can easily be integrated into portable ‘‘lab-on-chip’’ platforms to perform ‘‘point-of-care’’ analysis where portability is one of the major requirements. This section provides a review of several major biosensors transduction mechanisms and the recent achievements in each of the sensor categories.

1.3.1.1 Mechanical biosensors

Cantilever-based biosensors:

Microcantilevers are well-explored and characterized MEMS mechanical structures, which are also very promising platforms for micro- and nano-scale biosensors. Using highly sensitivity cantilevers as transduction platform, the biosensors can achieve local, high resolution and label-free molecular recognition measurements [13-15].

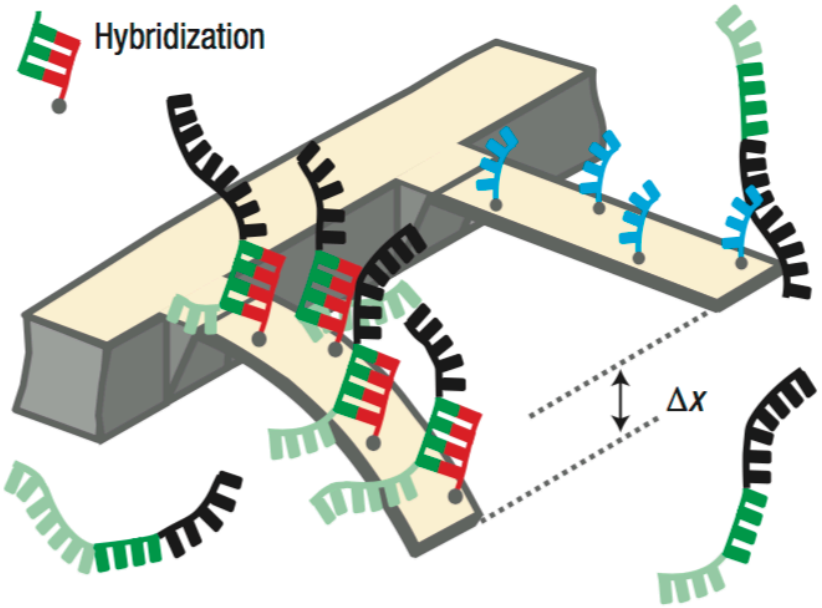

Figure 1-1 Principle of differential readout using sensor and reference cantilevers working in static mode. [16] (Reprinted with permission from J. Zhang, H. P. Lang, F. Huber, A. Bietsch, W. Grange, U. Certa, R. McKendry, H. J. Guntgerodt, M. Hegner, and C. Gerber, Nature Nanotechnology, 1,214 (2006). Copyright 2006, Nature Publishing Group)

The cantilever-based biosensor can be operated in static mode (cantilever deflection is measured) or dynamic mode (resonant frequency shift is measured). In the static mode, binding between analytes and the immobilized recognition molecules on one surface of the cantilever causes a change in cantilever surface stress and deflects the cantilever [17]. Figure 1-1 shows the schematic of the transduction mechanism of a static-mode cantilever biosensor for DNA hybridization analysis. In the dynamic mode, analyte–receptor

binding adds an additional mass to the oscillating cantilever, decreasing its resonance frequency. The static mode can operate well in both gas and liquid environments. The dynamic mode works efficiently in gas phase. However, in aqueous environments, the viscous damping during the oscillation hinders cantilevers working in the dynamic mode [18], which is not desirable. Overall, due to its high sensitivity, cantilever-based sensors can achieve label-free detection of various targeting molecules, including proteins such as cyanovirin [19]， prostate specific antigen [20], antibiotic oxytetracycline [21], and pollutants like atrazine [22], trimethylamine [23] and mycotoxin [24].

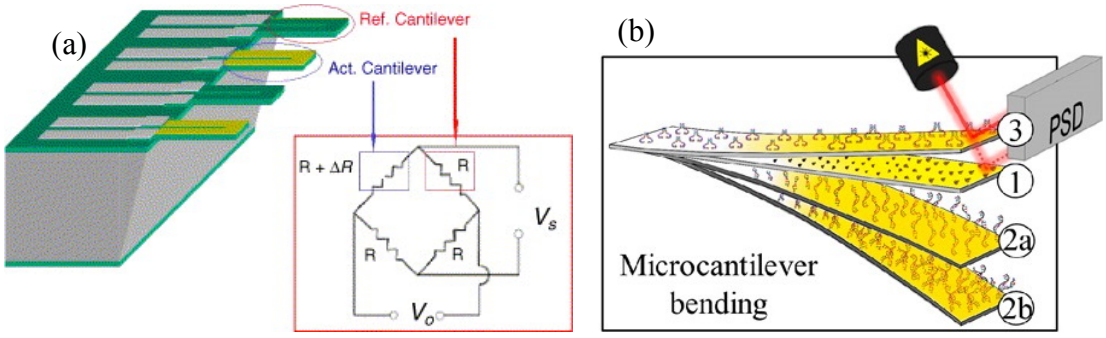

Figure 1-2 Cantilever biosensors with (a) piezoresistive [25] (reprinted with permission from K. W. Wee, G. Y. Kang, J. Park, J. Y. Kang, D. S. Yoon, J. H. Park, and T. S. Kim, Biosensors & Bioelectronics, 20, 1932 (2005). Copyright 2005, Elsevier) and optical [26] readout setups. (reprinted with permission from C. M. Dominguez, P. M. Kosaka, A. Sotillo, J. Mingorance, J. Tamayo, and M. Calleja, Analytical Chemistry, 87, 1494 (2015). Copyright 2015, American Chemical Society)

Piezoresistive and optical methods are two major readout mechanisms for cantilever biosensors. The core of the piezoresistive readout method is a half Wheatstone bridge placed on cantilevers. Due to the bending of cantilevers from the biological binding event, one of the resistors in the circuit changes its value accordingly, generating a potential in the circuit. This potential can be

measured and related to the target concentration. The other readout method is optical-based, which utilizes the change in a reflected laser beam to quantify the amount of cantilever bending. This method usually relies on an external point laser to shine on the tip of the cantilever sensor in order to generate the reflection light beam. When the biological binding changes the bending of the cantilever, the reflected laser beam changes the location on a position sensitive optical detector that can be related with the target molecule concentrations.

Electro-acoustic biosensor (piezoelectric biosensor)

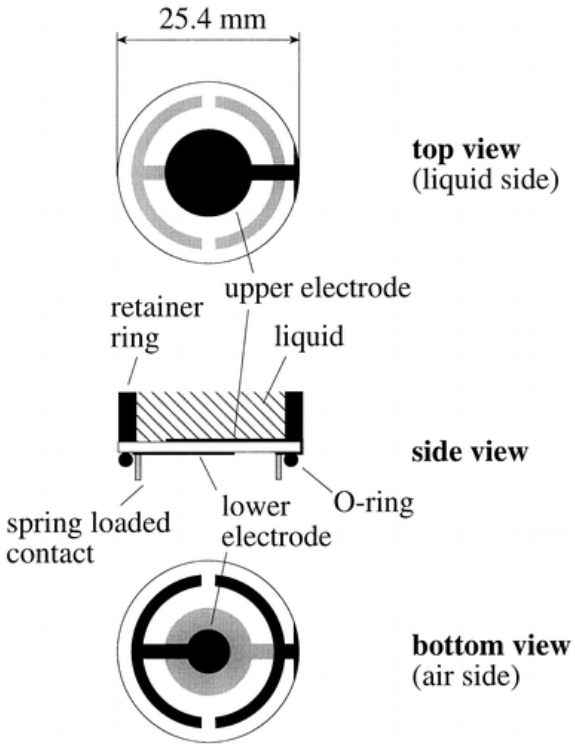

Figure 1-3 The electrode configuration of the Maxtek quartz crystal microbalance (QCM) chip [27]. (Reprinted with permission from M. Rodahl, F. Hook, and B. Kasemo, Analytical Chemistry, 68, 2219 (1996). Copyright 1996, American Chemical Society.)

The other major sub-category of mechanical biosensor is electro-acoustic sensors. These sensors utilize piezoelectric effect to generate mechanical wave oscillation within the crystal. Quartz crystal microbalance

(QCM) is one of the most established electro-acoustic sensors. QCMs are centimetre-scale mechanical resonators based on the property of an AT cut quartz crystal which oscillate when alternating voltage are applied. QCM sensors can measure the inertial mass of analytes attaching on their surfaces in vacuum, gas or fluid [28, 29]. A decrease in the resonant frequency occurs with molecules attachments, which can be measured in real time. When analysing a liquid-phase analyte, half of the crystal is exposed to the liquid in a flow-cell as shown in Figure 1-3. Fluid-based QCM biosensing capability spans the nano- to femtomolar range: nanomolar detection limit is reported for continuous analyte monitoring using an indirect-competitive assay [30], and 85 fM detection limit has been reported for end-point detection sandwich assays involving device removal from fluid, drying, and subsequent measurement in vacuum environment [31].

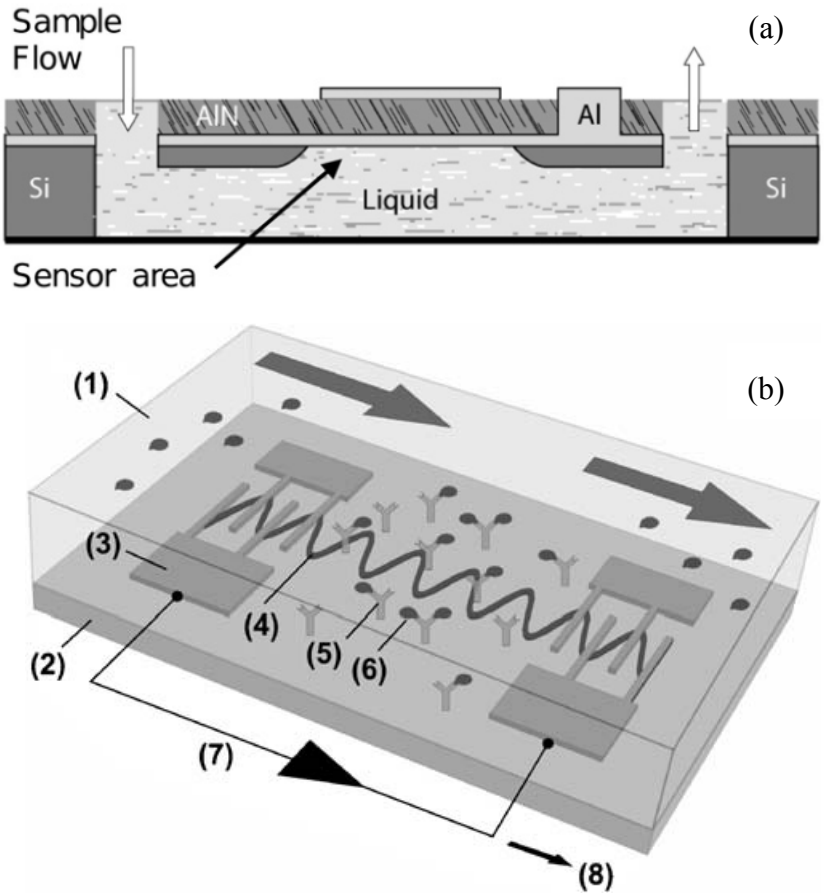

Figure 1-4 (a) Schematic cross section view of the shear mode thin film bulk acoustic resonator (FBAR) biosensor with an integrated fluidic channel beneath the active area [32]. (Reprinted with permission from G. Wingqvist, Surface & Coatings Technology, 205, 1279 (2010). Copyright 2010, Elsevier)(b) Basic SAW biosensor setup exemplified by a SAW immunosensor [33]. (Reprinted with permission from K. Lange, B. E. Rapp, and M. Rapp, "Surface acoustic wave biosensors: a review," Analytical and Bioanalytical Chemistry, vol. 391, pp. 1509-1519, Jul 2008.Springer)

Different from the QCM that is based on single crystalline bulk material oscillation, other piezoelectric resonator-based biosensors developed recently, including thin film bulk acoustic resonator (FBAR) and surface acoustic wave resonator (SAW), use thin films of polycrystalline materials deposited with IC-compactible process. These sensors operate based on piezoelectric effect, and oscillate in the frequency ranges from few hundred MHz to several GHz, thus

resulting in higher sensitivity compared to QCM. The advantages of the FBAR devices include: (1) the ability to fabricate the device using standard CMOS processing and materials allowing integration with CMOS control circuitry; (2) the size and volume can be significantly reduced [34]. The SAW sensors working in Love mode, where surface acoustic wave is much confined in the piezoelectric layer, are quite suitable for biosensing in liquid samples [33, 35].

1.3.1.2 Optical biosensors

In the past two decade, optical sensor development has been a fast-paced area because they are immune to electromagnetic interference, capable of performing remote sensing, and can provide multiplexed detection within a single device [36]. Two most popular optical biosensor formats are based on surface plasmon resonance (SPR) and optical fibers and Whispering-gallery-mode (WGM) recirculation. They are extremely sensitive devices with the low detection limit down to fM range. However, there is still challenges in the integration in a lab-on-a-chip platform and compatibility with the IC fabrication process for multiplexed on-chip sensor.

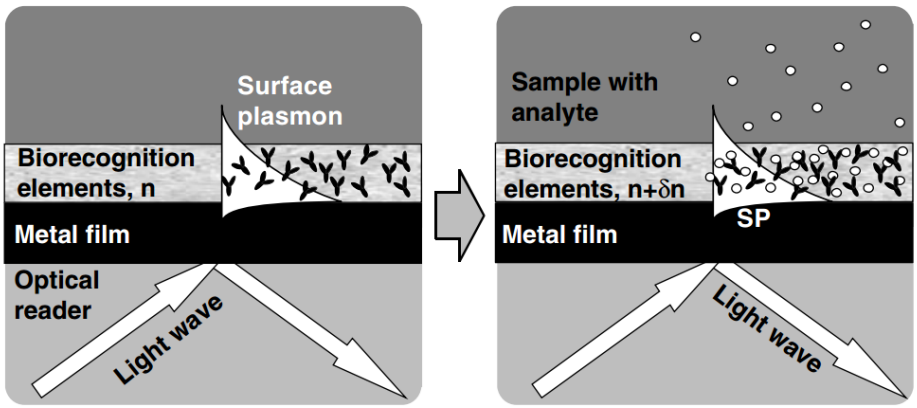

Figure 1-5 Formation of surface plasmon resonance wave for sensor. [37] (Reprinted with permission from M. Piliarik, H. Vaisocherová, and J. Homola, Biosensors and Biodetection, 65 (2009). Copyright 2009, Springer)

The SPR-based biosensor is based on total reflection of a laser beam in a glass prism attached on the backside of a thin (thickness smaller than 50nm) metal film. A light wave excites surface plasmon propagating along the on the metal/media interface [37]. The angle of incidence at which surface plasmon occurs is called the SPR angle and is determined by the angular frequency of the light source, dielectric constant of the metal and the geometry of the prism. However, if these are not changed, then the SPR angle depends only on the refractive index (n) of the ambient medium, on the far side of the gold film. Therefore, if an analyte is passed over an immobilized bioreceptor on the far side of the gold surface, a change in the SPR angle is produced.

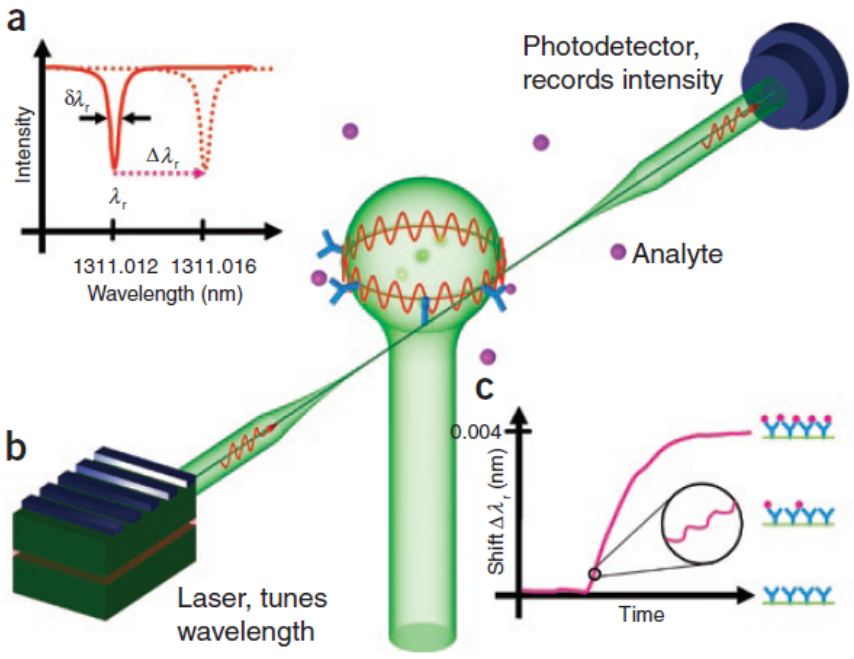

Figure 1-6 Concept of the WGM biosensor [38]. (Reprinted with permission from F. Vollmer and S. Arnold, Nature Methods, 5, 591, (2008). Copyright 2008, Nature Publishing Group)

The biosensing concept using a WGM biosensor is illustrated in Figure 6. First of all, the resonant wavelength/frequency and the shift in the wavelength/frequency can be identified through the transmission spectrum (Figure 6a); WGM in a dielectric sphere is driven by the evanescent coupling though the optical fiber (Figure 6b); when biomolecules bind on the receptor immobilized sphere, the refractive index changes on the sphere which causes resonant wavelength/frequency shift (Figure 6c). [38]

1.3.1.3 Electrical biosensor:

Electrical biosensors include biomolecule-functionalized filed effect transistors, voltammetric, amperometric and impedimetric electrochemical sensors. They rely solely on the measurement of currents and/or voltages to detect target binding [39-42]. Compared with other biosensors operating using optical, mechanical or magnetic principles, electrical biosensors do not require special excitations other than applied electrical potential or current. Electrical sensors are also independent from intermediate transduction mechanism such as transferring the biological binding events into mechanical displacements or light reflection angle changes. Thus, electrical biosensors can be fully integrated with integrated circuits, and are promising devices for point-of-care diagnostics and on-site analysis due to their low cost, low power and ease of miniaturization.

Amperometric and voltammetric electrochemical biosensors always utilize the electrochemical characteristics of the target analyte or the electrochemical reaction between analytes and coating on the electrode to

quantify the target concentrations. Glucose biosensors are of the well-investigated electrochemical biosensors that operate in amperometry mode. Amperometric enzyme electrodes, based on glucose oxidase (GOx), have played a leading role in glucose monitoring in blood. The enzyme electrodes concept was first proposed back in 1962, where the glucose level can be measured by the oxygen consumption through the enzyme-catalyzed reaction [43]. The recent development of amperometric glucose biosensors is more focused on performing reagentless glucose without the need for mediator. In these sensors, the electron is transferred directly from glucose to the electrode via the active site of the enzyme [44-46]. Figure 4 summarizes various generations of amperometric glucose biosensors based on different mechanisms of electron transfer, including the use of natural secondary substrates, artificial redox mediators, or direct electron transfer.

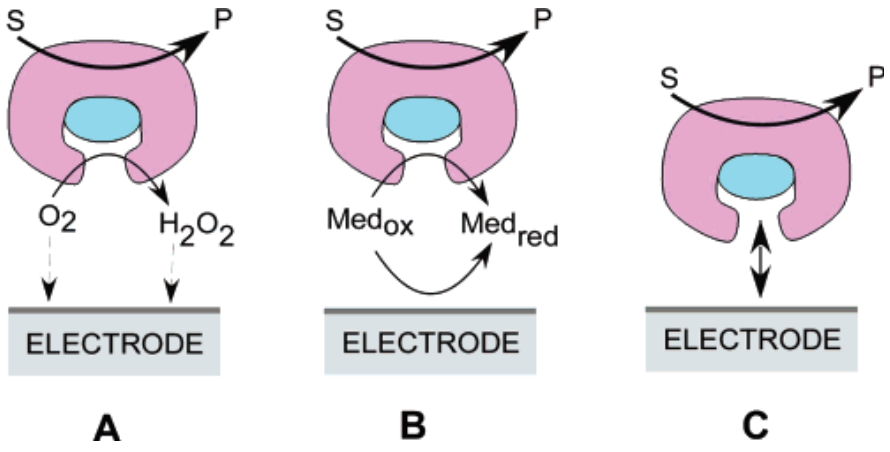

Figure 1-7 Three generations of amperometric enzyme electrodes for glucose based on the use of natural oxygen cofactor (A), artificial redox mediators (B), or direct electron transfer between GOx and the electrode (C). [44] (Reprinted with permission from J. Wang, Chemical Reviews, 108, 814, (2008). Copyright 2008, American Chemical Society)

Voltammetry is another versatile technique in electrochemical analysis, where redox current of electroactive species is recorded with the applied potential. The position of peak current is related to the specific analyte, and the peak current amplitude is proportional to the concentration of the corresponding species. Voltammetry is able to detect multiple compounds, which have different peak potentials, in a single electrochemical experiment (or scan), thus offering the simultaneous detection of multiple analytes [9]. Voltammetry has been widely used for detecting a wide range of chemical and biological targets such as TNT explosive [47], dopamine [48], carcinogen Sudan II [49], caffeine [50], etc.

Impedimetric biosensors measure the electrical impedance of an interface in AC steady state with constant DC bias conditions [39]. The method is usually referred to as electrochemical impedance spectroscopy (EIS), and usually requires imposing a small sinusoidal potential at different frequency and measuring the current between the electrodes. By combining the phase information, the voltage-current ratio provides complex electrical impedance. EIS has been used to study a variety of electrochemical phenomena over a wide frequency range [51-54]. EIS can be used to detect target binding on the electrode surface (which usually has receptor probes immobilized on the surface in advance) by monitoring the impedance of the electrode-solution interface changes.

Impedance biosensors can detect a variety of target analytes by simply varying the probe used. In the application of detecting suspended particles such

as bacteria, the changing in solution resistance Rs and dielectric capacitance between the microfabricated electrodes becomes more important.

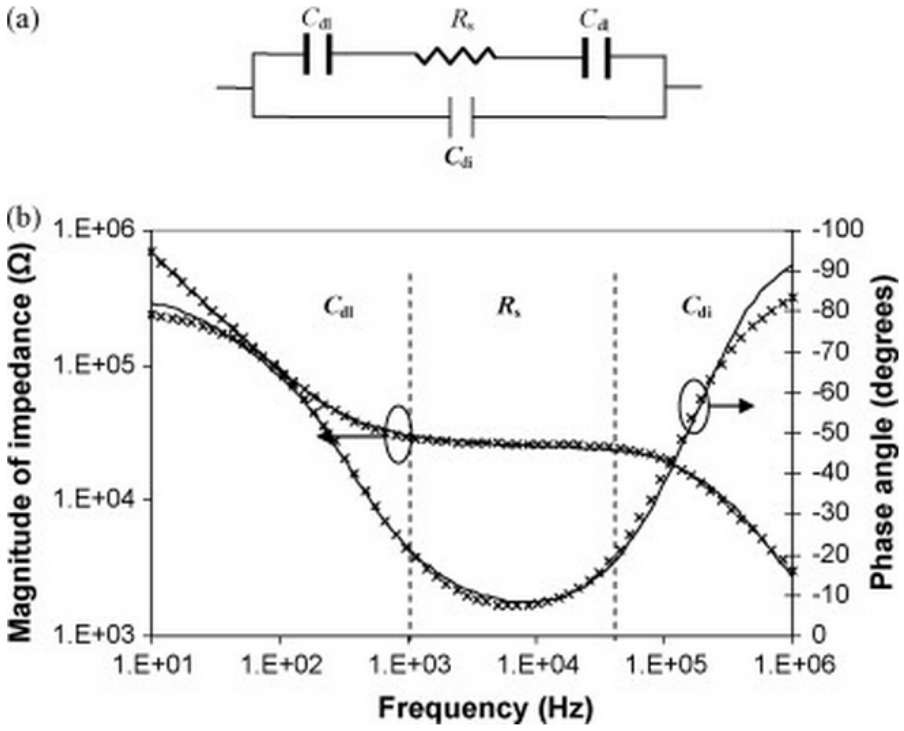

Figure 1-8 (a) The equivalent circuit for the label-free impedance measurement system coupled with magnetic nanoparticle-antibody conjugates for the detection of *E. Coli* O157:H7, (b) Bode diagrams of the impedance spectra of experimental and curve fitted data in a rang range of frequency from 10 Hz to 1 MHz [52]. (Reprinted with permission from M. Varshney, Y. B. Li, B. Srinivasan, and S. Tung, Sensors and Actuators B-Chemical, 128, 99 (2007). Copyright 2007, Elsevier)

From the bode diagrams of the impedance spectra in Figure 1-8b, at a relative low frequency, double layer capacitance in an impedance biosensors is the most dominant component which is more sensitive to surface binding. In general, impedance biosensors have potential for simple, rapid, label-free, low-cost detection of biomolecules [39].

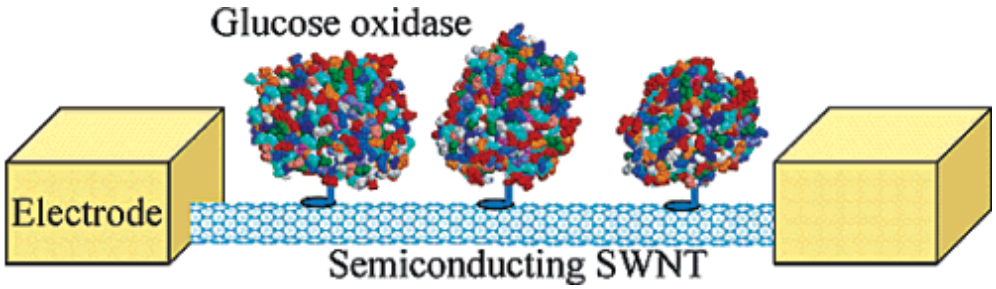

Figure 1-9 Carbon nanotube (CNT)-based transistor for biosensing of glucose.[55] (Reprinted with permission from K. Besteman, J. O. Lee, F. G. M. Wiertz, H. A. Heering, and C. Dekker, Nano Letters, 3, 727, (2003). Copyright 2003, American Chemical Society)

Another kind of electrical biosensors operates by field-effect modulation of carriers in a semiconductor due to nearby charged particles [56]. These field-effect sensors rely on the interaction of external charges with carriers in a nearby semiconductor and thus exhibit enhanced sensitivity at low ionic strength where counter-ion shielding effect is reduced [39]. Figure 1-9 demonstrates GOx-coated semiconducting SWNTs act as sensitive pH sensors and that the conductance of GOx-coated semiconducting SWNTs changes upon addition of glucose substrate.

1.3.1.4 Summary of biosensor transduction mechanism

Table 1 summarizes the state-of-the-art biosensors working under different sensing mechanisms.

Table 1-1 Summary of the biosensor transduction mechanisms and state-of-the-art

Sensor category	Note	Label-free	Receptor /functional material	Target	Detection limit	Reference
Mechanical:						
Cantilever	Static mode, Optical readout	Yes	single-chain variable fragment (scFv)	antigen	15 nM	[57]
	Static mode, Piezoresistive readout	Yes	antibody	protein (CRP), antigen (PSA)	300 pM	[25]
	Static mode, Optical readout	Yes	antibody	antigen (PSA)	100 pM	[58]
	Dynamic mode in liquid	Yes	antibody	activated leukocyte cell adhesion molecule	300 pM	[59]
	Static mode, sandwich assay	No	antibody	antigen (PSA)	1.5 fM	[60]
	Dynamic mode in air	Yes	Phosphoric acid / gelatin	TNT	70 pg	[61]
QCM, FBAR or SAW	QCM	Yes	antibody	protein (CRP)	1nM	[30]
	QCM, sandwich assay with Au-avidin conjugates amplification	No	ssDNA	DNA	1fM	[62]
	QCM	Yes	ssDNA	DNA - Human Papilloma Virus (HPV)	50nM	[63]
	FBAR, shear mode	Yes	avidin	antibody (anti-avidin)	2.3 ng/cm^2	[64]
	FBAR, shear mode	Yes	antibody	antigen (carbaryl)	3.2 ppb	[65]
	SAW	Yes	antibody	antigen (Ebola virus)	1.9 × 104 PFU/mL	[66]
Optical:						
SPR	SPR	Yes	Imprinted polymer	citrinin	6.8 fM	[67]
	SPR with Fe_3O_4-Au nanorod	Yes	antigen	antibody	155pM	[68]

Optical resonator	Microring resonator	Yes	antibody	antigen	0.6 nM	[69]
	Microring resonator with sandwich assay	No	antibody	antigen	6.5 pM	[70]
Electrical:						
Amperometric sensor	disposable	Yes	glucose oxidase	glucose	0.2 mM	[45]
	oxidized boron-doped diamond electrode	Yes	glucose oxidase	glucose	23 μM	[46]
	Graphene electrode	Yes	silk peptide	Bisphenol A (BPA)	0.72 nM	[71]
	screen-printed carbon electrodes	Yes	lactate oxidase	hydrogen peroxide	11 μM	[72]
Voltammetric sensor	screen-printed carbon electrodes	Yes	-	TNT	0.88 μM	[47]
	screen-printed carbon electrodes	Yes	-	TNT	0.4 μM	[73]
	Modified glassy carbon electrodes	Yes	electrochemically reduced graphene oxide-polymer hybrid	TNT	6.6 nM	[74]
	Modified glassy carbon electrodes	Yes	Titanate nanotubes	Dopamine	0.1 μM	[48]
Impedimetric sensor	Faradaic	Yes	Aptamer	Lipopolysaccharide	1 pg/mL	[75]
	Faradaic	Yes	Aptamer	*E. Coli* outer membrane proteins	0.1 μM	[76]
	Faradaic	Yes	Aptamer	17β-estradiol	2 pM	[77]
	Faradaic	Yes	Antibody	dengue serotype 2 viruses	1 pfu/mL	[78]
	Faradaic	Yes	ssDNA	ssDNA	4 nM	[79]
	Non-Faradaic	Yes	ssDNA	ssDNA	100 nM	[80]
	Non-Faradaic	Yes	Antibody	IgG	0.63 nM	[81]
Field effect transistors	Si Nanowire FET	Yes	Antibody	Antigen (PSA)	5 pM	[82]
	Si nanoribbon	No	Antibody	antigen	0.6 pM	[83]

Comparing all the transducers, electrochemical transducers are generally suitable for detection of both small chemical targets and relatively large

biological molecules. They are also more compatible with integrated circuitry and electronic components because of the requirements for direct electrical excitations and measurements. Because electrochemical sensor electrodes can be on the microscale to millimetre-scale, the sensors are relatively easy to be integrated with microfluidic platform for lab-on-chip applications.

1.3.2 Lab-on-a-chip (LOC) – sensor and microfluidics integration

The appealing feature of an LOC device is that it can perform laboratory operations on a small scale using miniaturized platforms. Small volumes reduce the time required to synthesize and analyze a product; the unique behavior of liquids at the microscale allows greater control of molecular concentrations and interactions; and reagent costs and the amount of chemical waste can be greatly reduced [84]. Compact LOC sensors also enable the analysis of samples at the point of need rather than in a centralized laboratory facility. Due to the favorable features of low volume, fast response, multiplexed operation and precise control, there has been an exponential increase in the LOC implementations in research fields such as gene expression analysis[85-87], cell manipulation and separation (Figure 1-10a) [88, 89], drug development[90, 91], biosensing (Figure 1-10b) [51, 92-97], etc.

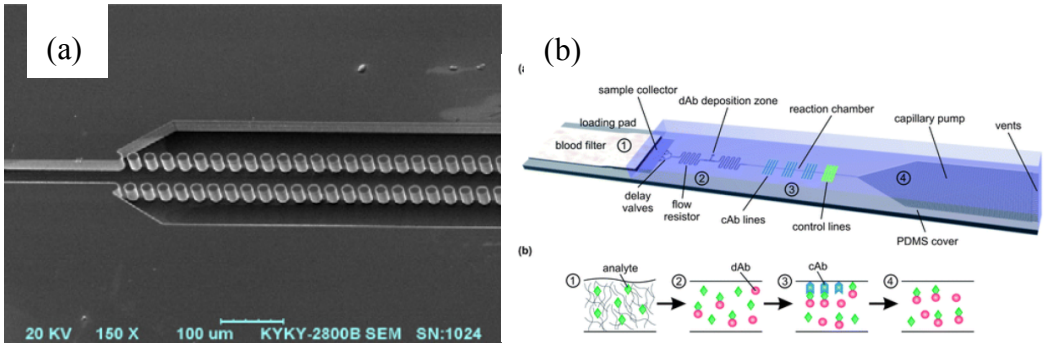

Figure 1-10(a) SEM micrographs of pillar-type barrier for blood cell separation[89] (Reprinted with permission from X. Chen, D. F. Cui, C. C. Liu, and H. Li, Sensors and Actuators B: Chemical, 130, 216,(2008). Copyright 2008, Elsevier) (b) Concept of a capillary-driven microfluidic chip for effecting immunoassays with one step[97]. (Reprinted with permission from L. Gervais and E. Delamarche, Lab on a Chip, 9, 3330, (2009). Copyright 2009, Royal Society of Chemistry)

In the sensing domain, LOC sensors are mainly aimed at achieving multiplexed sensor arrays on chip for drug discovery and portable sensing platform for point-of-care clinical diagnostics or in field bio-/chemical detections. A great diversity of transducers has been integrated with microfluidics to create LOC biosensor systems. The transduction mechanisms of these sensors are based on optical (optical density, surface plasmon [98] (Figure 1-11a) or Raman spectroscopy), electrical/electrochemical (amperometric, potentiometric, impedimetric or field effect transistor [99] (Figure 1-11b)), paramagnetic particle or mass loading (cantilever or acoustic) (Figure 1-11c, d) [33, 51, 57, 100-102]. These transducers need to be programed with functional receptors in order to selectively detect a specific target molecule or biomarker with immunoassays.

In a LOC system, microfluidics is the enabling technology to deliver and control the low volume of samples in the device. A microfluidic platform provides a set of fluidic unit operations that can be combined with microfabrication technology. The platform allows the implementation of different application specific systems (assays) in an easy and flexible way, based on the same fabrication technology [103]. Microfluidic systems are part of LOC technology which deals with minute amounts of liquids (biological

samples and reagents) on a small scale. They are fast, compact and can be made into a highly integrated system to deliver purified samples, perform separation, reaction, immobilization, labelling, as well as detection, and thus are promising for applications such as LOC and handheld healthcare devices [104].

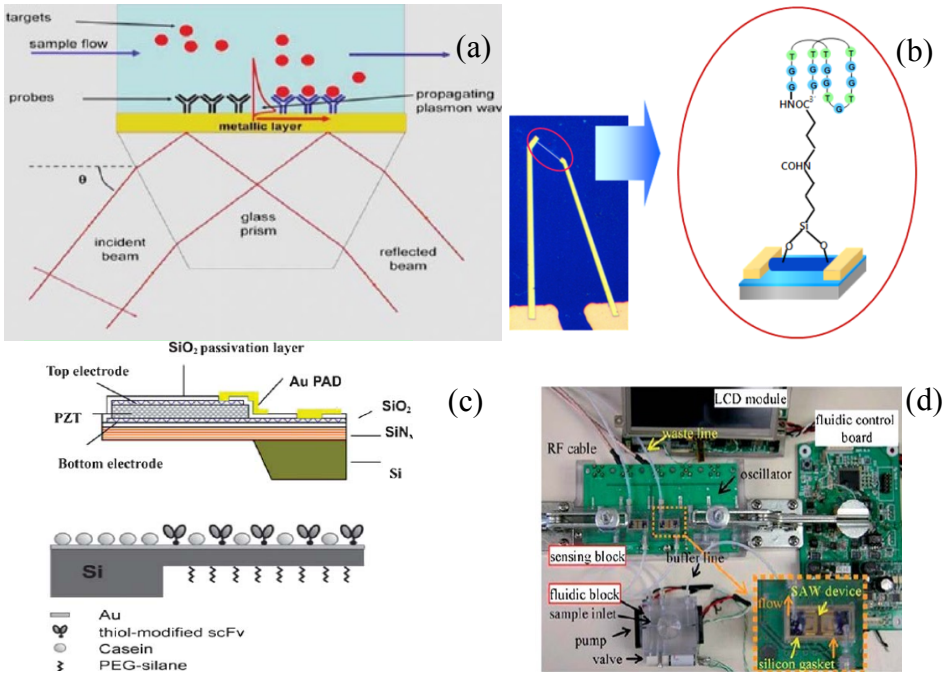

Figure 1-11(a) diagram of surface plasmon resonance sensor operation [98] (Reprinted with permission from A. Duval, F. Bardin, A. Aide, A. Bellemain, J. Moreau, and M. Canva, Copyright 2007, SPIE.org), (b) portable amperometric sensor [99] (K. S. Kim, H.-S. Lee, J.-A. Yang, M.-H. Jo, and S. K. Hahn, Nanotechnology, 20, 235501, (2009). Copyright 2009, IOP PUBLISHING, LTD), (c) microcantilever biosensors [57, 101] (N. Backmann, C. Zahnd, F. Huber, A. Bietsch, A. Pluckthun, H. P. Lang, H. J. Guntherodt, M. Hegner, and C. Gerber, PNAS, 102, 14587,(2005). Copyright 2005, National Academy of Sciences, USA) (Reprinted with permission from J. H. Lee, K. H. Yoon, K. S. Hwang, J. Park, S. Ahn, and T. S. Kim, Biosensors & Bioelectronics, 20, 269,(2004). Copyright 2004, Elsevier) and (d) surface acoustic wave sensors [102] (Reprinted with permission from M. I. Rocha-Gaso, C. March-Iborra, A. Montoya-Baides, and A. Arnau-Vives, Sensors, 9, 5740, (2009). Copyright 2009, MDPI)

Among the various applications that can be implemented in microfluidics, immunoassays and DNA analysis have been the most prevalent,

due to their significance in identifying infections and diseases [105-108]. This can be accomplished by screening for specific proteins, antibodies, or other biomarkers or through DNA separation and hybridization. Some characteristic examples include enzyme-linked immunosorbent assays (ELISAs), where antigen-antibody binding is detected by measuring the activity of an enzyme linked to a secondary antibody that is attached to the complex, and DNA hybridization, where the presence of a specific nucleic acid sequence is screened through attachment of the chain of interest to its complementary. The traditional bench-top processes are slow, consume large amounts of reagents, and cannot be easily automated. Consequently, efforts have been directed towards their miniaturization and in fact, multiple reports have been published on both LOC ELISA [109-115] and DNA analysis [116-121].

1.3.3 Nanostructured materials in microsensors

In addition to sensor and auxiliary component miniaturization, the overall performance of the down-scaled device can be improved through the use of nanostructured materials as binding agents. Indeed, nanostructures can offer significant benefits such as higher sensitivity, lower detection potentials, larger dynamic range, improved signal to noise ratios, and higher separation efficiencies [122, 123]. They can be used in suspended and stationary phases to facilitate electrophoretic or chromatographic separations as well as to directly detect a binding event on the transducer surface.

1.3.3.1 Nanoparticle Sensors

Various nanoparticles have been reported as detectors and separators in microfluidic sensors, including gold, silica, magnetic nanoparticles, and quantum dots. Composites of $NiFe_2O_4$ and SiO_2 were combined with electrochemical sensing for tumor marker screening, where the magnetic core allowed manipulation of the receptors in the microchannel and the silica cell facilitated functionalization with the specific antigen [124]. Similarly, core/shell/shell nanoparticles of Fe_3O_4/chitosan/Au have also been reported [125]. Chitosan promoted gold attachment which in turn bound to the probe proteins. Gold and silica nanoparticles have been used to improve electrophoretic separation efficiency by coating the sidewalls of microfluidic channels [116, 126, 127], or, in the case of gold, as SERS-active particles in microfluidic devices [128]. The unique size-tunable fluorescent quantum dots have also been employed. Hu et al. used DNA fragments and biotin/streptavidin conjugation chemistry to attach probe molecules onto CdTe/CdS nanoparticles [129], while Zheng et al. trapped quantum dots on microbeads in fluidic chambers using multi-depth microfluidics [130]. Notwithstanding the benefits of this approach, their utilization in low-cost autonomous LOC is hindered by the integration incompatibilities (they require magnetic, electrical, or chemical forces to be used in a device) as well as the need for post-integration biofunctionalization.

1.3.3.2 1-D and 2-D Nanosensors

Nanowires, nanotubes and 2-D materials such as graphene can overcome the device compatibility limitations of 0-D materials since they can

be patterned selectively in microfabricated sensors. This facile integration has enabled their use in microfluidics for both chemical and biological sensing. Ni nanowires [131] and carbon nanotubes [132] have been used to improve the detection efficiency of electrophoretic separations due to their catalytic properties, while silicon nanowires have served as high-surface-area pre-concentrators as well as sensitive field effect transistors (Figure 1-12a), where the conductivity of the nanowire is modulated by the charge of the bound molecule in a "bio-gating" effect [133-137]. Similar to the nanoparticles however, receptor functionalization of the nanowires is a tedious process that often requires up to three different steps of surface modification reactions to attach the molecule on the surface [137]; they also have to be used in buffer solutions with controlled conductivity. In other examples, the unique conductivity properties of graphene as well as the presence of aromatic rings that promote the attachment of proteins have also allowed it to be used as a transducer in microfluidics [138] (Figure 1-12b). In more sophisticated approaches, graphene has been modified with selective binding peptides that can bind both to the substrate and the analyte [139]. Most implementations have been focused on vapor-based disease biomarker and explosive detection sensors [139, 140]. While peptides enable a simplified device functionalization pathway, they provide limited binding sites and their production cost is not insignificant.

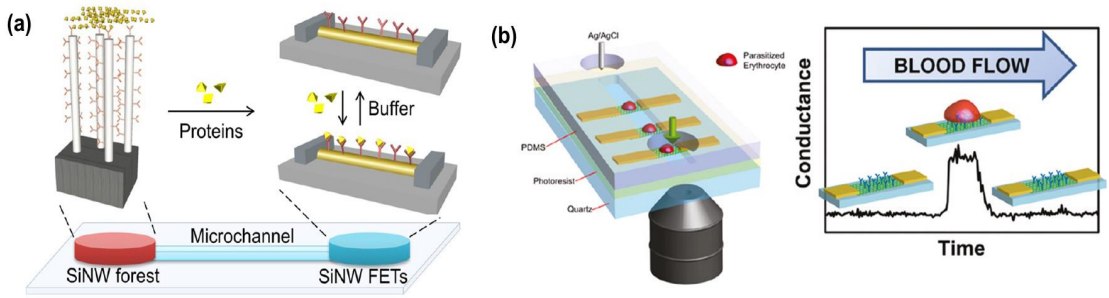

Figure 1-12 (a) Si Nanowire-based microfluidic device consisting of vertically attached arrays as protein pre-concentrators and Si-nanowire FETs where the proteins can then be sensed [133], (Reprinted with permission from V. Krivitsky, L. C. Hsiung, A. Lichtenstein, B. Brudnik, R. Kantaev, R. Elnathan, A. Pevzner, A. Khatchtourints, and F. Patolsky, Nano Letters, 12, 4748, (2012). Copyright 2012, American Chemical Society) (b) microfluidic malaria cell sensor with device patterned chemically functionalized graphene [138]. (Reprinted with permission from P. K. Ang, A. Li, M. Jaiswal, Y. Wang, H. W. Hou, J. T. L. Thong, C. T. Lim, and K. P. Loh, Nano Letters, 11, 5240, (2011). Copyright 2011, American Chemical Society)

1.3.3.3 Nanosensors Based on Virus Scaffolds

Filamentous viruses are simple, well-structured macromolecular assemblies of coat proteins that form rod or tube-shaped particles. These nanostructures can be ideal bio-recognition elements in sensor applications due to their high-aspect-ratio and genetic modification potential that enable expression of binding sites with very high density. The *Tobacco mosaic* virus (TMV) is a well-studied plant virus that consists of a single stranded RNA coated with 2,130 identical copies of coat proteins. Each of its physiological components (CP and RNA strain) has been used as a binding receptor. Previous work by our team has shown that TMV can facilitate DNA hybridization onto chitosan functionalized gold electrodes [141]. Chitosan was electrodeposited on the gold electrode and acted as an immobilization site for probe DNA; this was then linked with a complementary DNA attached to the viral RNA, exposed through partial protein disassembly on the bottom end of the TMV (Figure

1-13a). This process has been used by others to sense differentially labeled nano-templates as well as barcode-type biomolecules [142, 143]. The chemical modification capabilities of the virus coat proteins have also been reported, mostly in chemical sensors applications. For example, oligoaniline-modified and cysteine-modified TMV that promotes metallic particle nucleation have been explored as sensors for volatile organic compounds and hydrogen, respectively [144, 145].

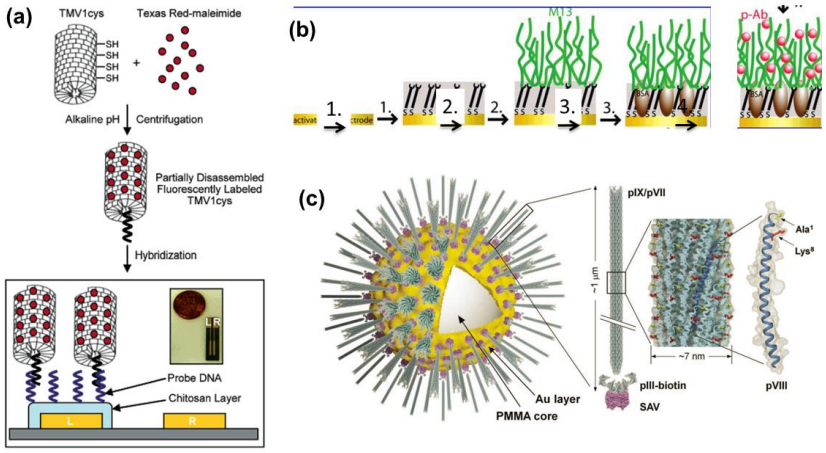

Figure 1-13 (a) DNA hybridization using partially disassembled TMV [141], (American Chemical Society) (b) M13 assembled on a quartz crystal microbalance for positive antibody immunoassays [146], (Reprinted with permission from L. M. C. Yang, J. E. Diaz, T. M. McIntire, G. A. Weiss, and R. M. Penner, Analytical Chemistry, 80, 933, (2008). Copyright 2008, American Chemical Society) (c) M13 assembled on gold-coated microbeads to mimic cellular structure for enhanced detection efficiency [147]. (Reprinted with permission from C. S. Jeon, I. Hwang, and T. D. Chung, Advanced Functional Materials, 23, 1484, (2013). Copyright 2013, Wiley)

M13 bacteriophage is another filamentous virus that can replicate in bacteria. It consists of 2,700 copies of major coat proteins and 5 minor coat proteins surrounding a DNA genome. Similar to the TMV, it can be genetically engineered to facilitate analyte binding. Addition of positive

antibodies on the coat proteins has enabled immunoassays with the M13, using quartz crystal microbalances (QCMs) as mass sensors (Figure 1-13b) [146], as well as Poly(3,4-ethylenedioxythiophene) (PEDOT) nanowires in microfluidic impedance sensors [148]. Binding efficiency can be increased by immobilizing M13 onto Au coated microspheres to form hierarchical surfaces resembling biological cellular structures and thus enhance ligand-receptor interactions (Figure 1-13c) [147]. The detection method can be simplified by incorporating thiolated coat proteins that capture gold nanoparticles and induce color changes associated with plasmon shifts [149]. More complex coat protein modifications have also been achieved to selectively target trinitrotoluene (TNT) molecules [150] and express ssDNA probes [151, 152] via a combination of genetic mutation and chemical conjugation.

These demonstrations indicate that viruses can be unique functional nanostructured building blocks in highly sensitive and selective platforms; however, most have been implemented in macro-scale experimental settings. Very little information is available on their integration in microfluidic devices as well as their behavior and stability under flow conditions. This could be a problem particularly with bacteriophages, which are longer, thinner, and less robust compared to the rigid rod *Tobacco mosaic* virus. This latter property that enables 3-D self-assembly makes the TMV an excellent candidate for efficient incorporation in microfabricated liquid flow configurations.

1.4 Structure of dissertation

Chapter 1 has presented the motivation for this research and the relevant work found in literature. Chapter 2 discusses the VLP receptor genetic modification, purification process, self-assembly morphology and validation of biosensing functionality using colorimetric methods. Chapter 3 discusses the integration of VLPs as receptors in microsensors for chemical explosive sensing. Chapter 4 studies the integration of VLPs in impedance microsensor for antibody sensing. Chapter 5 is focused on the design, fabrication and characterization of a sensor microsystem for rapid and enhanced VLP assembly and biosensing. Chapter 6 summarizes the contributions of this dissertation and discusses the future direction of this study.

Chapter 2: *Tobacco mosaic* virus-like particles as sensing receptors

This chapter discusses the genetic modification and purification methods of Tobacco mosaic virus-like particle (VLP) sensing receptors, surface morphology and biosensing efficacy of VLPs assembled through evaporation-based method on-chip.

Professor James N. Culver and Mr. Adam D. Brown contributed to developing the methods and protocols for genetically modifying *E. coli* bacterial cells to produce TMV coat proteins with self-assembly capabilities. Professor James N. Culver, Mr. Adam D. Brown, Ms. Lindsay Naves and Dr. Xiao Zhu Fan contributed to the purification of VLPs from bacterial cells.

2.1 *Tobacco mosaic* virus (TMV)

The *Tobacco mosaic* virus (TMV) is a highly infectious filamentous plant virus with a rigid high-surface-area nanorod structure. It is formed by 2,130 identical coat protein (CP) subunits stacked in a helix around a single strand of RNA. The length of TMV is about 300 nm controlled by the encapsulated genomic RNA, and the outer diameter of the nanorod structure is about 18 nm. The helical protein arrangement and the nanorod structure of TMV are shown in Figure 2-1. The molecular weight of each coat protein is 17.5 kDa; they self-assemble into a helical structure with 16 ⅓ coat proteins per turn around the RNA. Each CP of a wild type TMV is composed of a folded chain of 158 amino acids. Both N and C termini of the CP amino acid chain are exposed on the outer surface of the TMV. Thus, TMV can conveniently be

genetically engineered to show functional affinity to certain materials or target molecules by the expression of additional amino acid sequences on the N or C terminus of the CP.

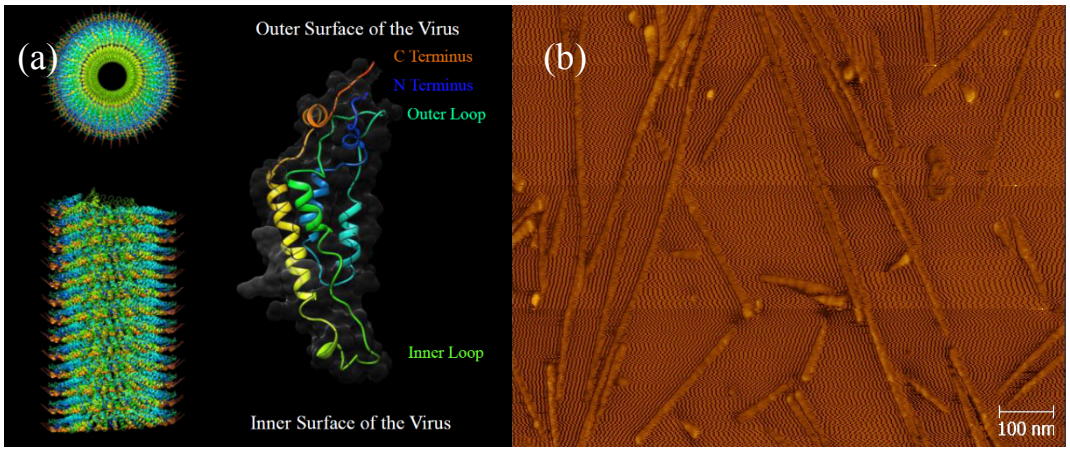

Figure 2-1(a) Diagram showing the structural composition of a TMV and one of its coat proteins. The top and side perspectives of the virus model show a helical tube viral structure. [153] (Reprint with permission from X. Z. Fan, E. Pomerantseva, M. Gnerlich, A. Brown, K. Gerasopoulos, M. McCarthy, J. Culver, and R. Ghodssi, *Journal of Vacuum Science & Technology A*, 31, (2013). Copyright 2013, AIP Publishing LLC.) (b) An AFM image showing TMV nanorod structure.

The typical preparation of TMV includes tobacco plant culture, infection and virus extraction, which take around one month. Also, from the experimental experience, the efficacy of plant infection and the final yield of TMV are closely related with the genetic modification on its RNA. To overcome the limitations in TMV preparation, research has focused on a different route to develop TMV virus-like particles (VLPs) that retain the TMV CP nanostructures and genetically programmable receptors, but feature shorten preparation time and higher yield.

2.2 Virus-like particles – genetic modifications

The virus-like particles (VLPs) are direct derivatives of the natural TMV. In order to achieve faster preparation with higher yield compared to TMV, the VLP culture uses bacterial cells as hosts other than plants. To achieve nanorod structures with receptors as TMVs from a bacterial cell host, several genetic modifications on the CP sequence are necessary.

2.2.1 Genetic modifications for stable coat protein assembly into nanorod

The VLP nanorod structure is self-assembled on the molecular level from TMV CPs inside *E. coli* cell. In order to achieve the similar nanorod structure as the TMV, special genetic modifications on the CPs are necessary to initiate the molecular level CP self-assembly and bind the individual CPs together.

In nature, the repulsive carboxylate groups located on opposite sides of CP subunits govern the stability of the TMV nanostructure. The negatively charged carboxylates are stabilized by protons and the Ca^{2+} ions that regulate the stability of the interrelationship between coat protein subunits to form a helical structure. The third axial carboxylate interaction that significantly drives the particle assembly occurs between the residues E50 and D77. The mutations of E50Q and D77N have been shown to block virus disassembly even in the absence of the nucleic acid backbone [154].

Therefore, both E50Q and D77N modifications have been engineered in the TMV coat protein open reading frame for the expressions in *E. coli*

bacterial cells. These genetic modifications have realized a VLP structure consisting of self-assembled TMV CPs but without the viral nucleic backbone.

2.2.2 Genetic modifications for surface attachment and target binding

As is introduced in 2.1, the N- and C-terminus of each CP is exposed on the outer side of the TMV (and thus also VLP) nanorods, providing biologically programmable affinity through the alternation of the amino acid sequence at the terminus. In microsensors for chemical or biological analysis, it is desired to integrate a selective functional surface layer of receptors with transducers to sense the presence of target molecules. Therefore, the VLP genetic modifications toward sensing applications are aimed at (1) promoting the attachment of VLPs on transducer surfaces and (2) providing highly specific binding affinity to the target molecules.

To address (1), the CP N-terminus has been genetically engineered to express a cysteine residue. Cysteine (C) is an α-amino acid with a thiol side chain that often participates in enzymatic reactions. Gold is a widely used electrode material for electrical transduction-based sensors. Since gold reacts to form a strong bond with both with reduced alkanethiols (-SH groups) and alkyldisulfides(-S-S-) [155], thiol-containing cysteine residue can be used as terminal thiol residue to enable the self-assembly of VLPs directly onto a gold surface.

As for the second aim, functional peptides have been expressed on the CP C-terminus aimed at conferring VLP specific affinity to target molecules., Two specific constructs of VLPs – with TNT binding peptides (VLP-TNT) or

FLAG-tag sequences (VLP-FLAG) – have been successfully expressed as model systems to study the feasibility of using VLPs as receptors in chemical sensor or biosensor. The TNT binding peptide contains 12 amino acids (WHWQRPLMPVSI) which shows high affinity for the target 2,4,6-trinitrotoluene (TNT) molecules even over other similar nitro aromatic compounds such as 2,4-dinitrotoluene (DNT) [156]. In VLP-FLAG (Figure 2-2), CPs are genetically modified to expressed the 8 amino acid FLAG-tag (DYKDDDDK) – a widely used labelling sequence that selectively binds with anti-FLAG antibody. These two variants of VLPs are used as biorecognition elements to selectively sense the biological or chemical targets.

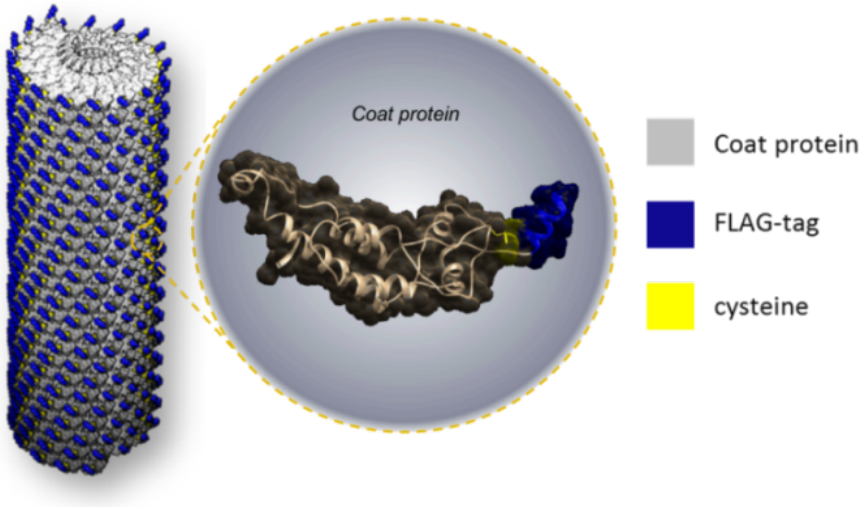

Figure 2-2 Diagrams of genetically modified VLP-FLAG sensing probes. [157] (Reprinted with permission from F. Zang, K. Gerasopoulos, X. Z. Fan, A. D. Brown, J. N. Culver, and R. Ghodssi, Biosensors and Bioelectronics, 81, 401, (2016). Copyright 2016, Elsevier)

2.3 VLP culture and purification procedure

The first step in the preparation of the VLP is to inoculate the *E. Coli* BL21 culture whose bacterial cells already contain desired vectors (a RNA

molecule that contains the code to produce the peptide modified CP sequence). A small stock sample of bacteria is placed in a test tube containing 5 mL of Lysogeny broth (LB) media supplemented with antibiotics to ensure only desired bacterial cells survive – 100 μg/mL of ampicillin, 50 μg/mL of chloramphenicol (for production of VLP-FLAG) or 20 μg/mL of nalidixicacid (for production of VLP-TNT) (Figure 2-3). The bacteria samples were cultivated in a 37 ^{o}C shaker/incubator overnight. The volume of the bacterial culture was then scaled the volume up to 50 mL on the next day by adding the original 5 mL bacteria samples into 50 mL LB media with the sample ratio of antibiotics described previously. The culturing process continued until the optical density reading of the bacteria growth solution at λ = 600 nm reached OD_{600} = 0.5.

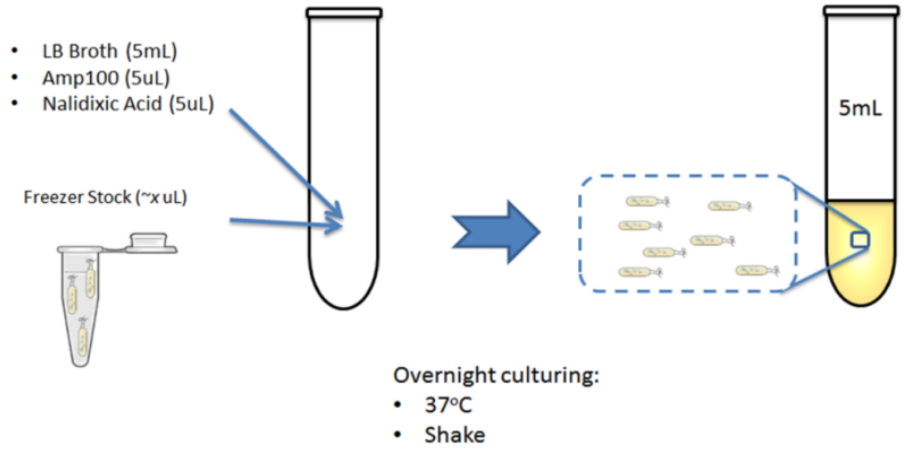

Figure 2-3 Schematic of the culturing process of *E. coli* bacteria from freezer stocks for producing VLP-TNT.

Once an OD reading of 0.5 was reached, the bacteria were induced to form TMV coat proteins by transcribing pre-programmed vectors. This was accomplished through addition of 0.1% v/v 1M Isopropyl β-D-1-

thiogalactopyranoside (IPTG), and leaving the solution overnight on a shaker at 25°C. During this process, CPs form and simultaneously self-assemble into helical nanorods in the bacterial cells due to the genetic modifications discussed in 2.2.1.

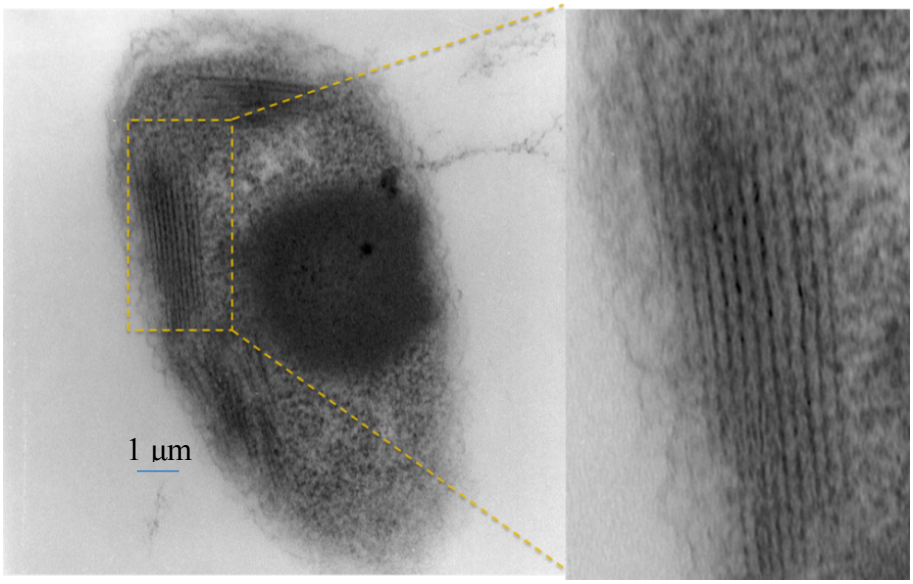

Figure 2-4 Transmission electron microscopy images of (left) *E. coli* bacterial cells with VLPs growing inside. The CPs assembled themselves into nanorod structures and closely packed in bacteria (right) [154]. (Reprinted with permission from A. D. Brown, L. Naves, X. Wang, R. Ghodssi, and J. N. Culver, *Biomacromolecules*, 14, 3123 (2013). Copyright 2013, American Chemical Society)

Figure 2-4 shows the *E. coli* bacterial cells containing VLP nanorod structures after induction. To extract the VLP from the bacterial cells, the solution was centrifuged at 10 thousands revolutions per minute (krpm) at 4°C for 10 minutes. The supernatant was discarded and the pellet containing the bacterial cells was re-suspended in 2.5 mL of Bug Buster Protein Extraction Reagent and 1 µL of Lysonase Bioprocessing Reagent. The re-suspending process was performed on a rotisserie for 45 minutes at room temperature to break the bacterial cell membrane. A 1 µL of Dithiothreitol (DTT) solution was

then added in solution and mixed for another 10 minutes to break the disulfide bond between the adjacent VLP rods. The solution was then transferred into microcentrifuge tubes and spun at 3 krpm for 1 minute in order to separate the VLPs from high density residues. The supernatant containing the VLPs was transferred into ultracentrifuge tubes and diluted in 0.1M phosphate buffer. Ultracentrifugation was then performed at 30 krpm for 30 minutes to collect the VLPs in the pellet. The purity of the VLP sample after re-suspension was assessed using protein gel electrophoresis (Figure 2-5). The lowest bands in Figure 4-3 represent TMV CPs. Comparing the density of these bands, it can be concluded that the VLP-FLAG has higher yield than VLP-TNT. This may be caused by the attachment of CPs in VLP-TNT samples to the pelleted high-density residues during the low-speed centrifugation due to the hydrophobicity of the TNT peptides.

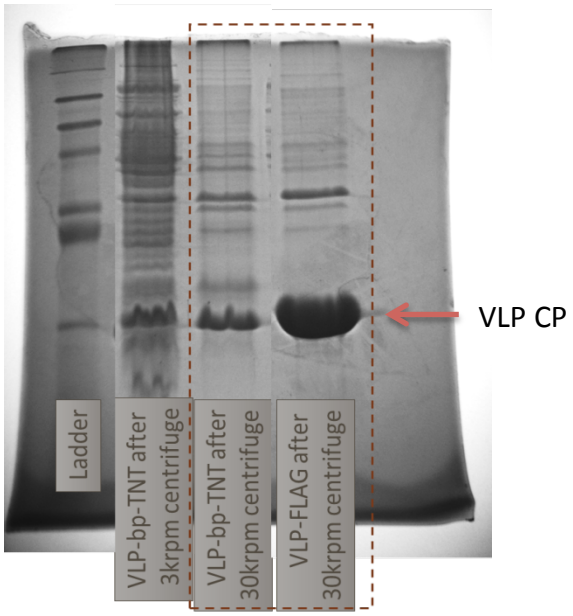

Figure 2-5 Protein gel electrophoresis of the VLP samples after centrifugations. Both VLP-TNT and VLP-FLAG samples showed clear and dense coat protein bands (lowest on each column) after centrifugations at 30krpm.

For VLP-FLAG samples, further purification steps were taken by first re-suspending the pellet and loading it onto a sucrose gradient solution with the total sucrose of 25%, which was followed by centrifugation at 22.5 krpm for 20 minutes to separate VLPs from residues with similar density. A bright section that contained VLPs in the sucrose gradient solution was observed under illumination. This section of the sucrose gradient solution was extracted and centrifuged in 0.1M sodium phosphate buffer at 30 krpm for 1 hour. The pellet was re-suspended overnight at 4^{o}C using either 0.1M sodium phosphate buffer or DI water to obtain the final VLP stock solutions for the device functionalization.

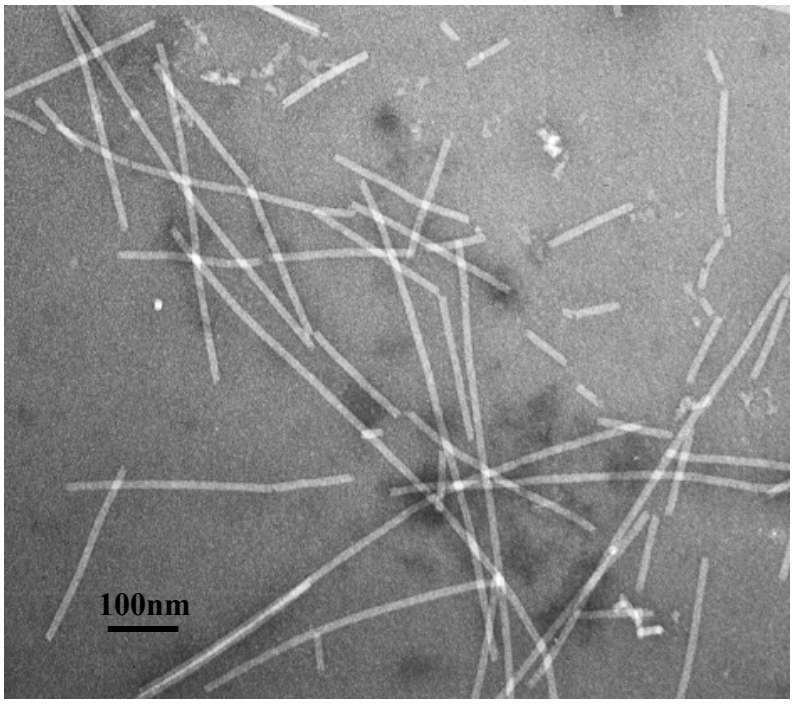

Figure 2-6 TEM image of the purified VLP-FLAG (sample is diluted for imaging purposes).

The purity and nanorod structure of the purified VLPs were verified using transmission electron microscopy (TEM), shown in Figure 2-6. It can be concluded that the VLP nanorods are successfully extracted from the bacterial

cell structures without major impurities in the purification process. The length of the VLP nanorods varies from around 50 nm to over 500 nm which is attributed to the lack of limitation from an RNA strand compared with TMVs. The successful purification of VLPs from bacterial growing media has established the foundation for the following self-assembly of these nanostructured sensing probes in transducers in a controlled manner.

2.4 VLP surface assembly process

2.4.1 VLP self-assembly

The VLP self-assembly on different materials was studied. These materials include gold, silicon oxide which is commonly used for electrode or insulating materials in microfabricated devices.

In the experiments, 0.2 mg/mL of cysteine-expressed VLPs were used as the VLP sample. The assembly of VLP was performed by immersion of the substrate chips in the VLP sample solution at 25^{o}C for 18 hours. The samples were visualized using scanning electron microscopy (SEM). For a better visualization, the metallization of surface self-assembled VLP was performed by 5 hours of palladium activation and a following 4 minutes of electroless plating of nickel. The metallization preserves the surface morphology of VLPs and forms a conductive nickel shell on the organic VLP nanorod surface, which lowers the charging effects during SEM imaging and improves the contrast against the metal substrate.

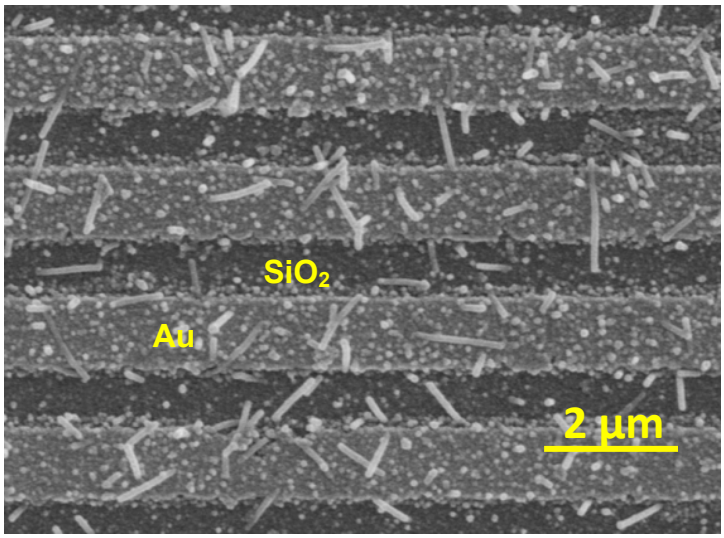

Figure 2-7 SEM images of interdigitated electrodes after VLP-FLAG assembly in deionized water.

The assembly of VLPs with binding peptide modifications (VLP-FLAG) was similarly studied on devices with gold and silicon oxide materials. As is shown in Figure 2-7, the VLP-FLAG self-assembled on both gold and SiO_2. The density of VLPs is higher on gold because of stronger interaction between the –SH group on cysteine residue and gold. Also, the overall assembly density of the VLP-FLAG on gold is lower than VLP-1cys. This may be attributed to the presence of the bulkier 8 amino acid FLAG-tag peptide sequence which potentially blocks some cysteine residues from interacting with the gold surface.

From the self-assembly experiments and SEM imaging, it can be confirmed that the cysteine residues on VLPs facilitated self-assembly on multiple kind of materials. This enables the use of VLPs as immobilized functional materials in a wide range of microfabricated sensors. On the other hand, there remain challenges such as long duration of the self-assembly process, insufficient selectivity to substrate materials and low assembly density

in the presence of binding peptides. Therefore, there is a need for an improved self-assembly method and process to precisely control the formation of VLP functional layer.

2.4.2 Evaporation-enhanced VLP assembly process

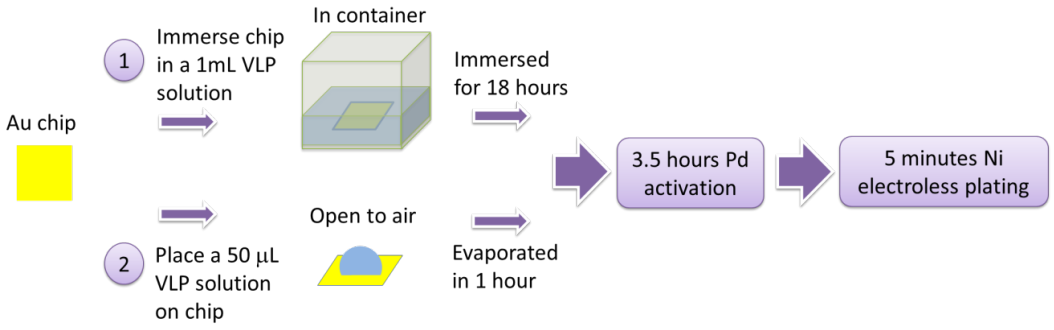

Figure 2-8 VLP assembly processes with or without evaporation.

Though the capability of VLP self-assembly on multiple materials has been validated, it is necessary to develop an enhanced VLP self-assembly method to minimize the amount of time and VLPs required functionalizing the sensor surface. Evaporation was studied as a means to achieve localized VLP assembly on chip using a much smaller amount of VLP stock solution. Figure 2-8 illustrates the process of the evaporation-enhanced VLP assembly on-chip. In this method, a droplet of VLP solution with the volume of less than 50 µL (instead of bulk VLP stock solution) is applied on the 1 cm^2 gold chip surface using a micropipette. By evaporating the VLP droplet in open environment for less than 1 hour, the VLPs can assemble on the gold surface due to self-assembly and van der Waals force in evaporation. The evaporation-assisted process is aimed at great improvement in the VLP localization as well as reducing the VLP assembly time.

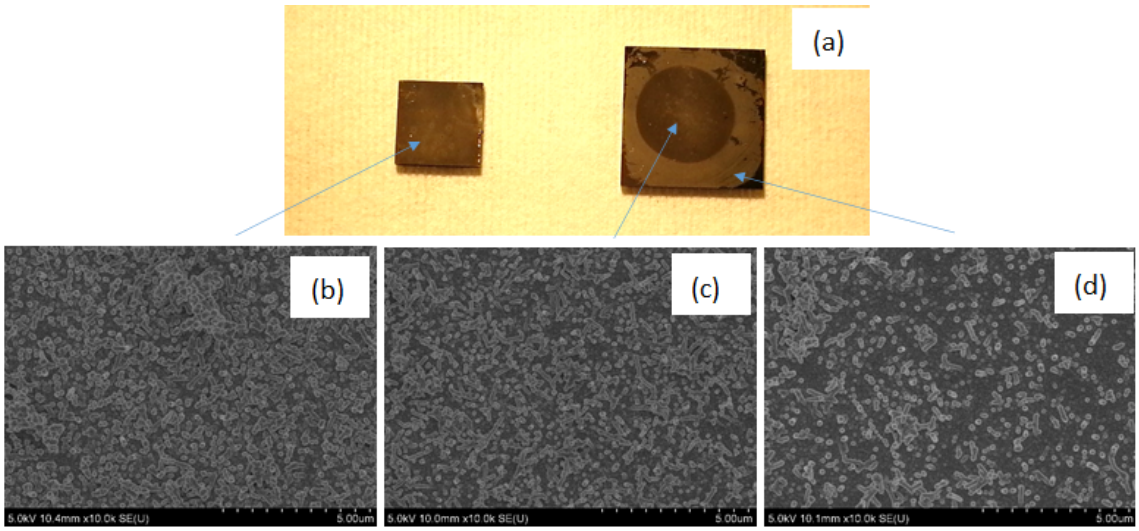

Figure 2-9 (a) Optical image of (left) VLPs assembled electrode by immersion for 18 hours and (right) VLPs assembled on electrode by evaporation of 50 µL of VLP solution at room temperature for 1 hour. (b) SEM image of the VLP assembled in 18 hours. SEM image of (c) the center and (d) edge of electrode that functionalized by evaporation of VLP droplet.

A VLP assembly test was carried out to determine whether immersion of a chip in VLP solution and evaporation of a VLP droplet on a chip surface yield significant differences in assembly morphology. From the optical image (Figure 2-9a), the electrode on the left (immersed in VLP solution) and the center area (where the 50 µL droplet of VLPs was located) of the electrode on the right showed the same dark colour. In the marginal region of the latter electrode the colour is light grey, meaning fewer VLPs were assembled there. Since electroless Ni plating was utilized to enhance the image contrast in SEM, the VLPs assembled on the marginal region is likely because of migration of non-specifically bound VLPs during the electroless Ni plating. The SEM images confirmed the density of VLPs assembled in Figure 2-9b and Figure 2-9c were similar while it was lower in Figure 2-9d. It indicates that, using evaporation, (1) a much lower amount of VLPs can be used for coating the

electrode while ensuring a good coverage, (2) the VLP assembly time can be significantly reduced and (3) localized VLP functionalization becomes possible.

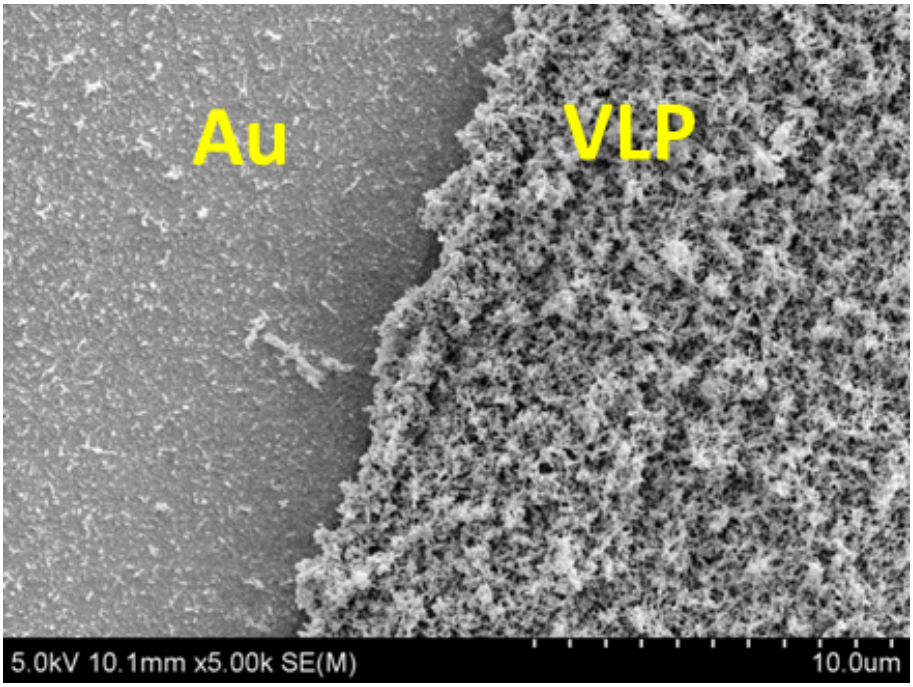

Figure 2-10 VLP morphology on the boundary of "coffee ring".

Due to higher surface tension, a thicker layer of VLP is formed on the edge of the VLP droplet on gold forming a "coffee ring". In the SEM image (Figure 2-10), VLP assembled on gold showed a clear boundary that is purely confined by surface tension and evaporation of VLP solution.

To advance the understanding of evaporation-enhanced assembly, the morphology, self-assembly time and peptide functionality of VLPs were studied with varying evaporation temperature during the assembly process. Table 2-1 lists the time corresponding to evaporation of 50 µL VLP solution on a 1 cm^2 gold substrate. As the temperature increased from 30°C to 60 °C, the total time for evaporation was decreased by 87%. During the assembly process, the ambient was at a temperature of 23°C with 10% relative humidity.

Table 2-1 Evaporation time of 50μL of VLP-1cys solution on gold surface (ambient: temperature 23°C, relative humidity 10%).

Chip temperature	Evaporation time
30°C	45 min
40°C	30 min
50°C	15 min
60°C	6.5 min

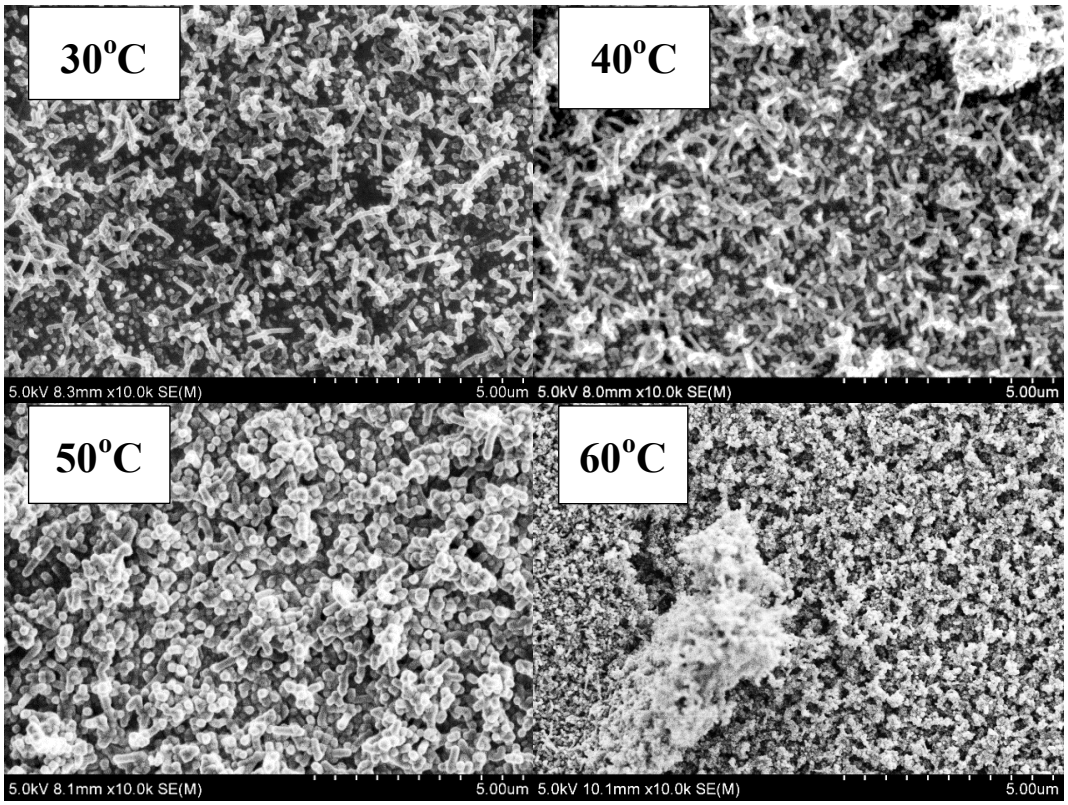

Figure 2-11 Morphology of metalized VLP-1cys assembled at 30°C, 40°C, 50°C, 60°C.

The evaporated VLPs were successfully metallized by Pd activation and Ni electroless plating, indicating that the cysteine residues on the VLP surface maintain their affinity to gold. From the SEM images shown in Figure 2-11,

VLPs are observed for all conditions. At lower temperatures, the VLPs keep their nanorod structure and show uniform coating, but with a lower assembly density. At higher temperature, the VLPs become closely packed at the expense of less uniformity. When the temperature reaches 60°C, the shape of the VLPs moreover changes from "rod" to "disk"-like, losing the high-aspect-ratio feature. The high temperature may weaken the affinity between CPs causing the VLP nanorods to dissemble.

2.4.3 Morphology of VLPs assembled through evaporation

In our previous work, VLP assembly was previously performed in a stationary bulk solution overnight. The VLP nanorods in this process have not experienced high surface tension due to immersion in a relatively large volume of stationary solution. The VLPs suspended in the bulk solution are therefore assembled vertically, owing to the attachment of cysteine at the end of the VLP nanorod to the material surface. However, this well-observed phenomenon does not translate identically when evaporation is introduced in the VLP assembly process, where surface tension plays an important role.

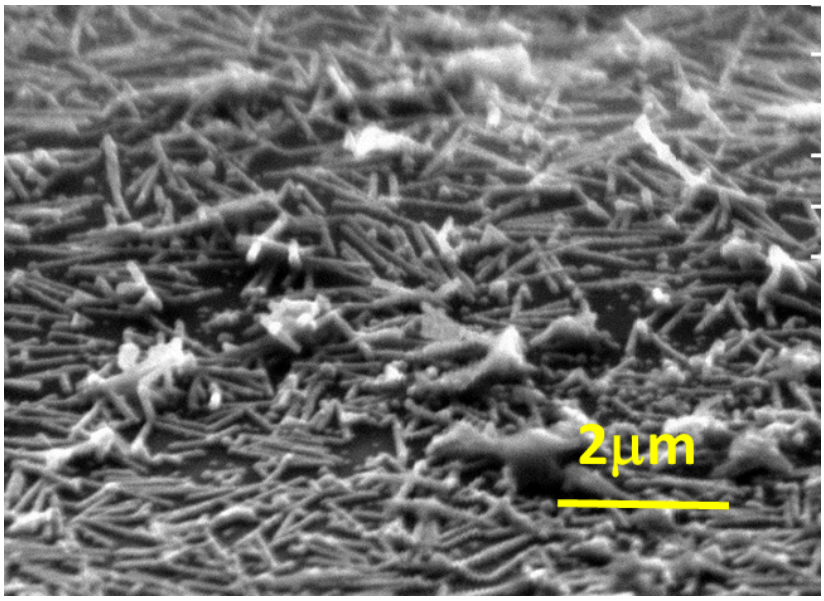

Figure 2-12 SEM image of VLP assembled on a flat silicon surface using evaporation-assisted process

SEM was utilized to study the influence of surface tension in the evaporation-assisted assembly on the morphology assembled VLPs. The SEM image in Figure 2-12 shows the VLPs attach horizontally onto the substrate. This parallel arrangement of VLP differs from the vertical VLP arrangement observed from VLP self-assembly process. Silicon is usually not a favourable surface for VLP assembly since –SH groups cannot form covalent bond with silicon. However, interestingly, the van der Waals force during the VLP solution evaporation "pulled" the VLP nanorods onto the silicon surface and forced relatively strong non-specific binding on the silicon. The VLP structures survived several washing steps and even the electroless Ni plating processes (for SEM imaging purposes).

Therefore, the surface tension is one of the important factors to determine the morphology of TMV-assembled surfaces. When surface evaporation is utilized during the VLP assembly, it is likely to create a flat

arranged VLP layer rather than a layer with vertically aligned VLPs. This brings the high density peptide receptors on VLPs much closer to the surface. When designing the transducers, the thickness of the VLP layer should be specially considered to achieve better sensitivity.

2.5 VLP biosensing efficacy in immunoassays

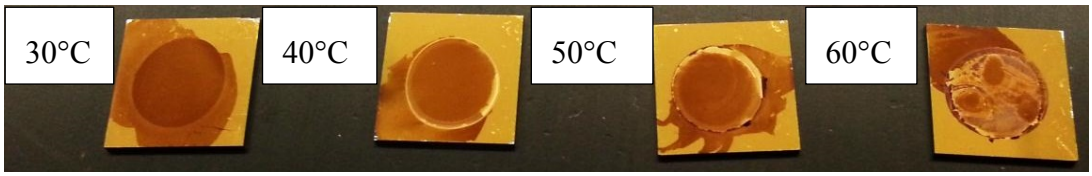

Figure 2-13 ELISA on gold chips with VLP evaporated at different temperatures.

ELISA was performed on the gold chips functionalized by VLP using the evaporation-assisted assembly process. The functionality of the VLP-FLAG as sensing probes in ELISA was independently validated by colorimetric experiments conducted in parallel with the impedimetric sensing experiments. Dark-purple colored precipitates due to the interaction between substrate and enzymes on the secondary antibodies were observed on gold chips which have VLPs assembled through evaporation. The pictures of the gold chips after the full ELISA process are shown in Figure 2-13. It is clear that the dark-purple color of the precipitate is much more uniform in the center of the chip where a lower evaporation temperature was utilized. At a higher evaporation temperature, there was still the colored precipitate from biological binding; however, the uniformity of the precipitate degraded significantly. Therefore, even though evaporation at a higher temperature can accelerated the process significantly, the process at a relatively low temperature can result in a much uniform VLP layer while keeping better biosensing efficacy of the binding

peptides on the VLP surface. Overall, by evaporating the VLP-containing solution on the gold surface, the assembly of VLPs can be significantly accelerated and the localization can be greatly improved. This method also keeps good biosensing efficacy of the peptide receptor sequence on the VLP coat proteins.

Appropriate evaporation temperatures need to be used to shorten the assembly time while keeping the integrity of VLP nanorods and the functionality of the peptides. Combining the results demonstrated in Figure 2-11 and Figure 2-13, the upper limit of the VLP evaporation temperature is estimated at 50°C. However, the VLP shows better structural integrity and receptor functionality from room temperature to 30°C. Under these conditions, the evaporation of VLPs is a feasible means to rapidly assemble these genetically modified macromolecules and create a localized functional layer in a device.

2.6 Chapter summary

This chapter studied the TMV VLP molecular structure, genetic modification, surface attachment, and bioreceptor affinity and stability. Through genetic engineering, *E. coli* bacterial cells are able produce VLP coat proteins and that form VLP nanorod structures inside the cell. Genetic modifications have been made on the C- and N-terminal ends of each VLP coat protein. On the C-terminal end, a TNT binding peptide or a FLAG-tag peptide have been successfully expressed and confer the VLP highly selective chemical and biological binding capabilities. On the N-terminal end, a cysteine residue is

expressed which enables self-assembly of VLP nanorods onto a variety of material surface without chemical treatment. The surface morphology of the assembled VLP can be controlled by the surface tension in different assembly processes. Under high surface tension during the assembly process, the VLP nanorods closely attached parallel to substrate and aligned according to the flow direction. This morphology is different from the self-assembly in bulk solution where the VLPs attached vertically on the surface. Further study using colorimetric ELISA showed good biosensing efficacy of the VLP receptors. Experiments also showed that VLPs are stable at a wide range of evaporation temperature, and the evaporation of VLP on a substrate can promote the VLP localization.

The fundamental study of the VLP sensing receptor genetic modification, preparation and characteristics provided important guidance to the later sensor design and system integration of VLPs. It also indicated that VLP is a versatile sensing probe which can be utilized as a universal platform for receptor expression.

Chapter 3: VLP-based chemical explosive sensor

Sensing of trace amounts of small toxic compounds such as explosive chemicals in complex aqueous environments faces significant challenges, including low signal level from the target molecules, large background signal as well as the requirement for ultra-sensitive transduction systems suitable for operation in solution. Conventional approaches are based on immobilization of receptors such as polymers, peptides, or antibodies on the transducer surface where the target species attach or react. The generated signal can be measured using fluorescent tags or in a label-free manner, as has been shown with field-effect transistors [158-162]. While these sensors are selective, they require sophisticated microfabrication processes with high precision, surface functionalization steps before the measurements, or additional labelling after the binding event, limiting their potential use in practical applications.

In this work, an alternative approach for sensing of small molecules that is based on VLP receptors as binding agents in solution is demonstrated. TNT is selected as a model target molecule to demonstrate the efficacy of this method, which can be readily expanded to other molecules with large contrast in size compared to the binding agents.

Dr. Konstantinos Gerasopoulos and Dr. Xiao Zhu Fan contributed to the discussion of the diffusion modulation-based TNT sensing methods and provided help in the experiment. Dr. Hadar Ben-Yoav contributed to the discussion and protocol of using square wave voltammetry for TNT sensing.

3.1 TNT electrochemical sensing

TNT is a widely used explosive and also a toxic chemical for organisms from bacteria to humans [163, 164]. The growing production and usage of TNT has resulted in contamination of soil and water in construction sites and weapon test grounds. When operating in solution, pulse voltammetric electrochemical sensors have been reported as the most sensitive approach to quantify TNT concentration, by analysing the peak current fingerprints from the electrochemical reduction of nitro groups ($-NO_2$) to amine groups ($-NH_2$) [165]. This method is not limited by the size of the analyte since it is based on charge transfer. However, selectivity is a bottleneck as the reduction peaks are very wide, and background subtraction is usually required to distinguish the TNT signal.

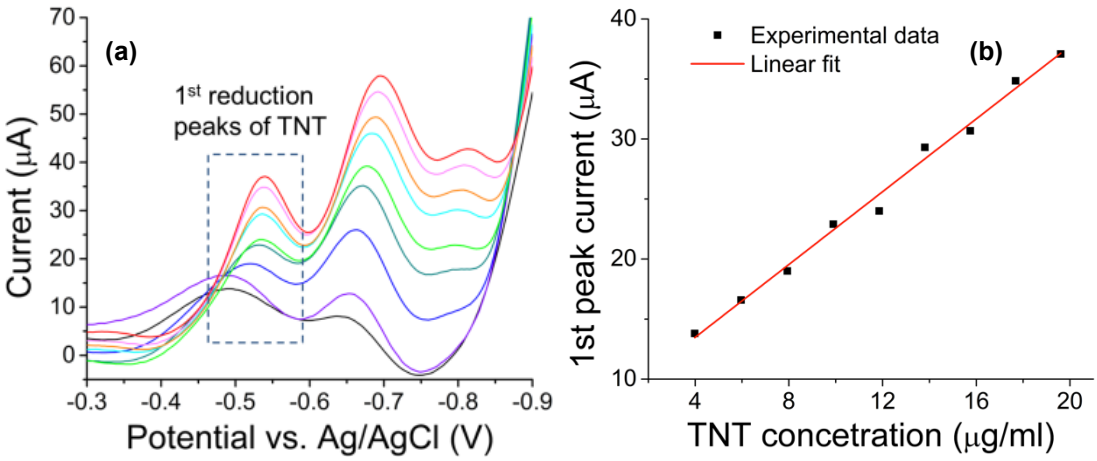

Figure 3-1 (a) Three characteristic peaks of TNT obtained using square wave voltammetry, and (b) the correlation between the 1st peak currents at -0.53V and TNT concentration [166]. (Reprinted with permission from F. Zang, K. Gerasopoulos, X. Z. Fan, A. D. Brown, J. N. Culver, and R. Ghodssi, Chemical Communications, 50, 12977, (2014). Copyright 2014, Royal Society of Chemistry)

The sensing methodology employed here utilizes square wave voltammetry featuring fast scan rate and high sensitivity. The peak current

signatures of TNT without VLP binding agents were first characterized using conventional square wave voltammetry where a 25 mV amplitude square wave was superimposed on a 4 mV step function at 50 Hz (Figure 3-1a). Three characteristic current peaks are observed in the voltage range from -0.3 V to -0.9 V (*vs*. Ag/AgCl). Among these, the first peak at -0.53V arises directly from the reduction of the nitro groups in the TNT molecule, and was used for quantifying the TNT concentration. For reactions on planar electrodes, the net peak current i_p can be expressed as,

$$i_p = nFS\sqrt{D_{eff}}\Delta\Phi_p f^{1/2} c^*$$

where the current is linear to the concentration c^* and the square root of the diffusion coefficient D of TNT in the bulk solution [167]. TNT in acetonitrile was introduced in an electrolyte containing 5 mL of 0.1 M NaCl and 0.01 M sodium phosphate. The TNT concentration was varied from 0 to 20 μg/mL, and the relationship between current and concentration was verified to be linear (Figure 3-1b). However, this conventional TNT electrochemical sensing method still has not rule out the possible electrochemical current overlapping from the interfering chemical species in real-world applications: it is hard for a sensor to tell whether a current peak is contributed purely by TNT reduction or comprehensively by all the species at the same reduction potential. Therefore, an enhanced electrochemical method is necessary to improve the selectivity in the electrochemical sensing of TNT.

3.2 VLP-based diffusion modulation method

The VLP-based TNT electrochemical sensing method breaks the selectivity limitation by combining the fast response and high sensitivity of conventional electrochemical sensors with the selectivity of VLP bioreceptors. A unique feature of this sensing method is the use of modified *Tobacco mosaic* virus (TMV)-like particles (VLP) as free-floating binding agents in the bulk sample solution that modulate the target TNT diffusion coefficient during sensing. This allows selective TNT detection within minutes without the need for surface functionalization of the transducer, a typically time-consuming added step. This "TNT filtering" enabled by the biological binding agents is quantified by a differential current measurement method, where the reduction currents with and without VLP are measured. The specificity of the bioreceptors and the simplicity of use make the sensor suitable for TNT detection in complex aqueous environments in a rapid and selective manner. The VLP binding agents are used in microfabricated electrochemical sensors to study the compatibility of this sensing mechanism with on-chip microsensors for TNT detection in low-volume solutions.

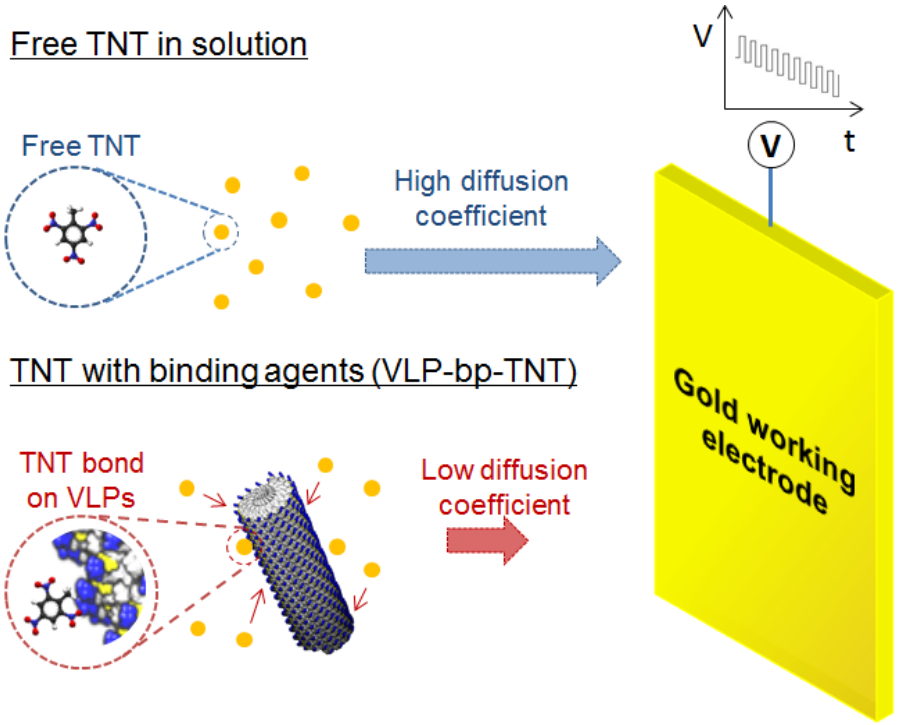

Figure 3-2 Diffusion modulations of TNT using VLP-TNT binding agents [166]. (Reprinted with permission from F. Zang, K. Gerasopoulos, X. Z. Fan, A. D. Brown, J. N. Culver, and R. Ghodssi, Chemical Communications, 50, 12977, (2014). Copyright 2014, Royal Society of Chemistry)

The integration of VLP binding agents in the TNT-containing solution changes the peak current by modulation of the effective diffusion coefficient, which is inversely proportional to the hydrodynamic radii of the molecules. VLP-TNT is a large macromolecule assembled from thousands of individual coat protein subunits (molecular weight ~17.5 kDa), which are significantly larger than free TNT (~227.3 Da). The hydrodynamic radius of TMV was previously reported to be approximately 42nm [168] while that of TNT is less than 0.4 nm. The suspended VLP binding agents bind free TNT molecules on the receptor peptides-displayed outer surfaces, and form "composite" macromolecules with extremely low diffusion coefficient (Figure 3-2). This biological binding event reduces effective diffusion coefficient in the system to

D'_{eff}, and generates a unique differential current ($\Delta i_p \propto (D_{eff})^{1/2} - (D'_{eff})^{1/2}$). In practice, the differential current is calculated from the peak current in the presence of VLP-TNT binding agents and a negative control (VLP-1cys, a construct without binding peptides) from two independent experiments in an identical experimental set-up. This method eliminates the need for obtaining environmental background from clean samples (without TNT contamination). The TNT concentration is now able to be quantified from the specific electrochemical current change caused by the VLP and TNT biological binding. Therefore, this method is extremely valuable for directly quantifying the TNT contamination level from samples obtained from unknown environments.

3.3 VLP nanoreceptors for TNT detection

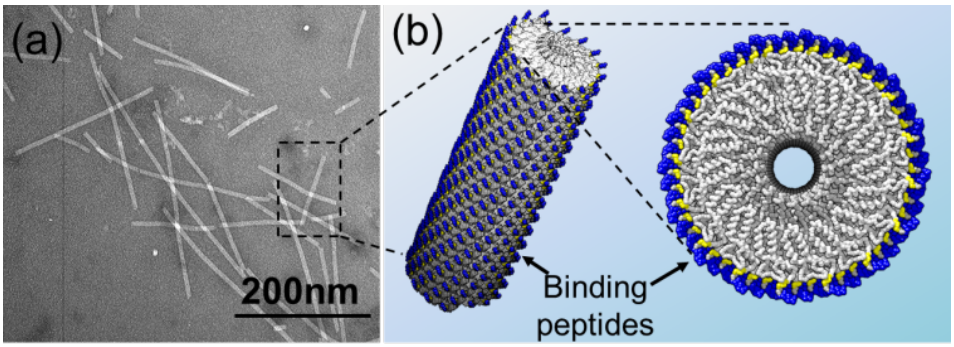

Figure 3-3 (a) TEM image of purified VLPs, and (b) genetic protein structure of VLP-TNT. [166] (Reprinted with permission from F. Zang, K. Gerasopoulos, X. Z. Fan, A. D. Brown, J. N. Culver, and R. Ghodssi, Chemical Communications, 50, 12977, (2014). Copyright 2014, Royal Society of Chemistry)

Figure 3-3 shows the TEM image and the schematic of the VLP-TNT receptor used in TNT sensing. Here, a previously identified TNT binding peptide [156] is utilized to genetically modify the TMV coat protein for expression and assembly in *Escherichia coli* (*E. Coli*) cells. This peptide

sequence has been shown to exhibit very high selectivity to TNT versus other competing molecules such as 2,4-dinitrotoluene, demonstrating its suitability for selective TNT sensing in a complex solution. The VLP coat protein gene was modified by PCR-based mutagenesis using a primer that augmented the gene with a bacterially optimized sequence coding for the 12-amino acid 2,4,6-trinitrotoluene (TNT) binding peptide WHWQRPLMPVSI at the C-terminus. The augmented coat protein gene did not produce full-length rods when subcloned into the pET21a bacterial vector and expressed in the BL21(DE3) bacterial expression system, possibly due to steric hindrance between adjacent coat proteins. To compensate for this, an amber stop codon was introduced between the 3' end of the VLP coat protein gene and the coding sequence for the TNT binding peptide. This construct was subcloned into the pET21a expression vector and transformed into the JM109(DE3) bacterial expression system, containing the *supE44* gene, which produces a tRNA that competes with the terminal TAG amber stop codon, allowing random read-throughs of the full, augmented coat protein. This produced a mixture of unaugmented and augmented coat proteins that self-assemble into nanorod structured VLP-TNT agents [166].

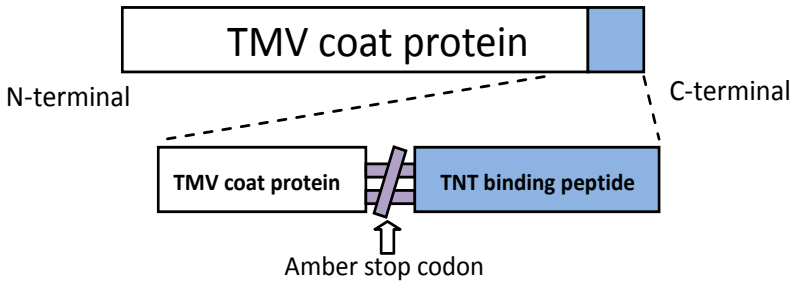

Figure 3-4 TMV coat protein genetic modifications and configuration.

The amino acid sequence of the VLP-TNT coat protein is

MSCYSITTPSQFVFLSSAWADPIELINLCTNALGNQFQTQQARTV
VQRQFSQVWKPSPQVTVRFPDSDFKVYRYNAVLNPLVTALLGAFDTR
NRIIEVENQANPTTAETLDATRRVDDATVAIRSAINNLIVELIRGTGSYN
RSSFESSSGLVWTSGPAT*WHWQRPLMPVSI*

The asterisks indicate stop codons.

3.4 Experimental results

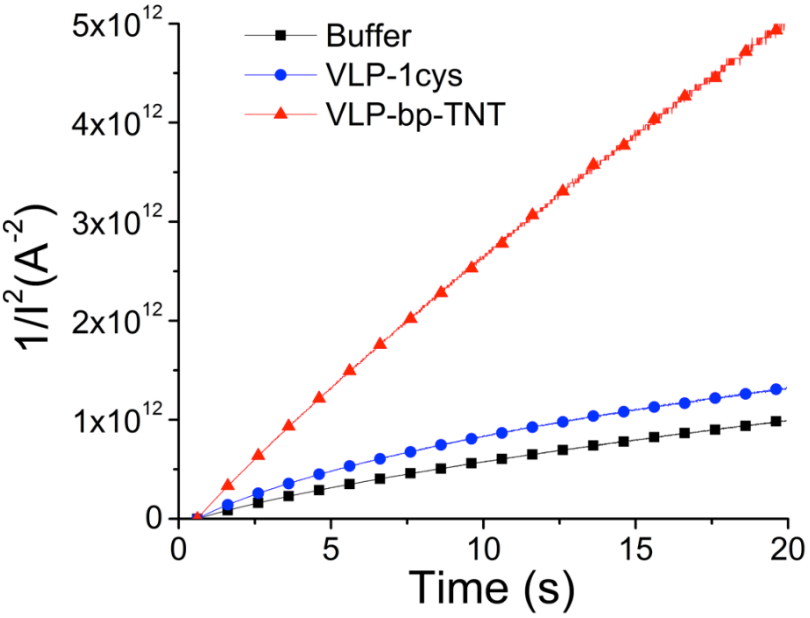

Figure 3-5 Chronoamperometry of 20 µg/mL TNT solution in the presence or absence of VLP-TNT binding agents. [166] (Reprinted with permission from F. Zang, K. Gerasopoulos, X. Z. Fan, A. D. Brown, J. N. Culver, and R. Ghodssi, Chemical Communications, 50, 12977, (2014). Copyright 2014, Royal Society of Chemistry)

The change of diffusion coefficient due to VLP and TNT biological binding was studied using chronoamperometry, where the current response was measured when applying a step potential from 0.2V to -0.6V (Figure 3-5). Faradaic currents from TNT reduction were recorded from 0.6s to exclude the

initial charging effect. The results were analysed using the Cottrell equation, which correlates the Faradaic current i_F, diffusion coefficient D and time t ($\Delta i_F(t) \propto (D/\Delta t)1/2$). The diffusion coefficient is inversely proportional to the change of $1/i_F^2$ over time. The calculated TNT diffusion coefficient in buffer was 5.70×10^{-6} cm^2s^{-1}, in good agreement with previously reported values (6.71×10^{-6} cm^2s^{-1}). The diffusion coefficient of 4.40×10^{-6} cm^2s^{-1} for unmodified VLPs (VLP-1cys) was 4.04 times higher than that of VLP-TNT (1.09×10^{-6} cm^2s^{-1}). This indicates a Faradaic current ratio of 2.01 between control experiments and the bioreceptor VLP-TNT at a 20 µg/mL TNT concentration.

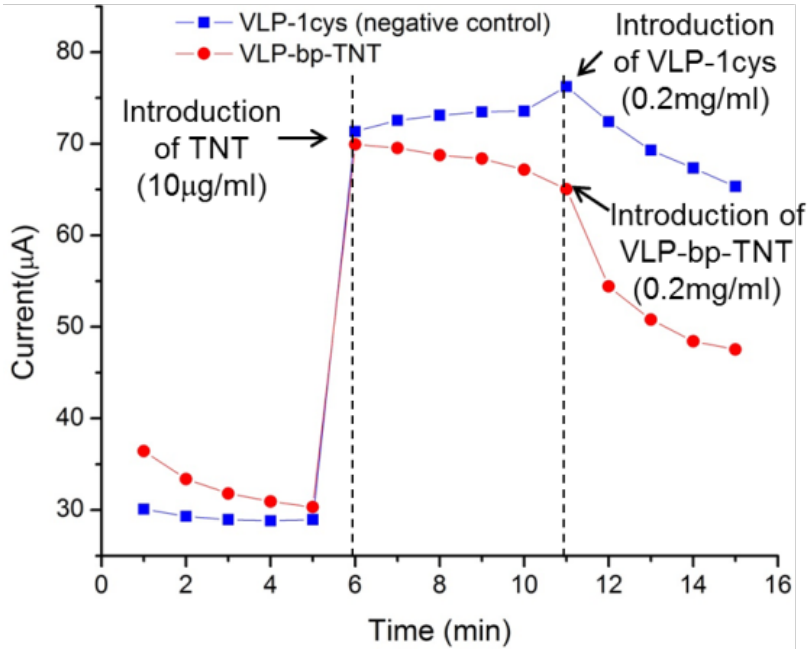

Figure 3-6 Dynamic responses of the peak current with sequential introduction of 10 µg/mL TNT and 0.2 mg/mL VLPs in solution. [166] (Reprinted with permission from F. Zang, K. Gerasopoulos, X. Z. Fan, A. D. Brown, J. N. Culver, and R. Ghodssi, Chemical Communications, 50, 12977, (2014). Copyright 2014, Royal Society of Chemistry)

The dynamics of VLP-TNT binding were studied by monitoring the peak current in response to the sequential introduction of TNT and VLPs in

solution (Figure 3-6). The current decrease for the VLP-TNT was significantly higher compared to the VLP-1cys. In both cases, the currents stabilized after three minutes post introduction of the biomolecules. The instability of the current level in the first 3 minutes is a combination of biological binding and fluidic turbulence. Therefore, in later experiments, the TNT peak current was measured after 3 minutes of stabilization from the introduction of VLPs.

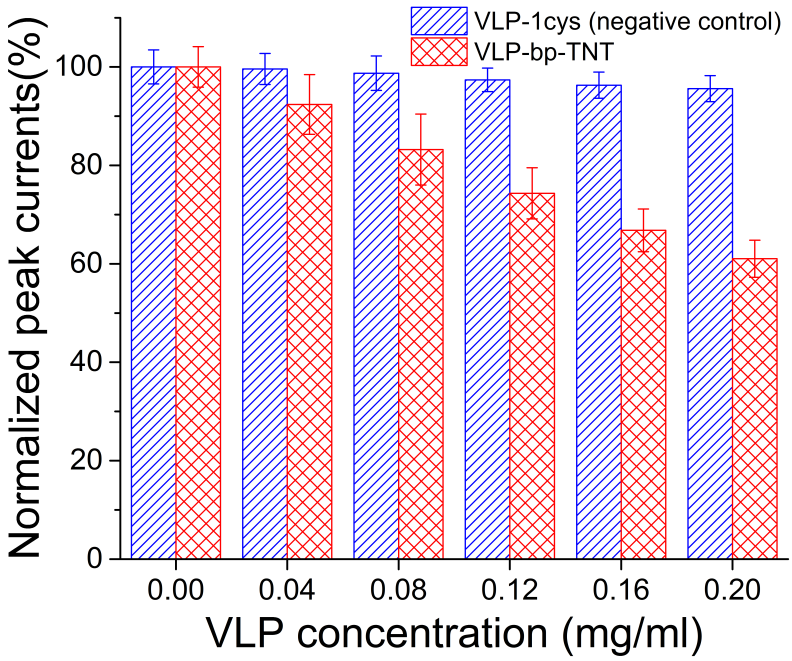

Figure 3-7 Normalized peak currents *vs.* VLP concentration obtained from the reduction of 10μg/mL TNT in solution. [166] (Reprinted with permission from F. Zang, K. Gerasopoulos, X. Z. Fan, A. D. Brown, J. N. Culver, and R. Ghodssi, Chemical Communications, 50, 12977, (2014). Copyright 2014, Royal Society of Chemistry)

The effective diffusion coefficient of the electroactive molecules was controlled by the ratio of bound and free-floating TNTs in solution. The TNT peak current in the presence of increasing concentration of VLPs is shown in Figure 3-7. The current decreases to 61.0% as concentration of the binding agent increases to 0.2 mg/mL. In the control experiment with VLP-1cys, the

peak current is stable with only a 4.4% variation. The strong correlation between the current and binding agent concentration enables tunability of the proposed sensor by adjusting the sensitivity and resolution through the differential current.

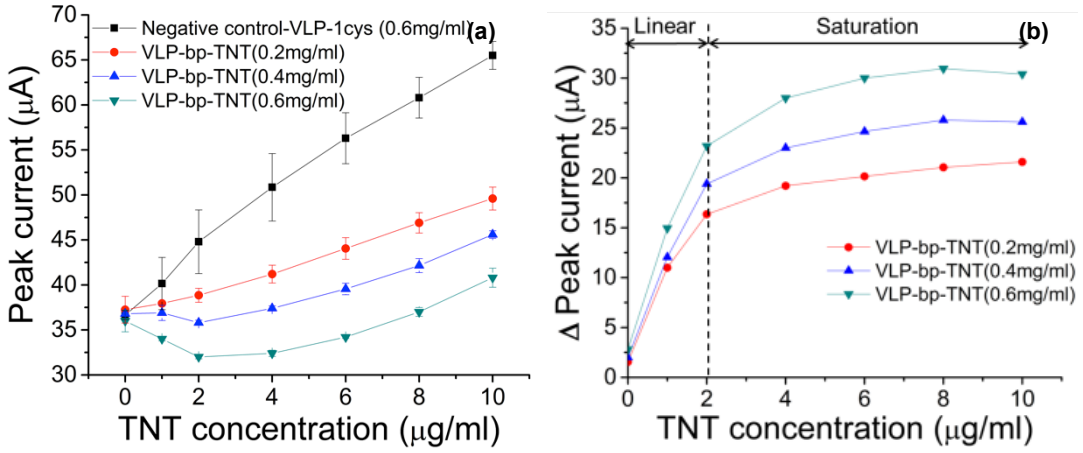

Figure 3-8 (a) Absolute peak currents and (b) differential currents of TNT reduction in the presence or absence of binding agents. [166] (Reprinted with permission from F. Zang, K. Gerasopoulos, X. Z. Fan, A. D. Brown, J. N. Culver, and R. Ghodssi, Chemical Communications, 50, 12977, (2014). Copyright 2014, Royal Society of Chemistry)

The response of the developed VLP-based sensor to increasing concentration of TNT was also studied. Due to TNT and VLP-TNT binding, the otherwise linear response of the current vs. TNT concentration that was observed in the negative control experiments (Figure 3-8a) is modified. The peak currents with VLP-TNT are subtracted from the peak currents of the control (Figure 3-8a), resulting in the differential peak currents (ΔI_{peak}) of Figure 3-8b. The differential current showed saturation when all the peptide binding sites on the VLPs were gradually occupied by TNT molecules. When the concentration of binding agent increased from 0.2 mg/mL to 0.6 mg/mL, the saturation point moved from 2 μg/mL to approximately 4 μg/mL TNT

concentration. The slope of the differential current vs. TNT concentration increases with the concentration of binding agents, indicating an increase in sensor sensitivity. The Faradaic current ratio of VLP-1cys (0.6 mg/mL) to VLP-TNT (0.2 mg/mL) is 2.03. This matches well with the Faradaic current ratio calculated from the Cottrell equation in Figure 3-5, which validates that the nonlinearity in the current is due to the difference in diffusion coefficient between the two systems.

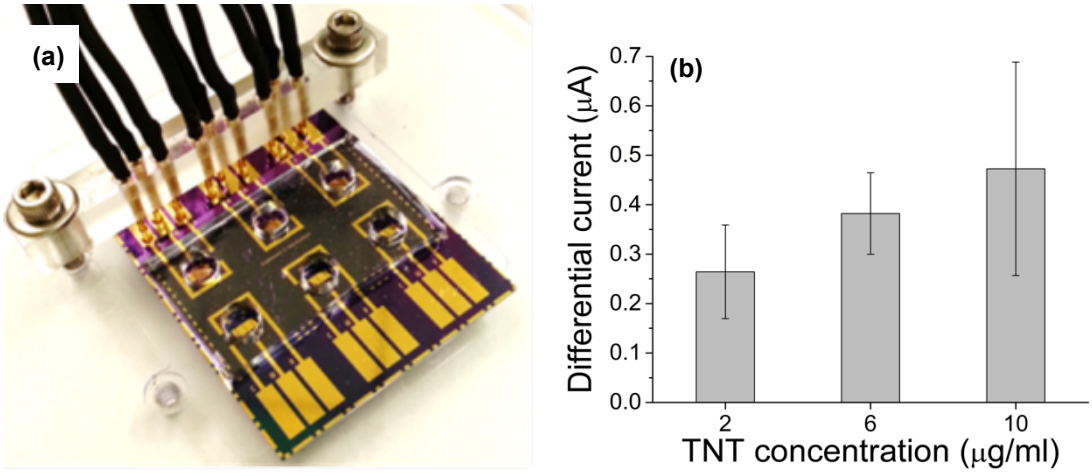

Figure 3-9 (a) Optical image of on-chip electrochemical sensor, and (b) differential currents for varying concentrations of TNT. [166] (Reprinted with permission from F. Zang, K. Gerasopoulos, X. Z. Fan, A. D. Brown, J. N. Culver, and R. Ghodssi, Chemical Communications, 50, 12977, (2014). Copyright 2014, Royal Society of Chemistry)

Field applications outside laboratory settings require sensors that are portable and compatible with limited amount of reagents without compromising fast response and high selectivity. The feasibility of applying the VLP-based TNT sensing method in miniature sensors was investigated through the development and characterization of an on-chip electrochemical sensor. Gold working, counter and pseudo reference electrodes integrated with 30 μL Polydimethylsiloxane (PDMS) reaction chambers were microfabricated

forming a sensor array (Figure 3-9a). An interdigitated electrode geometry optimized in previous work [169] (50 μm finger width and spacing) was selected. The differential current between sensors in the presence of VLP-TNT and the control VLP-1cys was measured for varying concentrations of TNT (Figure 3-9b). As in the case of the experiments in bulk solution (Figure 3-8b), the differential current increases with TNT concentration. A clear saturation was not observed, suggesting that the linear region can be extended in a microscale sensor. These results demonstrate that the developed sensing method is applicable for microscale sensors for low-volume TNT detection.

A differential sensing method using genetically modified macromolecules as binding agents for selective chemical sensing in aqueous environments was developed. The free-floating, suspended VLPs modulated the effective diffusion coefficient of the target TNTs within 3 minutes and contributed to unique differential current signatures that are proportional to TNT concentration. The genetically modified VLP bioreceptors were successfully tested in both beaker-scale and on-chip electrochemical sensors. This sensing method enables rapid label-free detection of TNT and can be expanded to a variety of electroactive species that have great size contrast with the programmable biologically engineered receptor macromolecules.

3.5 Chapter summary

This chapter focused on the development of VLP-based selective TNT sensor. The VLP binding agent is created by genetically modifying the VLP coat protein and expressing a 12 amino acid-long TNT binding peptide

sequence on its outer surface. Electrochemical sensor was adopted to detect the TNT molecule in solution by quantifying its characteristic electrochemical reduction current peaks. The use of VLP binding agent improves the conventional TNT electrochemical sensing method and avoids the influence of interfering species and background. This improved method quantifies the TNT concentration by the measuring the effect of diffusion modulation in the selective binding of VLP binding agent and the target TNT molecules. The binding creates a much larger particle compared to the target TNT, significantly lowers the TNT diffusion coefficient in the system and generates a differential current. This differential current only relates to the presence of (1) target TNT molecule and (2) VLP binding agent.

The method has been proved to be effective in both bulk sensor setups as well as in microfabricated sensor arrays. Therefore, the method is independent of any interfering species and environmental background signals, making it extremely desirable for directly quantify the TNT level in a blind sample. More importantly, this is a rapid method that does not need any sensor surface functionalization or VLP assembly process. With proper peptide modifications, the genetically modified VLPs are promising sensing probes or binding agent in detecting small electrochemically active molecules similar to TNT.

Chapter 4: VLP integration in impedance biosensor for antibody sensing

Selective and sensitive detection of pathogens are crucial steps in identifying sources of disease outbreaks and forming effective strategies to ensure public health and food safety [53, 170]. Among the most effective and widely used biosensing methods nowadays are immunoassays, such as enzyme-linked immunosorbent assays (ELISA), which are implemented to sense specific types of pathogens based on receptor-target interactions. This section explores and studies the feasibility of using self-assembled VLP layers on impedance microsensors as transduction layers.

Dr. Konstantinos Gerasopoulos and Dr. Xiao Zhu Fan contributed to the discussion, and provided help in the VLP-FLAG purification in this work.

4.1 Impedance sensor design and fabrication

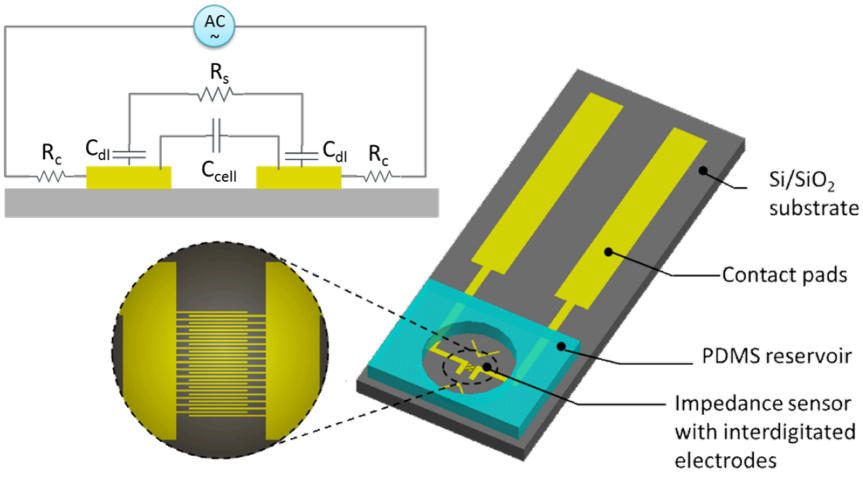

Figure 4-1 Schematic of the impedance microsensor [157] (Reprinted with permission from F. Zang, K. Gerasopoulos, X. Z. Fan, A. D. Brown, J. N. Culver, and R. Ghodssi, Biosensors and Bioelectronics, 81, 401, (2016). Copyright 2016, Elsevier)

Figure 4-1 shows a schematic of the impedance microsensor comprised of gold IDMEs, contact pads and a PDMS reaction chamber. In the fabrication process, a 500 nm thick SiO_2 layer was fabricated using plasma enhanced chemical vapour deposition (PECVD) (Plasmalab System 100, Oxford Instruments) on a 500 μm thick silicon wafer. A 1.6 μm thick layer of Shipley 1813 positive photoresist was spin-coated and patterned via photolithography to form contact pad and impedance sensor patterns. The exposed SiO_2 area after the photolithography was isotropically wet-etched in buffered HF to form 200 nm undercuts under the photoresist. Cr/Au (200Å/1400Å) layers were then deposited on a SiO_2/Si substrate using e-beam evaporation (EXPLORER 14, Denton Vacuum), and were lifted off in acetone to pattern contact pads and IDMEs with 2 – 8 μm finger width and spacing. Compared with the conventional one-step lift-off process, this process creates a SiO_2 barrier step between the neighbouring electrodes. Such barriers have been shown to provide higher sensitivity compared to coplanar electrodes [171]. Previously reported research has revealed that 95% of the effective electric fields and currents of IDMEs are concentrated above the electrode surface within a distance equivalent to an electrode spacing plus half of an electrode width [172]. Thus, in order to maintain high sensitivity in monitoring probe assembly and ELISA, the minimum width and spacing of the IDMEs were designed to be 2 μm, comparable with VLP layer thickness. The effective sensing area of the IDME

is 2 mm × 2 mm. The impedance sensors were cleaned with 10 minutes of O_2 plasma at 150 W to remove organic residues. A 3 mm-thick Polydimethylsiloxane (PDMS) with a 30 μL cavity was fabricated separately and attached to the sensor substrate as the reaction chamber. During VLP self-assembly on the impedance sensor, as well as the on-chip ELISA experiments, an additional layer of PDMS is temporarily attached on the PDMS reaction chamber to seal the cavity, therefore, preventing the 30 μL liquid sample from rapid evaporation, and maintaining constant analyte concentration and ionic strength. The reaction chamber and cover layer were used throughout the VLP self-assembly on the impedance sensor as well as the on-chip ELISA experiments.

Electrical impedance spectroscopy was performed using an electrochemical workstation (CHI660D, CH Instruments, TX). The excitation used a 50 mV amplitude of alternating current (AC) signal in the frequency range of 10 Hz – 1 MHz. Parallel experiments to monitor the impedance evolution on multiple microsensors were achieved by connecting the sensor electrodes to the CHI660D electrochemical workstation through a multiplexer (CHI684, CH Instruments, TX). The equivalent electrical circuit of the designed impedance microsensor while monitoring VLP self-assembly and immunoassays is shown in Figure 4-1. This circuit has been widely used for describing the biomedical impedance spectroscopy model in literature [173-175]. In this model, R_c represents the parasitic and contact resistance between the potentiostat and the contact pads of the impedance sensor, C_{cell} is the direct

capacitive coupling between the IDMEs, R_s represents the solution resistance between the electrodes, and C_{dl} is the double layer capacitance on the electrode/electrolyte interface. During electrical impedance spectroscopy, the conduction current will propagate through R_s and the displacement current will propagate through C_{cell}; therefore, the R_s and C_{cell} components are connected in parallel. The solution resistance R_s is connected in series with the interfacial capacitance C_{dl} of the two electrodes. The interfacial capacitance C_{dl} contributes primarily to the total impedance of this equivalent circuit when the operating frequency is below F_{low}, where the total impedance Z, critical cut-off frequency F_{low} and interfacial capacitance C_{dl} can be expressed as,

$$Z \approx R_s - j\frac{2}{\omega C_{dl}} \qquad (1)$$

$$F_{low} \approx \frac{1}{\pi \cdot R_s \cdot C_{dl}} \qquad (2)$$

$$C_{dl} \approx \frac{\varepsilon_r \varepsilon_0 A}{d} \qquad (3)$$

In equation 3, ε_r is the relative dielectric constant of the media directly in contact with the electrode surface and A is the area of the electrode that is directly in contact with the ionic solution. In the frequency range lower than F_{low}, the total impedance increases with decreasing frequency. The decrease in dielectric constant ε_r and effective electrode area A during biological molecule binding on the surface results in the reduction of C_{dl} value, which can also induce the increase in impedance.

4.2 Impedimetric ELISA procedure

The VLP sensing probes (VLP-FLAG) are synthetized by the helical arrangement of thousands of genetically modified and identical TMV coat proteins inside *Escherichia coli* bacterial cells. Each coat protein produced expresses a cysteine residue that promotes surface attachment and a FLAG-tag sequence (DYKDDDDK) that enables selective binding with the target anti-FLAG antibody. The genetic modification, culture and purification procedures were reported in detail previously [154]. The purified VLPs were diluted and suspended in deionized (DI) water at a concentration of 0.2 mg/mL. This VLP stock solution was used in the surface functionalization of the impedance sensors.

After the VLP-FLAG sensing probes were self-assembled on the impedance sensor surface, on-chip ELISA was performed to validate the VLP probe efficacy in sensing the target anti-FLAG antibodies. Determining factors such as IDME geometries and VLP concentrations used in sensor functionalization were studied in order to achieve better sensing performance in the ELISA process.

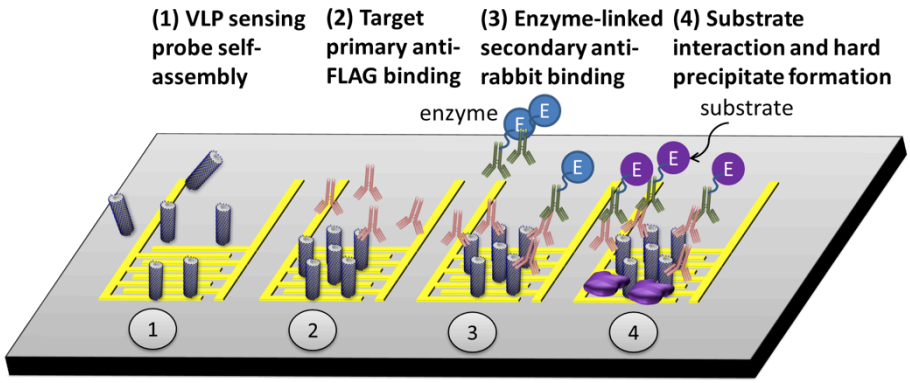

Figure 4-2 Schematic of the procedure of sandwiched on-chip ELISA using VLP-FLAG [157] (Reprinted with permission from F. Zang, K. Gerasopoulos, X. Z. Fan, A. D. Brown, J. N. Culver, and R. Ghodssi, Biosensors and Bioelectronics, 81, 401, (2016). Copyright 2016, Elsevier)

Sandwiched ELISA (Figure 4-2) was used as a model system to investigate the sensing efficacy of assembled VLP-FLAG sensing probes to anti-FLAG antibody targets. In the process, VLP-FLAG sensing probes were introduced in the reaction chamber and self-assembled on the impedance sensor surface. After washing off excessive VLPs on the device using buffer solution, a Tris-buffered saline (TBS) (1X) solution containing 12 ng/mL – 1.2 μg/mL of target primary anti-FLAG IgG antibodies, produced from rabbit (dilution of F7425, Sigma-Aldrich) was introduced in the reaction chamber. A 1:10000 dilution of Goat anti-Rabbit IgG (whole molecule)-Alkaline Phosphatase antibody (A3687, Sigma-Aldrich) was subsequently introduced in the reaction chamber. In the final step, the nitro-blue tetrazolium chloride and 5-bromo-4-chloro-3'-indolyphosphate p-toluidine salt (NBT/BCIP) substrates (Fischer Scientific) were added into the chamber for interaction with the enzyme on the secondary antibody, producing dark-purple insoluble precipitates on the surface. Between all steps, the devices surfaces were washed 3 times using TBS and one time using TBS with 0.05% Polyoxyethylene (20) sorbitan monolaurate (Tween 20) buffer solutions. The impedance changes were continuously monitored during these experiments.

4.3 Experimental results

4.3.1 VLP assembly on impedance sensor

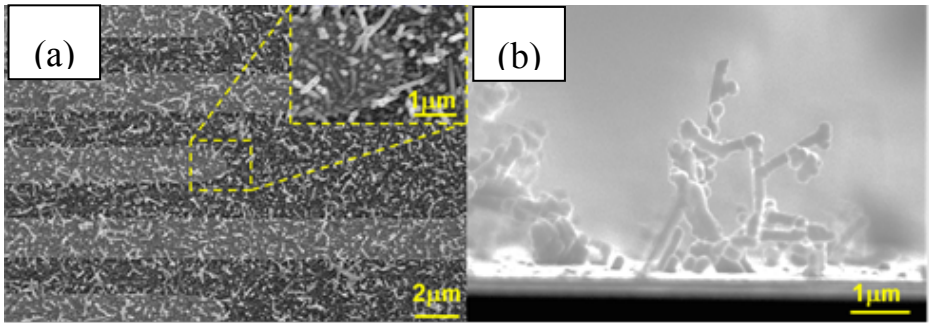

Figure 4-3 Scanning electron microscopy (SEM) images of the (a) top-down and (b) cross-sectional views of self-assembled VLP layer on IDMEs. [157] (Reprinted with permission from F. Zang, K. Gerasopoulos, X. Z. Fan, A. D. Brown, J. N. Culver, and R. Ghodssi, Biosensors and Bioelectronics, 81, 401, (2016). Copyright 2016, Elsevier)

Figure 4-3a shows the SEM image showing the impedance sensor surface after functionalization using 18-hour self-assembly of VLP-FLAG at a concentration of 0.2 mg/mL. Before SEM imaging, the surface was pre-treated with one hour palladium activation and 4 minutes nickel electroless plating to enhance the contrast in SEM. The nanorod shaped VLPs (white particles in Figure 4-3a) uniformly cover the impedance sensor surface, forming a functional layer. The cross-sectional SEM image (Figure 4-3b) shows that the VLPs are quasi-vertically aligned on the electrode surface due to the interaction between the sensor surface and exposed cysteines at the end of each VLP rod. The average length of each VLP is about 1 μm, and the maximum VLP layer thickness reaches around 3-4 μm due to stacking of VLPs. Impedance sensors with IDME features of 2 μm and 8 μm (two times the lengths of a single VLP and the maximum VLP layer thickness, respectively) were utilized.

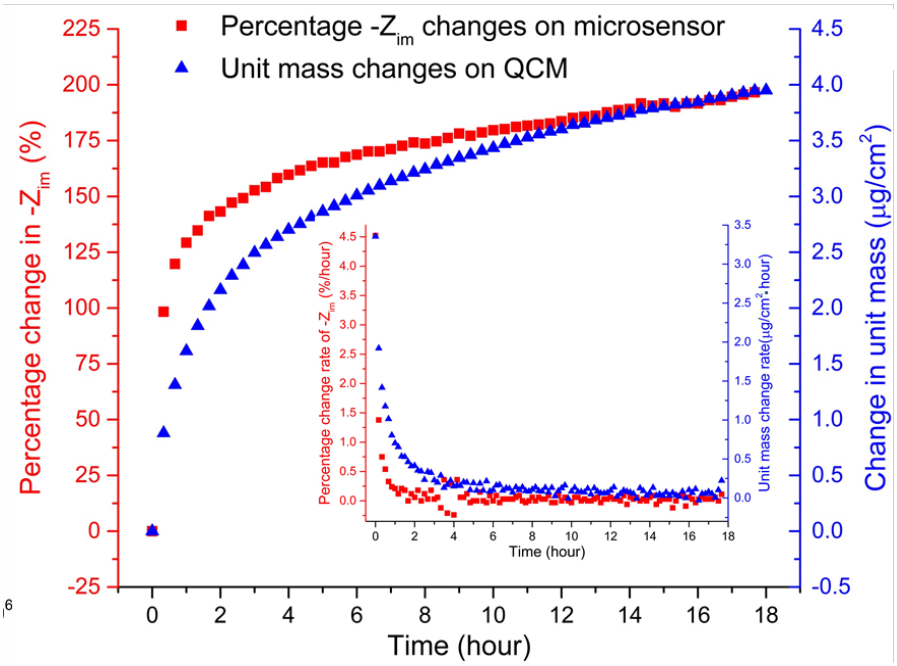

Figure 4-4 Real-time impedance and mass loading measurement using the developed impedance microsensor. [157] (Reprinted with permission from F. Zang, K. Gerasopoulos, X. Z. Fan, A. D. Brown, J. N. Culver, and R. Ghodssi, Biosensors and Bioelectronics, 81, 401, (2016). Copyright 2016, Elsevier)

The imaginary part of the complex electrical impedance on a sensor with 8 μm electrode feature size, was measured to analyse the VLP self-assembly dynamics over an 18-hour duration. Figure 4-4 shows the impedance (red squares) changes detected by the designed impedance microsensor during VLP self-assembly. The impedance amplitude trends reflected the rapid attachment of VLP sensing probes to the surfaces in the initial 3 hours followed by a gradual increase of attachment throughout the 18 hours of self-assembly. These results show that the impedance sensors are capable of real-time monitoring of VLP sensing probe self-assembly on the transducer surfaces of a more compact platform. The impedance change reveals that the first 3 hours during VLP self-assembly is the most critical period to saturate a sensor surface.

4.3.2 Detection of antibodies using on-chip ELISA

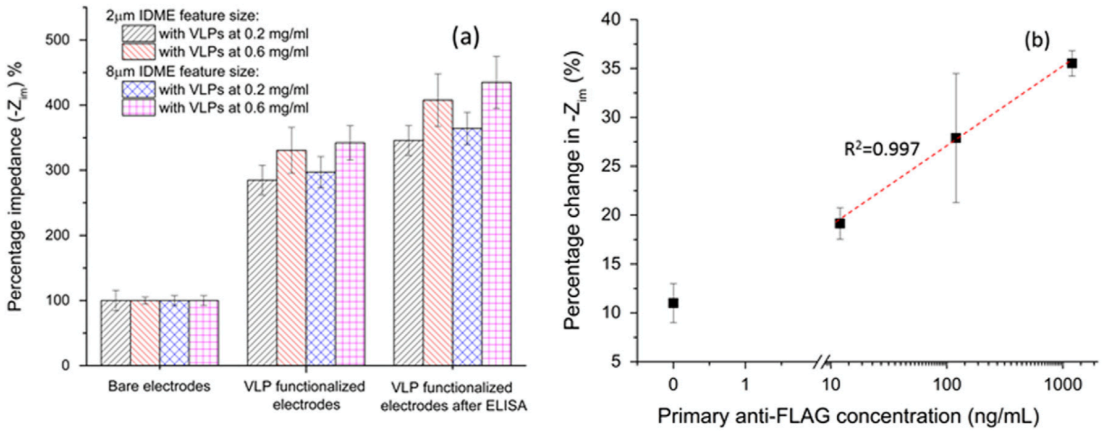

Figure 4-5 Percentage impedance change $-Z_{im}$ % (a) during VLP self-assembly and ELISA process, and (b) after ELISA process with different target primary antibody concentrations. The error represents the standard deviation of the mean (n=3) [157] (Reprinted with permission from F. Zang, K. Gerasopoulos, X. Z. Fan, A. D. Brown, J. N. Culver, and R. Ghodssi, Biosensors and Bioelectronics, 81, 401, (2016). Copyright 2016, Elsevier)

Figure 4-5a shows the changes of the imaginary part of the electrical impedance observed using different IDMEs functionalized by VLPs at different concentrations. The impedance increases significantly during the VLP assembly process due to both the decrease in direct electrode/electrolyte interfacial area and the lower effective dielectric constant, as discussed previously in section 4.1. The slight decreases in the impedance during both antibody binding steps may be attributed to the disassociation of the non-specifically bound VLPs on the sensor surface (through bonds other than thiol-gold), and diffusion into the Tris-buffer during the testing. The sensor responses in the full ELISA also showed that the largest overall impedance shifts are from experiments using the IDMEs with 8 μm feature size and 0.6 mg/mL concentration VLPs.

In order to understand the determinant factors influencing the sensing efficacy such as VLP concentrations and electrode geometric parameters, two-way analysis of variance (ANOVA) is utilized to analyse the statistical significance of the data sets in Figure 6a. The ANOVA test shows that VLP concentration is the only major source of variation ($F=15.72>F_{crit}$, $p=0.0041<0.05$) that controls the percentage impedance level after ELISA process. The test also shows that, regardless of electrode feature size, all impedance sensors response similarly as the VLP concentration increases. These analytical results indicate that VLP concentration is the dominant factor for the VLP-based impedance biosensor performance. A higher VLP concentration will contribute to enhanced impedance sensor responses in the immunoassay.

Table 4-1 Percentage changes in capacitive impedance during sensor surface functionalization and ELISA process

Percentage impedance changes (Δ-Z_{im}%)	2 µm electrode features		8 µm electrode features	
	0.2 mg/mL VLP-FLAG	0.6 mg/mL VLP-FLAG	0.2 mg/mL VLP-FLAG	0.6 mg/mL VLP-FLAG
In VLP assembly	185%	231%	197%	242%
In ELISA	21%	23%	22.62%	27%

Table 4-1 summarizes the percentage impedance changes in the VLP assembly and the ELISA processes. In VLP assembly, the relative changes of impedance (imaginary part) amplitudes measured were compared between VLP functionalized IDMEs and bare IDMEs. In the ELISA, the relative changes in

imaginary impedance were compared between measurements after VLP self-assembly (step 1 described in section 4.2) and after precipitate formation (step 4 described in section 4.2). Both sensor designs show high sensitivity to VLP attachment on the surface, measuring up to about 240% increase in imaginary impedance using 8 μm IDMEs and 0.6 mg/mL VLP concentration. However, compared with the 8 μm feature size sensors, those with finer electrode features of 2 μm do not show higher impedance shifts during the ELISA process, and it showed less VLP-FLAG concentration dependency. This may be attributed to the saturation of the effective sensing area by the dense VLP layer, which degrades the sensor performance during the immunoassay.

Figure 4-5b shows the total percentage of imaginary impedance amplitude change in the ELISA process when different concentrations of anti-FLAG antibody were used. Sensors with 8 μm electrode width and spacing functionalized by 0.6 mg/mL VLP-FLAG sensing probes were used in this study. Tris-buffer solution with no anti-FLAG was introduced as the control in the ELISA. In the control experiment, the impedance change was 12% due to non-specific binding of secondary antibody and precipitate formation on the sensor. In the sensing experiments, the impedance sensors detected 19%, 28% and 36% of total impedance increases after the entire ELISA procedure when 12 ng/mL, 120 ng/mL and 1200 ng/mL of target anti-FLAG primary antibody were used, respectively. The error bars in Figure 4-5b represent the standard deviation of the results from three independent experiments using newly functionalized sensors at identical conditions. Based on the linear correlations

(R^2=0.997) between the percentage impedance change and antibody concentration (log scale), the sensitivity of the VLP functionalized microsensor can be calculated as 8.7% of the total impedance per magnitude of antibody concentration (ng/mL). The detection limit of target antibody for the on-chip impedimetric ELISA is 9.1 ng/mL.

4.4 Chapter summary

The study in this chapter explored the VLP as sensing probes in an affinity-based biosensor whose transduction mechanism relies on binding of target molecules onto immobilized sensing probes of a transducer. The transducers used in this study were impedance microsensors, which detected the complex electrical impedance shifts on the interdigitated electrode due to biological molecule binding. An antigen-antibody binding model system was utilized to evaluate the biosensing efficacy of the VLPs. Each VLP coat protein was genetically modified with an 8 amino acid-long FLAG-tag peptide and a cysteine residue. These modifications enabled selective binding with the target anti-FLAG IgG and promoted surface assembly on gold electrodes.

The impedance sensor detected the complex electrical impedance changes on the electrode surface during biological binding. By real-time monitoring of the impedance at 100 Hz, the dynamics of VLP self-assembly was studied revealing the saturation on the surface in 3 hours. On-chip immunoassay process was performed on the VLP-functionalized impedance sensor in order to quantify the concentration of the target anti-FLAG IgG. The impedance sensor functionalized through VLP self-assembly can detect the

presence of 9.1 ng/mL targets using the full ELISA process. This work revealed VLP self-assembly dynamics and demonstrated the potential of VLPs as immobilized sensing probes in affinity-based sensors.

Chapter 5: Microsystem solution for controlled and accelerated VLP integration and biosensing on-chip

In this chapter, a microsystem solution is developed for accelerated VLP sensor functionalization and performance-enhanced VLP-based biosensing. Capillary microfluidic devices – capillary micropumps and stop valves – are utilized to achieve autonomous VLP assembly directly on impedance microsensor surface. With the dense VLP coverage, the impedance sensor is able to detect the presence of target antibody label-free.

Dr. Konstantinos Gerasopoulos contributed to the discussion of the capillary microfluidic design and microfabrication. Mr. Adam D. Brown contributed to generating the model and purification protocol of the VLP-FLAG receptors.

5.1 Microsystem design

The integrated sensing microsystem is composed of capillary microfluidics and an impedance sensor, aiming at autonomous liquid sample delivery, receptor localization, accelerated sensor functionalization, and real-time label-free sensing of target molecules.

The three main **modules** and their functions are:

Sensing module: impedance sensing to monitor VLP sensing probe assembly and the target antibody binding on the VLP receptor layer.

Control module: confining the VLP solution to the sensing module area during assembly and triggering flow in antibody sensing process

Venting module: withdrawing the liquid from the sensing and control modules to wash unbound target molecules on impedance sensor

The three main **components** of this LOC system are:

Impedance sensor: the impedance between microscale interdigitated electrodes will be continuously monitored during the VLP self-assembly and target molecule binding processes. The impedance change will be used to evaluate the quality of the self-assembled VLP receptor layer and quantify the concentration of target molecules.

Capillary microfluidics: capillary microfluidics created by micropillar structures using hydrophilic materials will be used to autonomously deliver the VLP and target molecules in the system. Capillary stop valves will be used in the control module to limit the VLP solution in the sensing area.

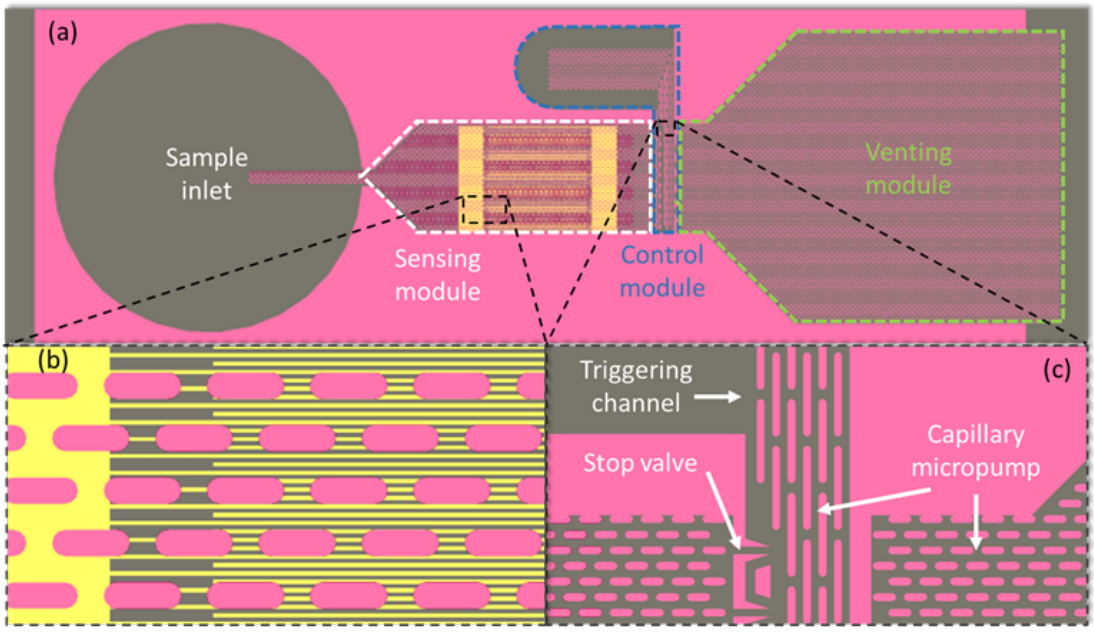

Figure 5-1 Schematic of the capillary microfluidics and impedance sensor-integrated sensing microsystem. (a) The top-down view of the microsystem design showing three main modules: sensing, control and venting. The exploded views show the (b) interdigitated electrode of the

impedance sensor in the sensing module and (c) the details of the stop valve and triggering channel designs in the control module.

Figure 5-1 shows the schematic of the integrated sensing microsystem. According to the different functions, the system components can be catalogued into three essential modules: sensing, control and venting. An impedance sensor and a capillary micropump comprise the sensing module. The impedance sensor spans a 4 mm × 4 mm area with interdigitated electrodes in 4 μm width and spacing. The capillary micropump in the sensing module can autonomously deliver the VLP-containing solution onto the impedance sensor through capillary action. Owing to its large micropump area and open top surface, the micropump will rapidly evaporate the VLP-containing solution, and enhance the attachment of VLPs to the impedance sensor surface through both thiol-gold interactions and van der Waals forces. The control module contains capillary stop valves and a triggering micropump with the channel direction perpendicular to the sensing and venting micropumps. During the sensor functionalization with VLPs, the stop valves can confine the VLP solution to the left sensing module due to the local energy barrier induced by the sharp change in the sidewall geometry. During antibody sensing, a triggering fluid will be introduced from the triggering channel in the control module. This triggering fluid will mix with the test antibody sample and break the liquid/air interface at the stop valves, and will eventually induce continuous flow through the VLP functionalized impedance sensor. The large capillary micropump in the venting module will provide the major capillary force to

keep the antibody test sample flowing during sensing. The detailed principle of operation of the sensing microsystem is included in the supplementary material.

5.2 Capillary microfluidics sub-system

The LOC sensor system is designed toward on-site sensing applications. The portability and the convenience in operation are important. To achieve this, the complex external tubing and pumping setups for conventional microfluidics need to be eliminated. Here, autonomous open-channel capillary microfluidics is proposed to accomplish VLP sample delivery in the self-assembly process as well as the transfer of test samples to the active sensing area in the LOC system. The liquid in the reservoir will be automatically driven into microfluidic channels due to one-directional capillary force.

As shown in Figure 5-1c, the two major types of capillary microfluidic components are capillary pumps and capillary stop valves, which are responsible for generating autonomous flow in the channels and limit the liquid passively in certain areas, respectively. In the following sections, the detailed analysis on the capillary force generation and stop valve design will be discussed.

5.2.1 Capillary microfluidic channel design and simulation

The calculation of the designed open channel capillary microfluidics is based on the following model:

With XY as the substrate plan, the open microfluidic channel is created along the X direction. The width and depth of the open microfluidic channel

are w and d, respectively. The meniscus of the flow advances along the +X direction (Figure 5-2). Gravity and the initial transit phenomena when the flows first enter the channel are neglected.

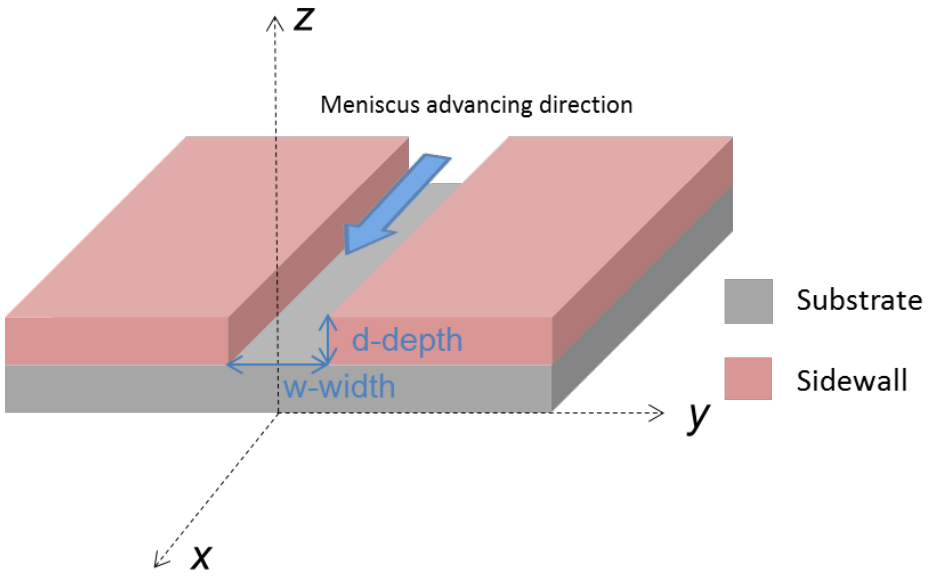

Figure 5-2 3D schematic of the open microcapillary with the definition of parameters

The capillary force is due to the change of interface free energy E along the microfluidic channel experienced by the moving fluidic meniscus. Figure 5-3 shows the analysis of the interface free energy changes that are considered in the calculation. A is the interface area, γ is surface tension. E_1 is the surface energy between liquid/air interfaces on the top of the microfluidic channel. As the meniscus of flow advances in the channel, the initial solid/air interfaces on the substrate and sidewall are changed to solid/liquid interfaces. The changing energy ΔE in this process equals to the sum of E_2 and E_3 on the substrate and sidewalls, respectively.

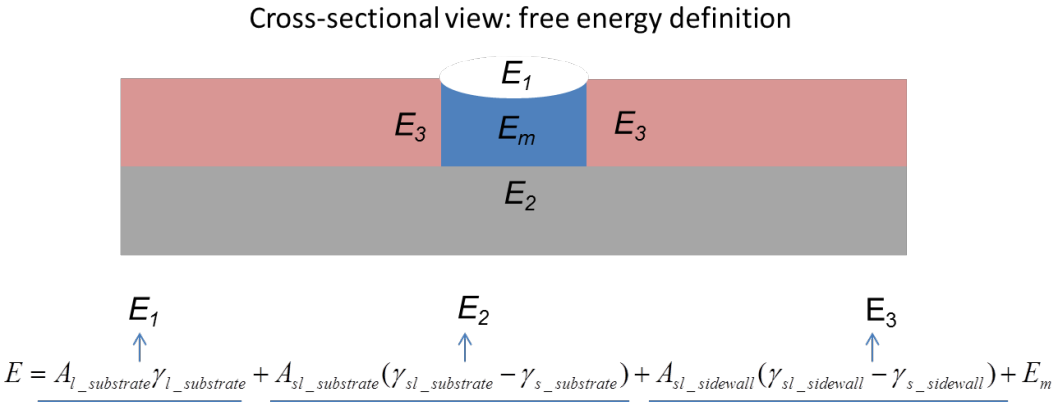

Figure 5-3 Cross-sectional schematic of the microcapillary with free interfacial energy definitions

The surface tensions between the interfaces of solid, liquid and air can be correlated using Young's equation, which is expressed as

$$\gamma_{\text{sl\_substrate}} - \gamma_{\text{s\_substrate}} + \gamma_{\text{l\_substrate}} \cos\theta_{\text{substrate}} = 0 \qquad (1)$$

Where, $\theta_{\text{substrate}}$ is the contact angle of substrate (defined in Figure 5-4).

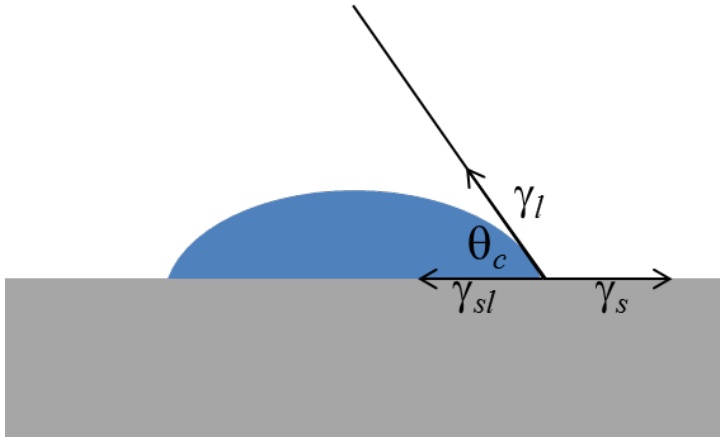

Figure 5-4 Contact angle and the surface tensions of a drop of liquid on solid substrate

Therefore, the change of free energy can be rewritten as,

$$\Delta E = A_{\text{l\_substrate}} \cdot \gamma_{\text{l\_substrate}} - A_{\text{sl\_substrate}} \cdot \gamma_{\text{l\_substrate}} \cos\theta_{\text{substrate}} - A_{\text{sl\_sidewall}} \cdot \gamma_{\text{l\_sidewall}} \cos\theta_{\text{sidewall}} + E_{\text{m}}$$

$$(A_{\text{l\_substrate}} = A_{\text{sl\_substrate}} = wx = dx/p, A_{\text{sl\_sidewall}} = 2dx) \qquad (2)$$

In which, the w and d are width and depth of microfluidic channel. The p is the microfluidic channel aspect ratio equalling to d/w.

And, capillary force can be calculated as,

$$F_\gamma = -\frac{\mathrm{d}E}{\mathrm{d}x} = d\left[2d\gamma_{\mathrm{l\_sidewall}}\cos\theta_{\mathrm{sidewall}} - \frac{1}{p}\gamma_{\mathrm{l\_substrate}}\left(1-\cos\theta_{\mathrm{substrate}}\right)\right] \quad (3)$$

To ensure the liquid can automatically flow in the capillary microfluidics, the capillary force expressed in equation (3) needs to be positive.

Using Matlab simulation, the influence of aspect ratio (channel depth/width (p)), sidewall contact angle, and substrate contact angle on the capillary force can be evaluated.

Aspect ratio (microfluidic channel depth/width)

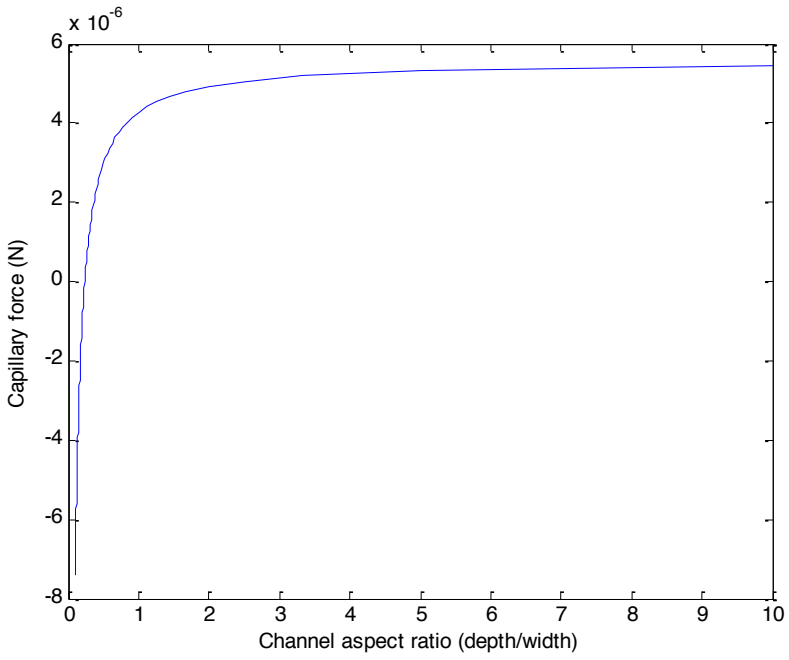

Figure 5-5 Capillary forces vs. the aspect ratio (depth/width) of the microfluidic channel

At constant contact angles of the sidewall and substrate material, the capillary forces can be calculated with respect to the change of aspect ratio

(depth/width, p in the equation). From Figure 5-5, the capillary force is decreased to 0 at the aspect ratio of 0.236 (depth/width). The force shows a dramatic increase when the aspect ratio increases from 0 to 1. Therefore, the microfluidic channels on the chip need to maintain an aspect ratio of greater than 0.236 to ensure one way flow. The capillary force then gradually reaches a saturated level as the aspect ratio increases further beyond 2~3. It can be concluded that a higher aspect ratio will result in a larger capillary force to keep the advancing of flow. And the aspect ratio of around 2 to 3 is optimized considering the difficulty in fabricating high-aspect-ratio structures using photolithography on the KMPR photoresist.

Sidewall contact angle

To study the effect of sidewall contact angle on the capillary force, SiO_2 (contact angle: 50^o) is used as substrate material in the calculation. Water is used as liquid sample. Two aspect ratios of microfluidic channel (depth/width), 1 and 2, are studied in the calculation.

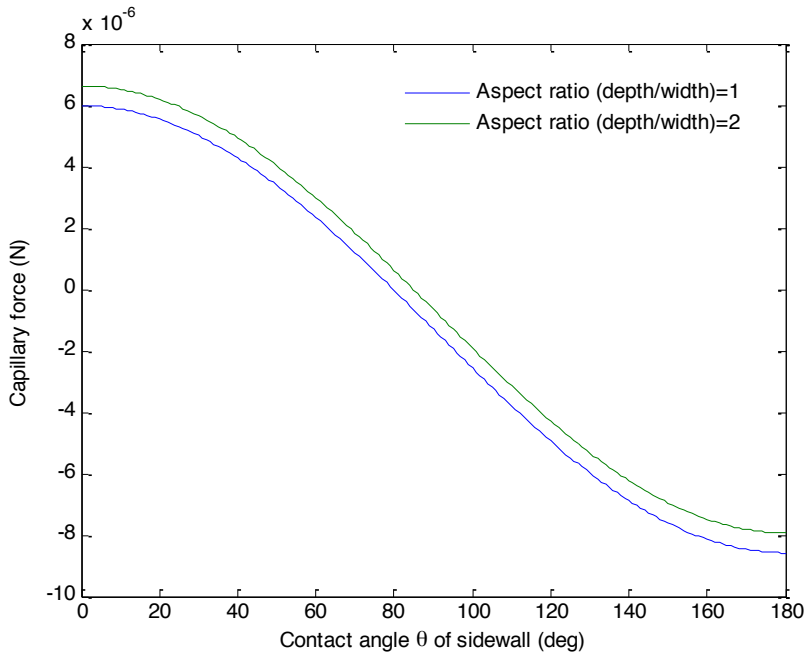

Figure 5-6 Capillary force vs. the contact angle of sidewall material with different aspect ratios

From the results in Figure 5-6, capillary force is positive if the contact angle of microfluidic sidewall $\theta_{l\_sidewall}$ is lower than 80^o for aspect ratio of 1. If the aspect ratio is increased to 2, capillary force can be positive for contact angle lower than 85^o

Substrate contact angle

Use 1:1 aspect ratio for microfluidic channel geometry and O_2 plasma treated KMPR as sidewall material (fixed contact angle $\theta_{l\_sidewall}=40^o$), the relation of capillary force and substrate material contact angle is studied.

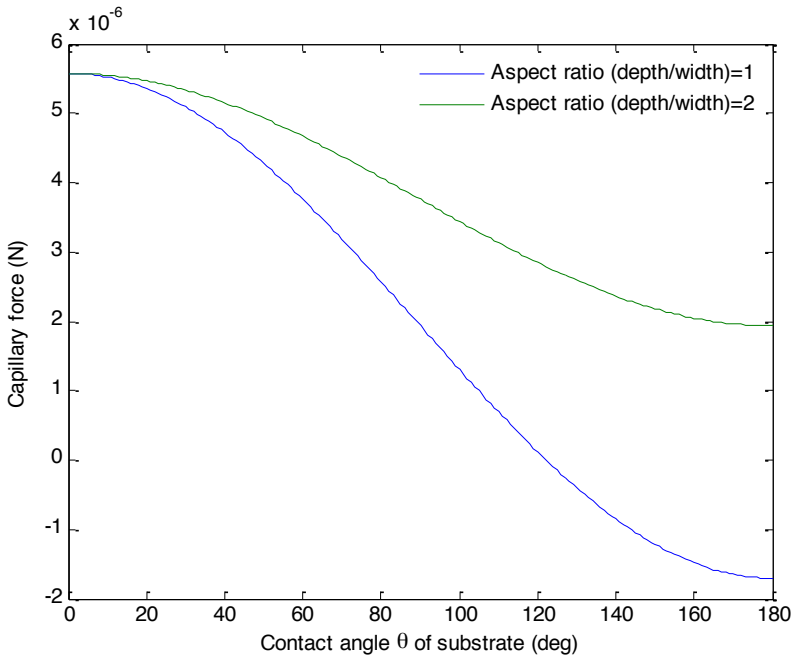

Figure 5-7 Capillary force vs. the contact angle of substrate material with different aspect ratios

When the contact angle of substrate is larger than 123^{o}, the capillary force is around 0 for aspect ratio of 1. If the aspect ratio increases to 2, the capillary force will always be positive no matter what the contact angle is for the substrate (Figure 5-7).

The Matlab simulation results indicated that aspect ratio and sidewall contact angle are the two most important factors that determine the capillary force in a capillary microfluidic device. The sidewall need to be higher than 0.236 and the sidewall contact angle should be smaller than ~80^{o} to ensure a positive capillary force as the driving force. Therefore, achieving a higher aspect ratio around 2-3 and selecting more hydrophilic sidewall material are favourable for device function.

5.2.2 Calculation of capillary valve design

The capillary stop valve is a passive valve that operates based on localized low surface energy created by a rough change in channel-flow direction angle (β in Figure 5-8). In Figure 5-8, the curvature of liquid front is defined by angle α which is related with the surface tension. Assuming the contact angle of the substrate and sidewall to be similar $\theta_{l\_sidewall} \approx \theta_{l\_substrate} = \theta_c$ =40°.

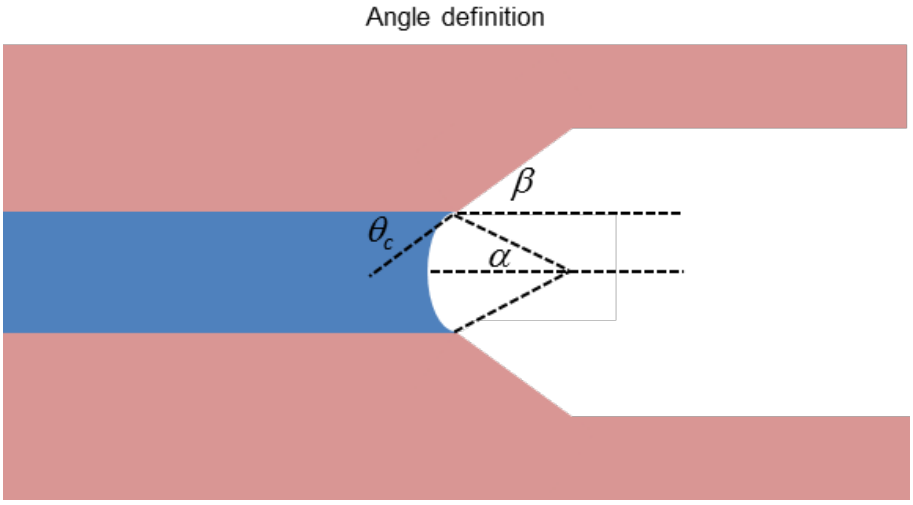

Figure 5-8 Angle definition: top-down view of microfluidic capillary stop valve

As shown in Figure 5-9, at the critical point, the capillary pressure should be 0, which means the meniscus is a flat surface (α=0°). The equilibrium angle between liquid and solid will be $\pi-\theta_c = \pi/2+\beta_c$. Therefore, the change of sidewall-flow direction angle should be $\beta_c \geq \pi/2 - \theta_c$.

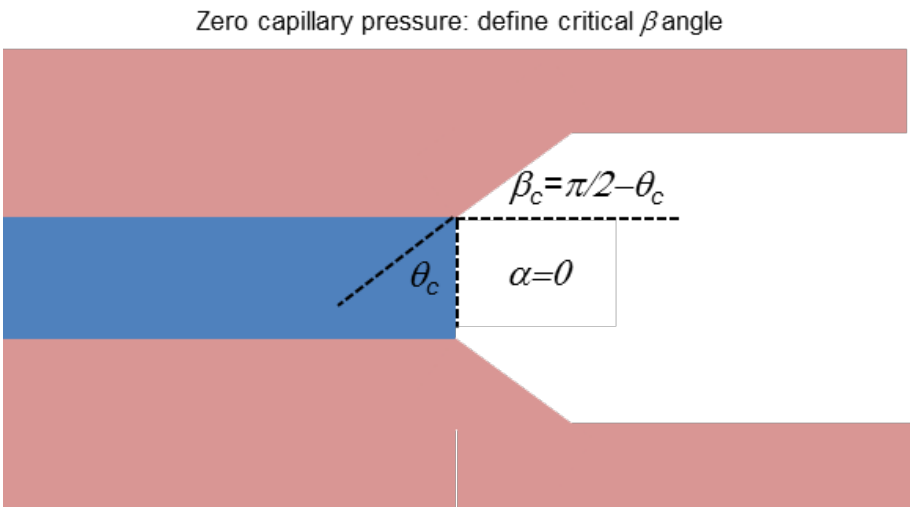

Figure 5-9 Capillary stop valve design at critical point of "zero" capillary force

For the hydrophilic surface material with a contact angle of 40°, the change of angle $\beta \geq \beta c = 90° - \theta_c = 90° - 40° = 50°$ in order to change the capillary pressure from positive to zero.

5.3 Principle of operation

A test sequence of the proposed LOC system includes (a) VLP localized self-assembly (b) target molecule binding, and (c) washing and measurement.

5.3.1 VLP localized self-assembly

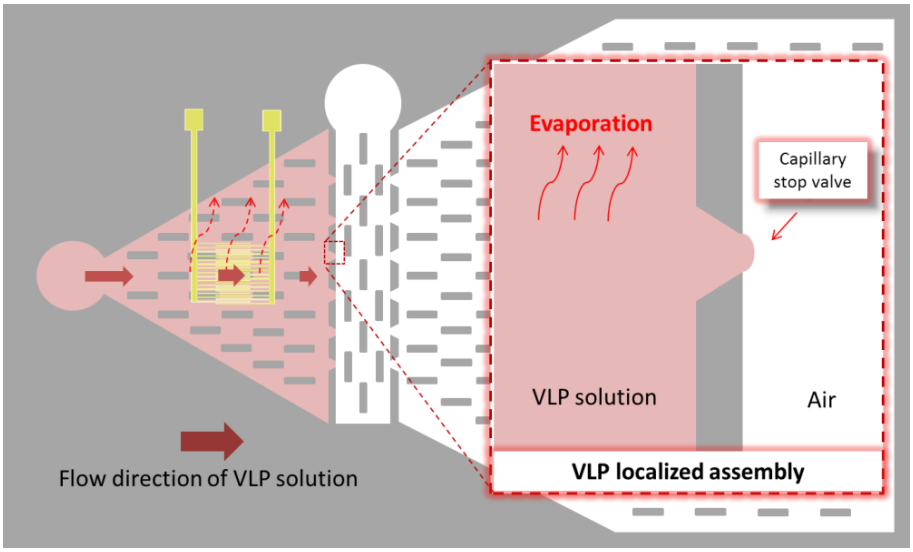

Figure 5-10 Schematic of VLP assembly in LOC system

As shown in Figure 5-10, during the VLP assembly process, the VLP suspended in DI water is introduced from the sample reservoir and limited in the sensing module because of the capillary stop valves. The VLP solution evaporates at room temperature. Impedance sensor will monitor the impedance change to evaluate the assembly process of VLP through the change in the imaginary part of the complex electrical impedance.

5.3.2 Target molecule binding

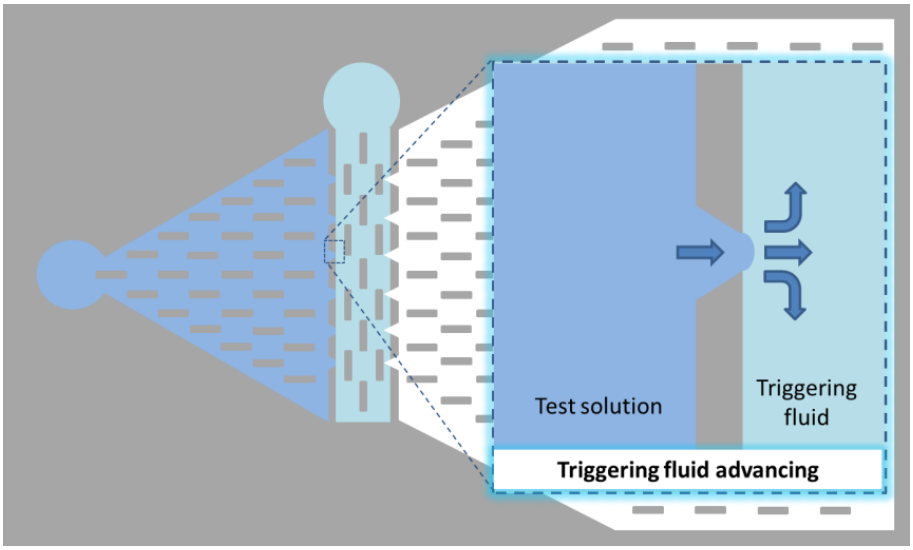

Figure 5-11 Schematic of fluidic triggering before antibody sensing

The buffer solution is first introduced in the device to establish baseline impedance after VLP assembly. After the impedance measurement, a triggering fluid is applied in the control module to trigger the venting of the liquid from the sensing to the venting module (Figure 5-11). Then, the buffer solution that contains target antibody will be introduced to the left sample reservoir and enter the sensing area. The impedance change during the antigen-antibody binding will be monitored.

5.3.3 Real-time antibody sensing

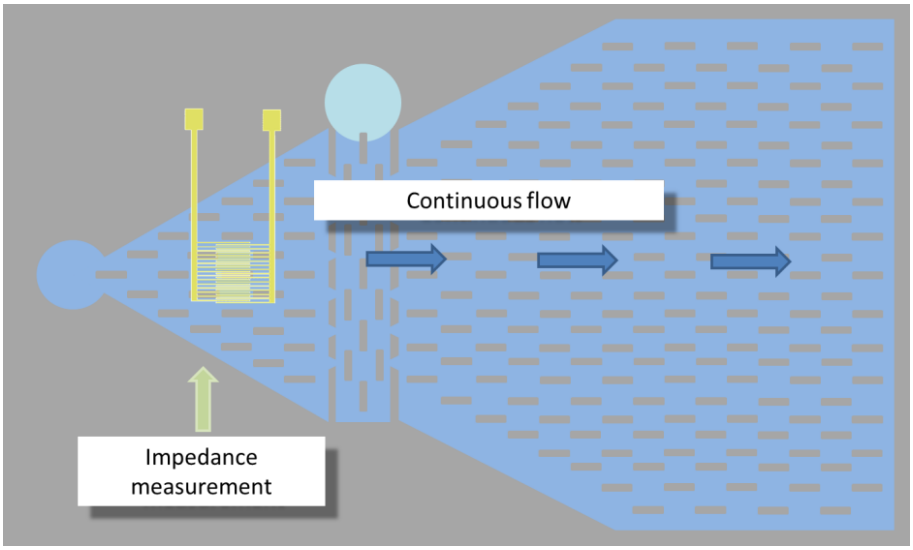

Figure 5-12 Schematic of impedance measurement in continuous flow

Once the impedance in step (b) stabilizes, buffer solution will be introduced again to wash off all the unbound residues in sensing area. The electrical impedance at this stage will be measured and compared with the initial value before the introduction of target molecules (Figure 5-12).

5.4 Microsystem fabrication

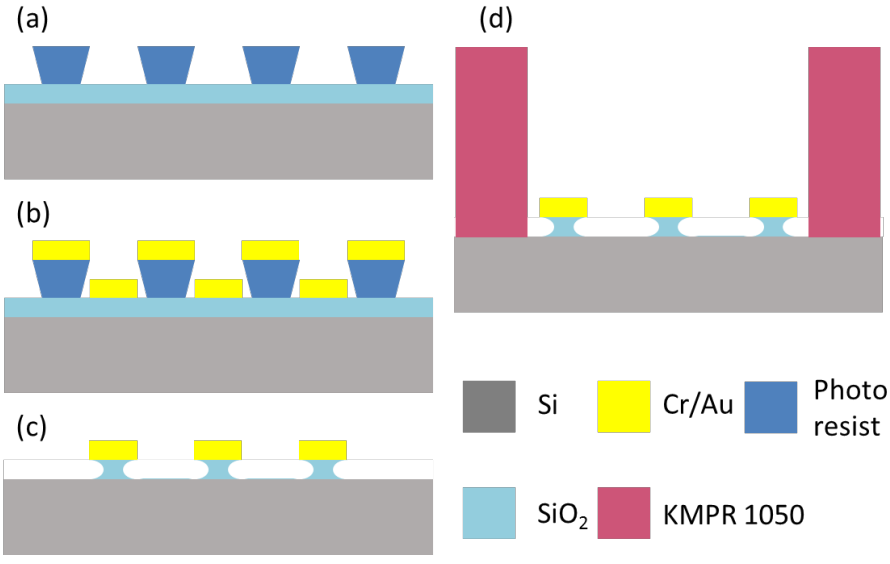

Figure 5-13 Microfabrication process flow of the microfluidics integrated impedimetric sensing microsystem: (a) patterning of photoresist, (b) e-beam deposition of Cr/Au, (c) lift-off of photoresist to create interdigitated impedance sensor electrodes, and etching of SiO_2 in BOE, and (d) creating capillary microfluidic layer through patterning of KMPR

The fabrication process flow of the microsystem is demonstrated in Figure 5-13. A 500 μm-thick silicon wafer with a 200 nm-thick SiO_2 passivation layer deposited using Plasma Enhanced Chemical Vapour Deposition (PECVD) was utilized as the substrate. Negative photoresist NR9-1500PY (Futurrex Inc., NJ, USA) was spin-coated at 3000 RPM for 30 seconds to form a 1.5 μm-thick photoresist layer. The photoresist was patterned using photolithography with an exposure energy dose of 280 mJ/cm^2 at 365 nm wavelength (Figure 5-13a). After development, Cr/Au (20 nm/140 nm) was coated on the patterned wafer using NEXDEP E-beam Deposition (Angstrom Engineering, Ontario, Canada) (Figure 5-13b). The metals deposited on the photoresist were then removed in a lift-off process in acetone, creating the impedance sensor features on the wafer. A 45-second buffered HF etch was performed to expose the silicon (Figure 5-13c), a more hydrophobic substrate material. The driving capillary force is mainly provided by the changing interfacial energy on the sidewall, which largely depends on the sidewall geometries. After impedance sensor fabrication, KMPR 1050 (MicroChem Corp., MA, USA) was spin-coated at 3000 rpm for 30 seconds, to form a 60 μm-thick layer. The KMPR was soft-baked at 100 ^{o}C for 20 minutes before exposure at a dose of 1000 mJ/cm^2 at 365 nm with UV light. The wafer was then post-baked at 100 ^{o}C for 4 minutes. The KMPR development process was

completed in SU-8 developer for 4 minutes followed by rinsing in isopropyl alcohol (Figure 5-13d).

After fabrication, the integrated sensing microsystem was exposed to O_2 plasma (50 W, 0.5 Torr) for 5 minutes in order to remove residues in the microfabrication process as well as render the KMPR microfluidic layer hydrophilic[176, 177].

5.5 Label-free antibody sensing procedure

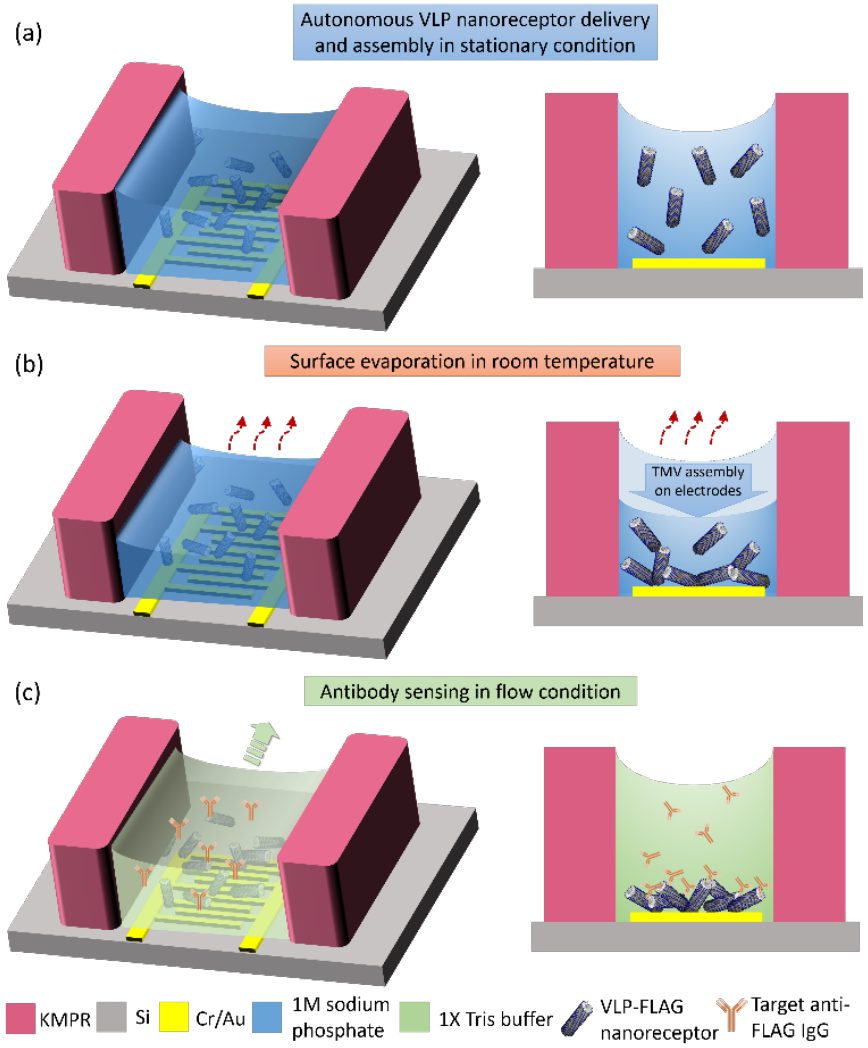

Figure 5-14 Experimental procedure for the VLP-FLAG surface functionalization and antibody sensing

For impedance sensor functionalization, 5 μL of 0.1 M sodium phosphate buffer solution containing VLPs at concentrations of 0.2 mg/mL, 2 mg/mL or 4 mg/mL were pipetted in the sample inlet shown in Figure 2. Due to capillary action, the VLP solution was automatically distributed on the impedance sensor surface (Figure 5-14a). The VLP concentration above the impedance sensor increased as the solution evaporated, promoting high-density assembly of VLPs on the sensor through both thiol-gold binding and van der Waals forces (Figure 5-14b).

In the subsequent antibody sensing, the sensor was rinsed twice with 5 μL of 1X Tris-buffered saline (TBS) solution to remove non-specifically attached VLPs from the sensor surface. Then, the target anti-FLAG antibodies with increasing concentration from 10 ng/mL to 10 μg/mL in 5 μL 1X Tris buffer were added from the sample inlet. 1 μL of 1X Tris buffer was introduced from the triggering channel after the antibody-containing buffer solution filled the entire sensing module, which broke the barrier of the stop-valves and induced continuous flow of test samples from the sensing to the venting module (Figure 5c). The electrical impedance on the sensor was measured in real-time during both VLP sensor functionalization and target antibody binding. Specifically, an AC signal at 100 Hz with amplitude of 50 mV was applied between the IDT electrodes using a VSP-300 potentiostat (Bio-Logic Science Instruments SAS, France) to analyze the VLP assembly dynamics and quantify the target molecule concentration.

5.6 Characterization of the capillary microfluidics operation

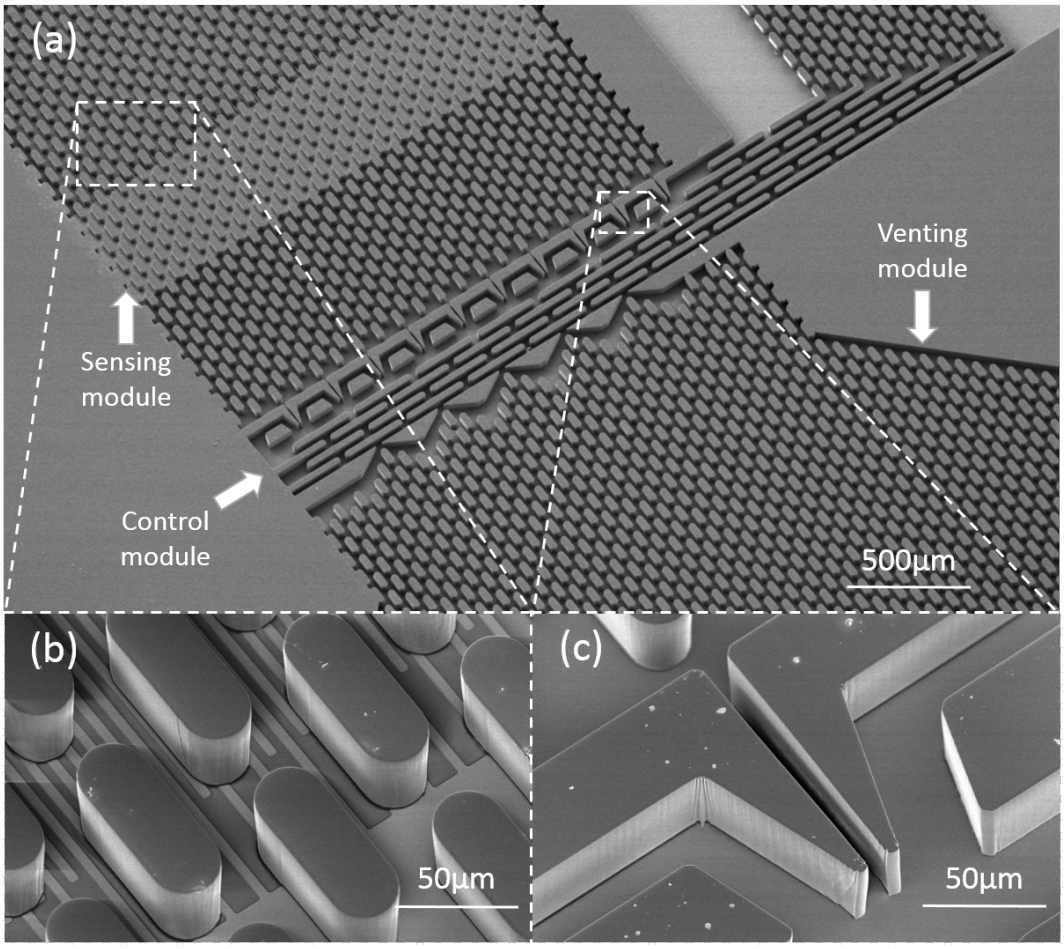

Figure 5-15 SEM image of the microfabricated sensing microsystem. The SEM image shows (a) the overview of the integrated sensing microsystem containing sensing, control and venting module, (b) the interdigitated electrodes of the impedance sensor in the sensing module, and (c) the capillary stop valve in the control module

The surface morphology of the microfabricated sensing system was characterized using scanning electron microscopy (SEM) and optical interferometry. Figure 5-15a is the SEM image showing the fabricated capillary stop valves, and the micropumps in the sensing and triggering modules. The KMPR 1050 negative photoresist shows high-aspect-ratio pillar structures with smooth sidewalls. KMPR micropillars show good adhesion on the impedance sensor IDT electrode area (Figure 5-15b). The stop valves change the initial

liquid meniscus-sidewall angle to more than 150^{o}, forming sharp nozzle shapes and a localized free energy barrier (Figure 5-15c). Optical profilometry was utilized to further inspect the geometric dimensions of the microfluidic layer.

The geometric dimensions, such as depth and width of the developed capillary system, were measured using WYKO NT 1100 optical profilometer (Veeco Instruments Inc., AZ, USA). The depth of each channel in the capillary micropump is measured as 60 μm (Figure 5-16), while the width is 25 μm, resulting in an aspect ratio (channel depth/width) of 2.4. At the stop valves, aiming at an increased controllability of sidewall geometry to the liquid meniscus advancing, the width of the channel is reduced to 15 μm, resulting in an aspect ratio of 4. This enhanced aspect ratio improves the isolation of liquid using the stop valves.

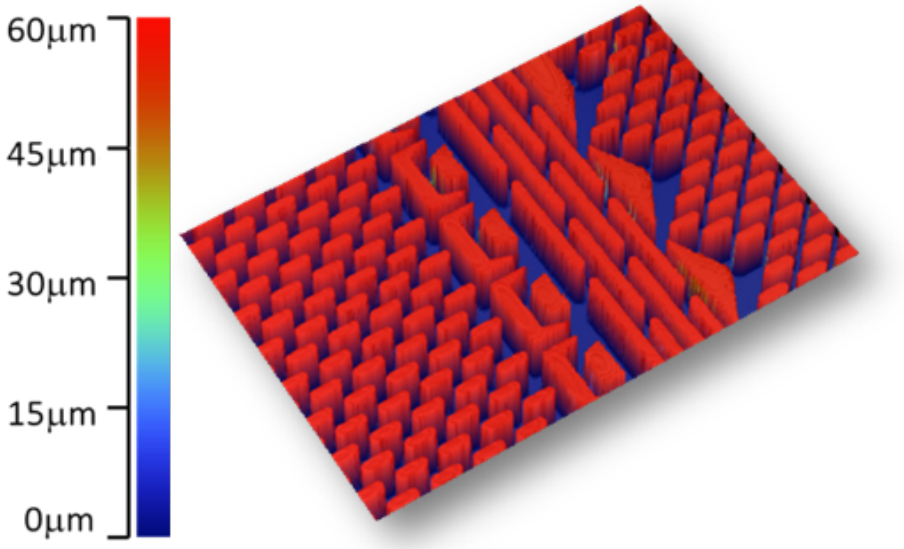

Figure 5-16 Optical profile of the microfluidic system

A 5-minute O2 plasma treatment was performed on the KMPR microfluidic layer surface to render the microfluidic sidewalls hydrophilic

(contact angle of 6°). Long-term stability test also showed the water contact angle on the O_2 plasma treated KMPR stabilized at around 40° after two months of storage, still more than sufficient to achieve a positive capillary force (Figure 5-17).

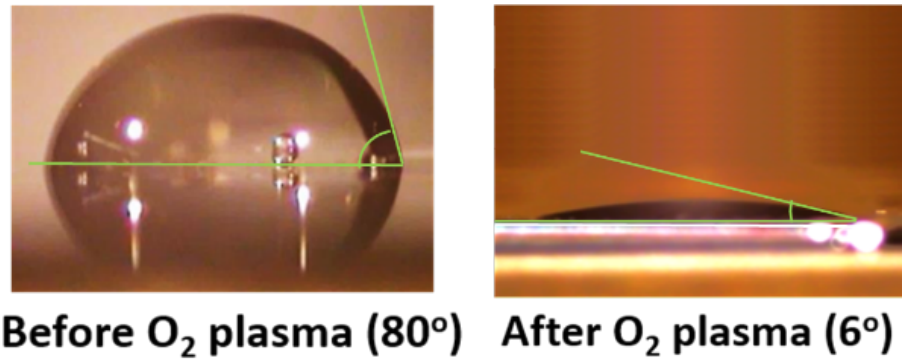

Figure 5-17 KMPR Contact angles before and after O_2 plasma activation at 50W for 5 minutes

The flow regulation function of the stop valves before triggering, and the flow distribution in the system after the triggering of stop valves, were characterized using optical interferometry. A 5 μL water sample containing polystyrene microbeads of 10 μm diameter were loaded from the sample inlet. These microbeads were confined in the sensing module due to the presence of capillary stop valves. The movements of the microbeads due to the initial filling in the channel and the Brownian motion distorted the water/air interface, creating a different reflection patterns compared with water. The trajectories of these microbeads were recorded using vertical scanning interferometry through the optical profilometer operating at a low scan rate of 1 μm/s (Figure 7). It can be clearly seen that the microbeads suspended in DI water were confined only in the sensing modules on the left of the stop valves, leaving both triggering

and venting modules unfilled. This scenario is analogous to when VLP-containing solution was introduced during the sensor functionalization process.

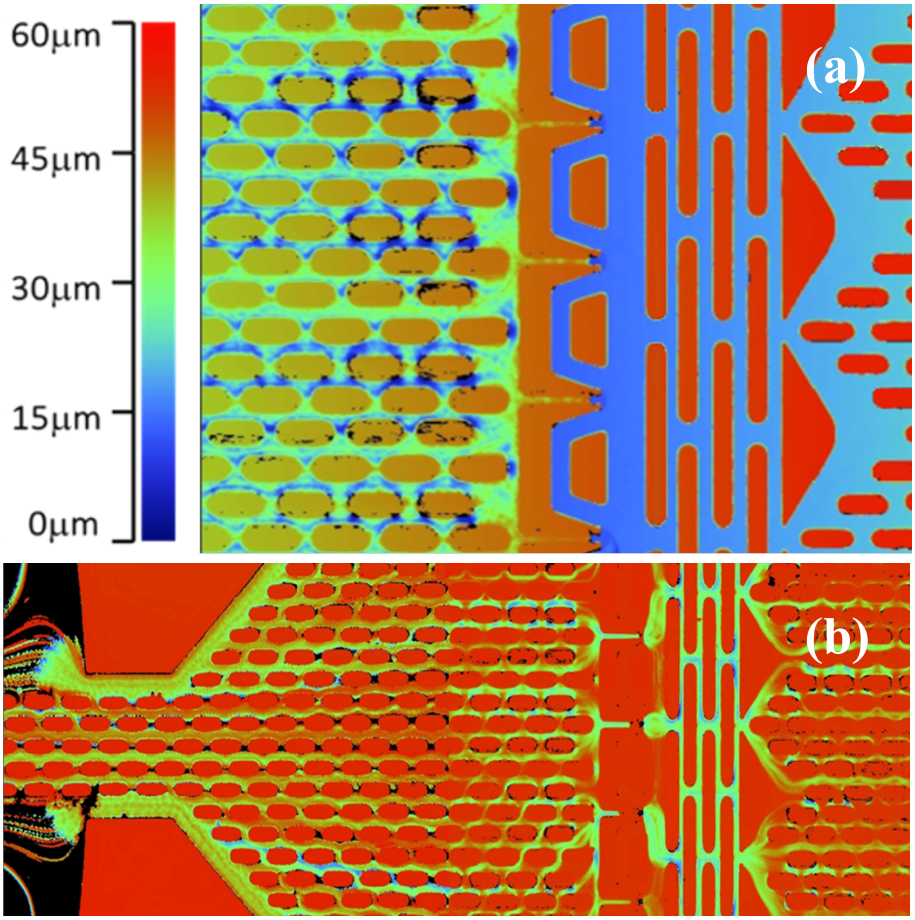

Figure 5-18 (a) Liquid sample filling in the sensing module before triggering of stop valves. (b) Trajectories of microbeads in the capillary microfluidic sub-system after stop valves triggering

Optical profilometry image in Figure 5-18a shows that the microbeads suspended in DI water were confined only in the sensing modules on the left of the stop valves, leaving both triggering and venting modules unfilled. This reflects the circumstances present when the VLP-containing solution is introduced during the sensor functionalization process. Figure 5-18b demonstrates the distribution of flow in the microsystem after triggering of the stop valves. The liquid sample that contains polystyrene microbeads flew

evenly through the sensing module on the left side and left an evenly distributed trajectory pattern of the microbeads. This even distribution will enable the delivery of target molecules on the full area of the sensor, thus maximize the use of assembled VLPs toward sensitive antibody detection.

Figure 5-19 demonstrates the distribution of flow in the sensing microsystem after triggering of the stop valves. The white parts in this grayscale image represent the trajectories of the microbeads traveling within the microfluidics. These suggest that, after triggering of the stop valves, the liquid samples could flow evenly through the sensing module. This maximizes the effective impedance sensing area and contributes to a more sensitive impedance sensor for quantifying antibody binding. The flow distribution in the sensing and venting modules were further quantified and compared using the image analysis program – ImageJ [178, 179].

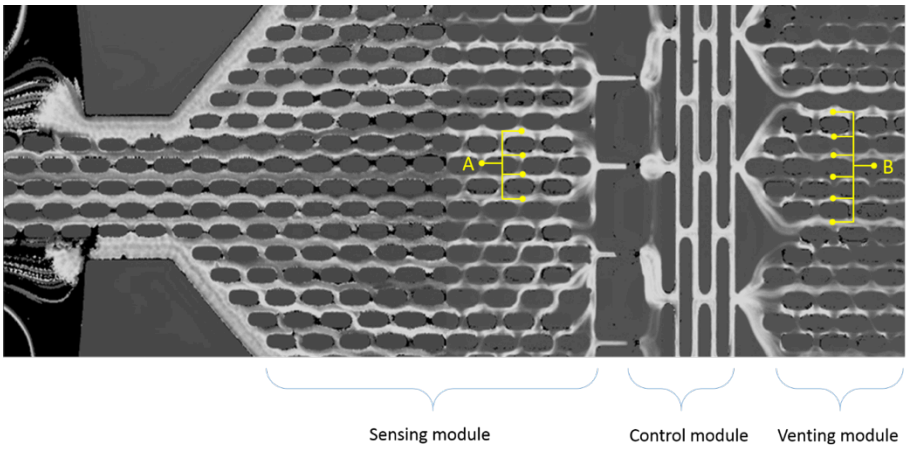

Figure 5-19 Grayscale optical profilometry image of trajectories of microbeads flowing in the capillary microfluidic device after triggering the stop valves

As is shown in Table 5-1, the percentage deviation of the flow distribution in the sensing area is only 3.5%. However, in the venting area, due

to large capillary force and changes in the channel width from large to small, the particles have a larger probability of flowing into the channels on the side of the nozzle. This results in a 46.78% deviation in the greyscale level on the trajectory plot. This analysis validated that the current design can ensure an even distribution in the sensing area in the antibody sensing stage, which ensured the maximum usage of the effective impedance sensor electrode area on-chip.

Table 5-1 Grayscale levels in "Area A" in the sensing module and "Area B" in the venting module in Figure 5-19

	Average gray (0-255)	Standard deviation	Percentage deviation
Area A (Sensing)	221.25	7.76	3.5%
Area B (Venting)	143.67	66.97	46.78%

5.7 Experimental results

5.7.1 VLP assembly in capillary microfluidics

A 5 μL drop of 0.1 M sodium phosphate buffer solution containing VLP-FLAG nanoreceptors was introduced in the inlet of the capillary microfluidics. The concentration of VLPs in the solution was varied from 0.2 mg/mL (a previously characterized minimum concentration to ensure coating uniformity) up to 4 mg/mL (the highest concentration achieved after purification). The VLP-containing solution was delivered autonomously in the micropump, and immobilized on the impedance sensor surfaces due to flow

constraints from the stop-valve array. The stationary VLP solution in the sensing area completely evaporated within 15 minutes at room temperature.

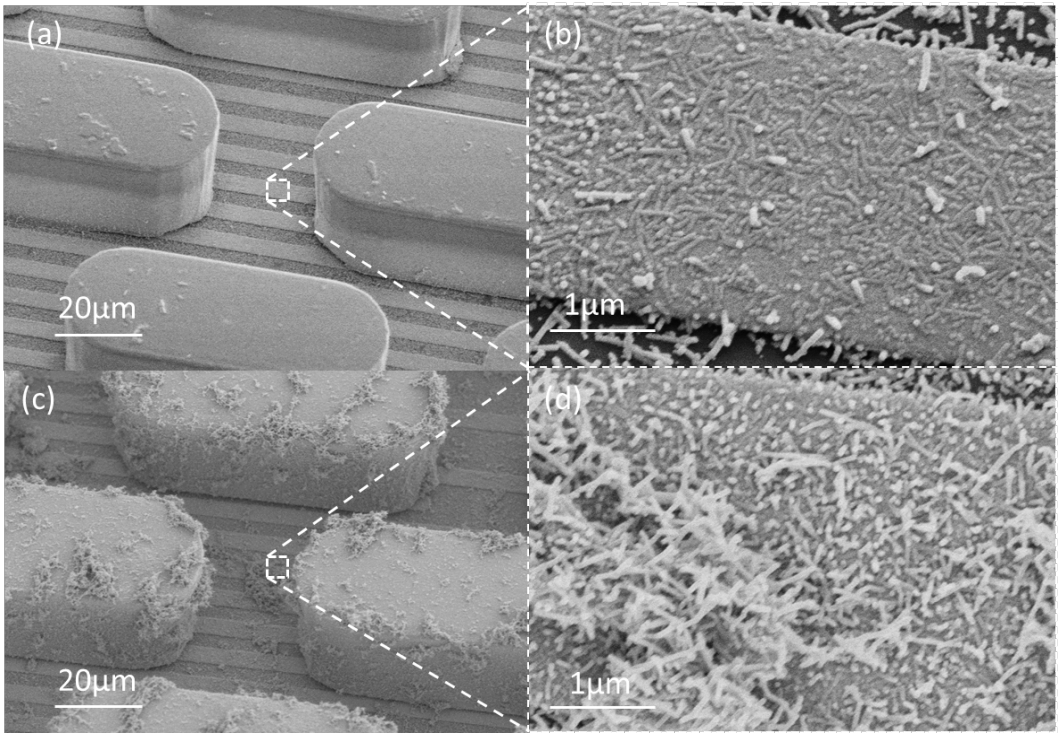

Figure 5-20 SEM images of the VLP-FLAG functional nanoreceptor layer assembled through autonomous delivery and enhanced evaporation in the open-channel capillary microfluidics. The morphology of VLP nanoreceptors assembled using (a) 0.2 mg/mL VLP-FLAG in 0.1M phosphate buffer, where the enlarged view (b) shows the VLP nanorod assembled in parallel with the impedance sensor surface, forming a flat arrangement of nanoreceptors, and the morphology of VLP nanoreceptors assembled (c) 4 mg/mL VLP-FLAG in 0.1M phosphate buffer, where the enlarged view (d) shows the VLP nanorods forms clusters and piled-up on the impedance sensor electrode due to van der Waals force or electrostatic interactions

The surface morphology of the VLP nanoreceptor assembled through evaporation in the capillary microfluidic device was studied using scanning electron microscopy (SEM). Palladium activation and electroless nickel coating were performed on the VLP-assembled device to enhance the SEM imaging contrast. Figure 8a shows the uniform coating of VLP-FLAG nanoreceptors on the impedance sensor IDT electrodes and the sidewall of the microfluidic

channel using 0.2 mg/mL VLPs in the buffer solution. Both the impedance sensor and microfluidics retained their original profiles. The enlarged view in Figure 8b shows flat and dense attachment of VLP-FLAG nanoreceptors on the IDT electrode surface, forming a thin VLP functional layer. When the concentration of VLPs was increased to 4 mg/mL, the VLPs form clusters due to the non-specific binding caused by van der Waals forces and electrostatic interactions (Figure 8c). These clusters of VLP nanoreceptors increase the total volume of VLPs available in the sensor system; however, a closer view of the VLP morphology on the electrode also shows that the high concentration VLPs result in the aggregation of these nanoreceptors with random orientation (Figure 8b). Overall, with both low and high VLP concentrations, the density of the assembled VLPs on the impedance sensor through evaporation in the open capillary microfluidics is much higher compared to that previously achieved in a closed chamber.

The cross-sectional SEM images of the VLP-assembled sensor electrode (Figure 5-21) show distinct difference in the VLP layer when difference VLP concentrations are utilized in the assembly process. A low VLP concentration (0.2 mg/mL) resulted in a low thickness of 0.53 μm. And, a higher VLP concentration (4 mg/mL) in the assembly process formed a thicker VLP stacking up to 1.78 μm (a 3-fold increase compared to that achieved using a lower VLP concentration).

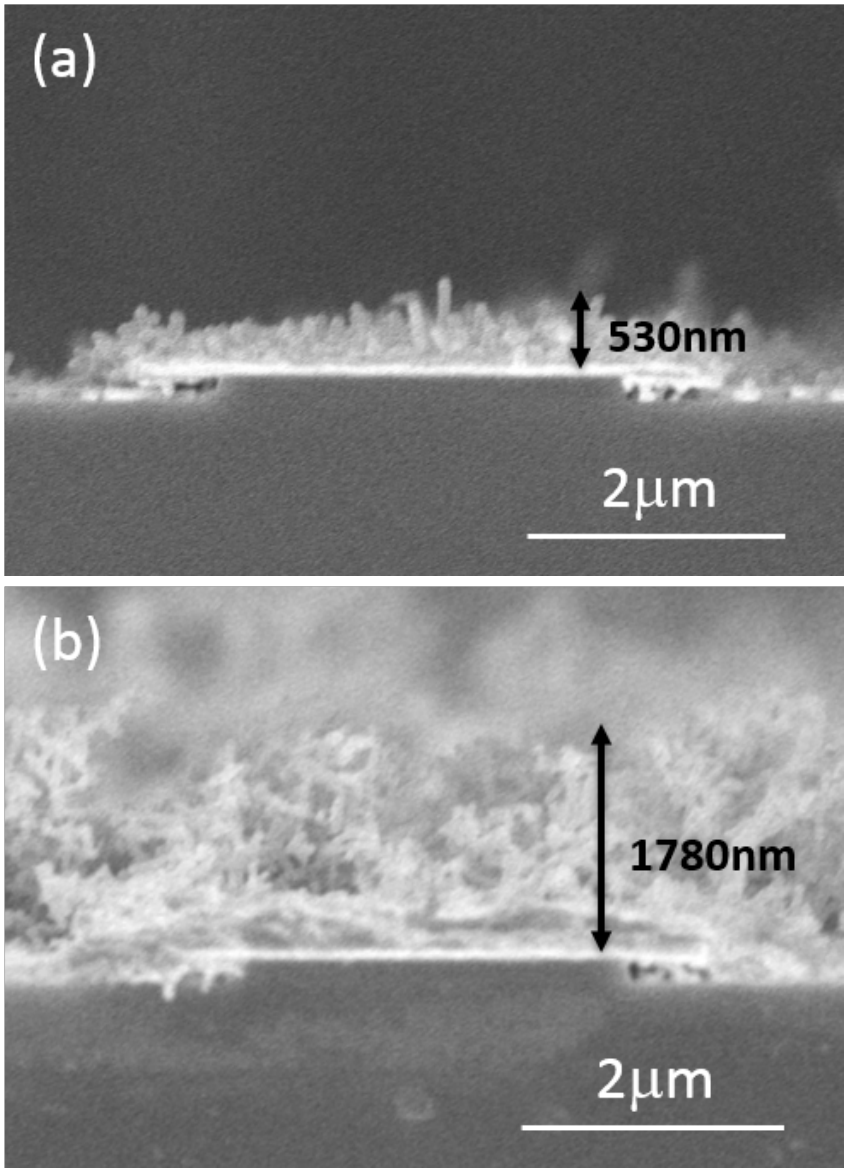

Figure 5-21 Cross-sectional SEM images of the VLP-assembled sensor electrode. The VLP concentrations used in the assembly were (a) 0.2 mg/mL and (b) 4 mg/mL.

5.7.2 Label-free antibody sensing

The electrical impedance between the interdigitated electrodes was measured every 10 seconds during both VLP assembly on-chip and antibody sensing. The percentage impedance change (imaginary part of the complex impedance) at 100 Hz was utilized to analyse the VLP and antibody attachments on the electrode surface. When biological particles (relative

permittivity of 4-13) attach to the electrode surface, they will displace water (relative permittivity of ~80) on the electrode/liquid interface. This will lower the effective dielectric constant on the electrode surface, and will reduce the area (and thus the associated capacitance capacitance) of the ionic double layer defined by the electrode/electrolyte interface. Therefore, an increase in the amplitude of impedance (imaginary part) is expected as biomolecules attach to the electrodes.

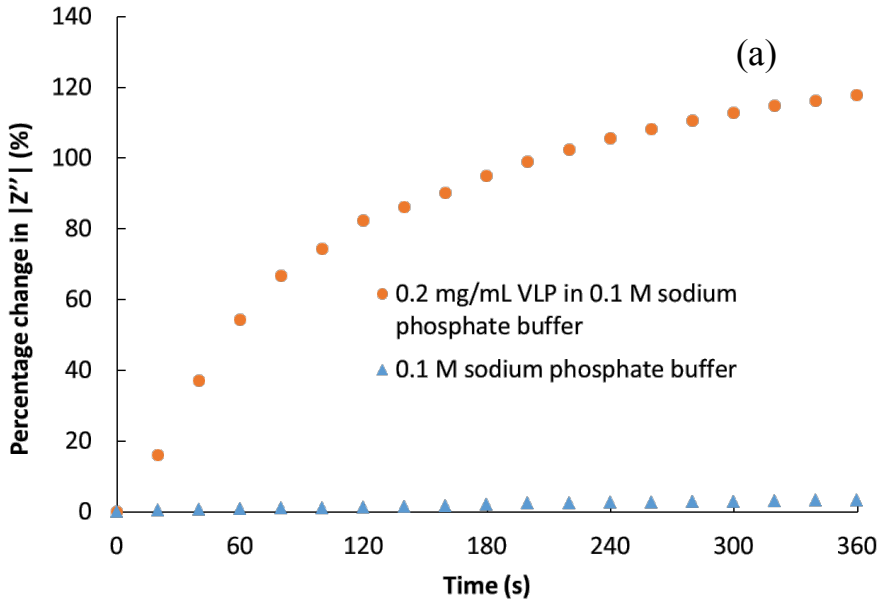

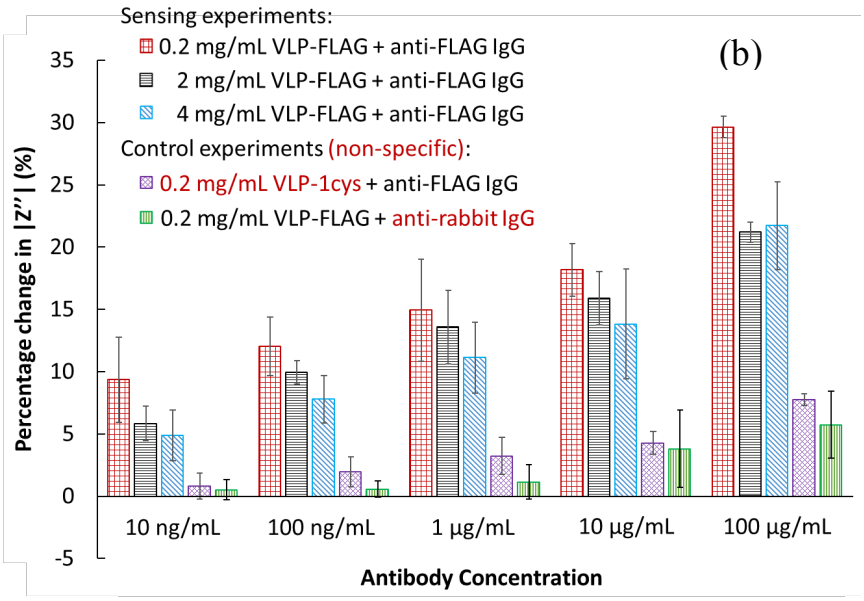

Figure 5-22 (a) Real-time percentage changes in the impedance (amplitude of imaginary part) between IDT electrodes during VLP assembly. (b) Percentage impedance changes when antibodies were introduced to the VLP-functionalized impedance sensors. Complimentary receptors and targets – VLP-FLAG and anti-FLAG IgG – were utilized in the sensing experiments. In the two control experiments, non-specific receptors (VLP-1cys at 0.2 mg/mL) or non-specific target antibodies (anti-rabbit IgG) were used. Experiments with the same conditions have been repeated independently on multiple sensors (n=3). The error bars represent the standard deviations

Figure 9a shows the evolution of the relative impedance during the assembly of VLP on the sensor's IDT electrodes. It is shown that, using the open capillary microfluidic device as delivery platform, the impedance between the IDT electrodes increased by more than 120% and saturated within 6 minutes after introducing a drop of 0.2 mg/mL VLP-FLAG nanoreceptors. In contrast during the control experiment, the impedance changed less than 2% when only buffer solution was delivered. In previous work that utilized VLP self-assembly, the VLP could saturate the electrode surfaces in 3 hours. The accelerated VLP assembly process using the capillary microfluidic system may be due to the local increase in VLP concentration as buffer evaporates and

more solution is drawn in via the capillary pump. These results show not only the capability of using impedance sensors in studying the dynamics of nanoreceptor assembly on sensors, but the great advantage of using open-channel capillary microfluidics to accelerate the assembly process through enhanced evaporation as well.

After the accelerated VLP assembly, the VLP-functionalized impedance sensor was utilized to perform label-free antibody sensing. The binding of target anti-FLAG antibodies with concentrations ranging from 10 ng/mL to 100 μg/mL in the 1X TBS buffer were studied. The increasing antibody concentrations were sequentially applied onto the VLP-functionalized impedance sensors surfaces. The sensors were functionalized using 0.2 mg/mL, 2 mg/mL or 4 mg/mL of VLPs in order to reveal the optimized sensor conditions for a better sensitivity.

Figure 9b shows the resulting percentage change in imaginary impedance of the VLP-functionalized sensors. Impedance shifts from non-specific bindings were studied in two control experiments. In the first control experiment, non-specific VLP-1cys at 0.2 mg/mL concentration were used to functionalize the sensors, which generated the impedance changes of less than 7.8% at the maximum anti-FLAG concentration of 100 μg/mL. In the second control experiment, the 0.2 mg/mL VLP-FLAG functionalized sensors responded to non-specific binding anti-rabbit IgG with the maximum of 5.7% impedance changes.

On the other hand, the impedance sensors functionalized using VLP-FLAGs at various concentrations all showed significantly larger impedance increases. This indicates that VLP-FLAG is a highly selective biosensing probe with respect to the target antibody. Interestingly, when the impedance sensor was functionalized using the lowest concentration of VLP-FLAG (0.2 mg/mL), the highest sensitivity during antibody binding was observed. At the maximum target antibody concentration of 100 μg/mL, the impedance sensor functionalized using 0.2 mg/mL VLP-FLAG showed an impedance increase of 29.6% while the one functionalized using 4 mg/mL VLP-FLAG only showed an increase of 21.2%. This substantial difference in the sensor performance may be a result of the significant difference in the VLP morphology achieved by using different VLP concentrations during assembly. Though the amount of VLPs attached on the sensor is considerably larger using a higher VLP concentration, it also decreased the porosity of the VLP layer, thus losing the surface area. Also, a higher VLP concentration also leads to a larger thickness of the VLP layer, which kept the subsequently attached antibodies away from the electrode surface, thereby decreasing the sensor sensitivity. Using a lower VLP concentration, the VLPs assembled as a closely packed flat monolayer on the electrode surface, allowing the attached antibodies to directly impact the double layer capacitance, thus increasing the sensitivity of the system. Therefore, among all the tested VLP concentrations, the 0.2 mg/mL is the optimized sensor functionalization condition to achieve a better antibody sensing.

From the sensing experiments in Figure 9b, the maximum sensitivity of the sensors is 4.12% impedance change per $\log_{10}$(ng/mL) antibody concentration. The resolution of the VLP functionalized sensors was calculated to be 3.9% impedance change (3 times the standard deviation when measuring buffer solution). Therefore, the detection limit of the VLP-FLAG functionalized sensor is 8.84 ng/mL (equivalent to 55 pM anti-FLAG IgG). The results showed great potential of using VLP-functionalized impedance sensors to perform rapid label-free biosensing in the real-time.

5.7.3 System regeneration

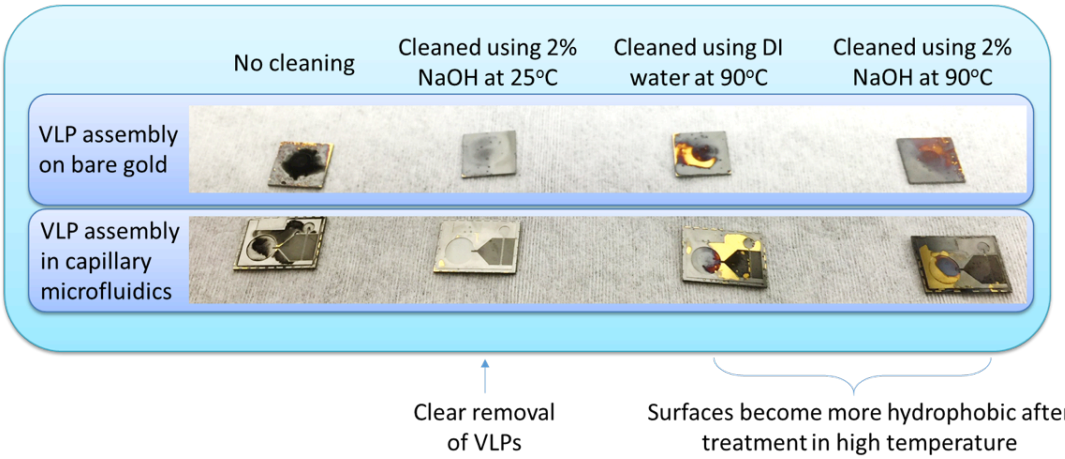

Figure 5-23 Surface regeneration using DI water and NaOH treatments at room temperature and 90°C

NaOH is a commonly used base for cleaning organic compounds in experiments or life. The positive photoresist developer contains about 0.6% NaOH to remove the cross-linked photoresist. In the experiments, both DI water and 2% NaOH were compared at both room temperature and 90°C in terms of their VLP removal efficacy. Figure 5-23 shows the optical observations of the DI water and NaOH treated bare gold chip and microfluidic

devices at different temperature. From the images, the 2% NaOH treated gold chip and microfluidic device both show good surface cleaning efficacy, removing the black-colored VLP layer from the surfaces.

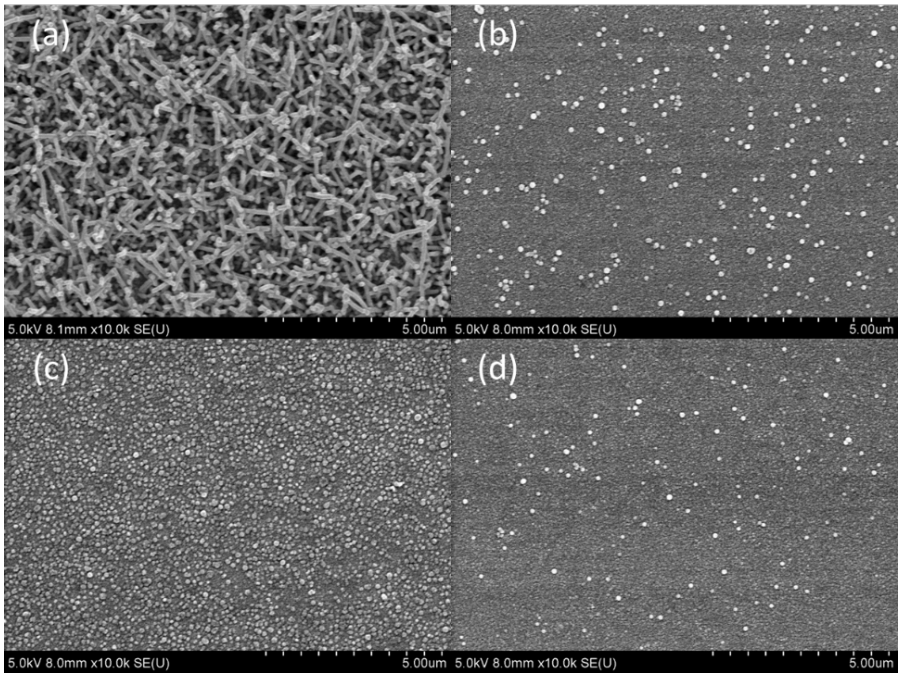

Figure 5-24 SEM images showing the morphology of the metalized VLP-coated surfaces with or without cleaning procedure in different chemicals and conditions. (a) No cleaning, (b) 2% NaOH cleaning at room temperature, (c) DI water cleaning at 90°C, (d) 2% NaOH cleaning at 90°C

Figure 5-24 shows the SEM images of the device surfaces after the aforementioned different surface treatment. The VLP coated gold chips have gone through four different surface treatments: (a) no cleaning, (b) cleaning using 2% NaOH at room temperature, (c) cleaning using DI water at 90°C, and (d) cleaning using 2% NaOH at 90°C. The aim is to find the best procedure to remove the VLPs without affecting the properties of the device. As the control experiment, the VLPs assembled firmly on both bare gold surfaces if no cleaning procedure is performed, which formed the VLP nanorod forest on the surfaces (Figure 5-24a). Interestingly, by cleaning the surfaces using 2% NaOH

solution before metallization, only scattered distribution of VLP subunits can be observed (Figure 5-24b). When the temperature of the chips were elevated up to 90°C, both DI water and NaOH treated surface lost the original VLP rod structures (Figure 5-24c and Figure 5-24d); however, the DI water treated surface still have a much larger quantity of VLP subunit attached on the gold surface compared with NaOH treated one. The better surface regeneration efficacy using NaOH may owe to the denaturisation of VLP coat proteins after exposing to high pH-level base solution.

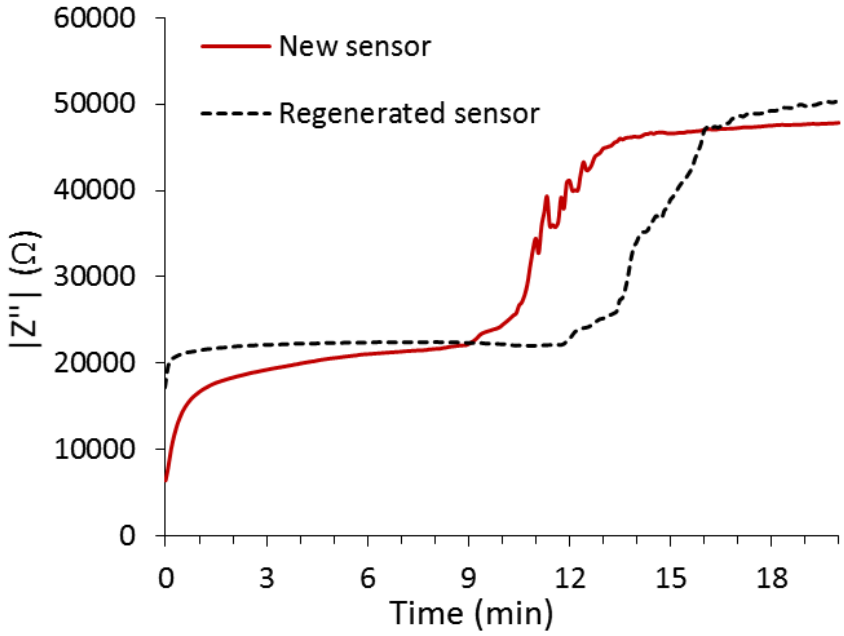

Figure 5-25 Impedance responses in VLP assembly before and after sensor regeneration

Figure 5-25 shows the detailed impedance responses of the VLP assembly on a new sensor surface (red solid curve) and on a sensor surface that was regenerated using 2% NaOH at room temperature (black dashed curve). The VLP assembly shows much faster saturation on the regenerated sensor compared with on the new one. This may be resulted from the incomplete

removal of VLPs on the sensor surface. On the other hand, the overall impedance responses are similar between the two devices, and the impedance of the sensor after VLP functionalization is comparable between the two devices. This indicates that the sensor can be functionalized with VLPs again after cleaning the surface, but the quality of VLP assembly on the sensor may not be completely the same as the new one.

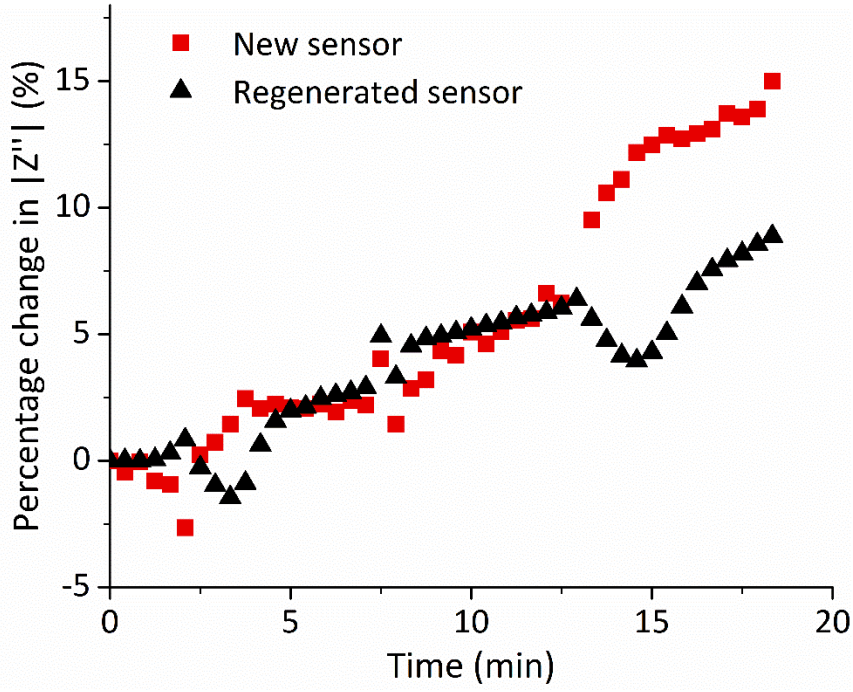

Figure 5-26 Impedance responses to increasing target anti-FLAG concentration on a sensor before and after surface regeneration

The VLP assembly and sensing efficacy of the sensor microsystem after surface regeneration were validated. The impedance responses from the same sensor before and after surface regeneration were compared in Figure 5-26. With either new sensor or regenerated sensor, the impedance responses were very similar to the increasing target antibody concentration from 10 ng/mL to 1 µg/mL, and the maximum impedance increase was of around 7%. However, the

new sensor showed more stable and continuous impedance increase compared with the regenerated sensor. As the antibody concentration further increased to 1 μg/mL, the new sensor showed higher impedance change of 15% compared with lower than 10% from the reused sensor. The impedance fluctuation in the regenerated sensor may attribute to the detachment of VLPs on the surface due to degraded VLP binding strength on the surface. The new sensor also showed slight larger relative impedance increase compared with the regenerated one. Though there are differences in the sensor characteristics due to the regeneration, the VLP-functionalized regenerated sensor can still be utilized to perform label-free antibody sensing and quantify the concentration of the target molecule. Therefore, the VLP-based impedance sensor is reusable and reconfigurable in the integrated capillary microfluidic system.

5.8 Chapter summary

Based on the fundamental understanding of VLP material characteristics and the self-assembly limitation in sensors, a microsystem comprising capillary microfluidics and impedance microsensors is developed to further enable accelerated VLP assembly and rapid biosensing. The open channel capillary microfluidic components include capillary micropumps and stop valves, aiming at controlled and accelerated assembly of VLP receptors on impedance sensor surface. The capillary micropumps autonomously deliver the VLP-containing solution into the sensor microsystem due to capillary driving forces in the microfluidic channel surface. The evaporation of the VLP solution from the capillary micropump surface results in the accelerated VLP assembly within 6

minutes, a significant reduction of time compared to the existing 3-18 hours of VLP self-assembly process. Owing to the dense VLP receptor assembled closely on the impedance sensor electrode surface, the sensor is able perform label-free antibody sensing within 5 minutes after sensor functionalization, and is able to achieve a detection limit of 55 pM of target anti-FLAG IgG. This microsystem platform greatly enhanced the VLP assembly process in the aspect of time, density and morphology. It is also an integrated sensor microsystem that is capable of controlled sensor functionalization and rapid target molecule quantification for on-demand biosensing applications. This is also the first time that capillary microfluidics is utilized for enhanced sensor functionalization.

Chapter 6: Summary

6.1 Summary

A systematic study has been performed to establish the integration of the macromolecule – *Tobacco mosaic virus* virus-like particle (TMV VLP) – as selective receptor in electrochemical microsensor systems in both chemical and biological sensing applications. This work explored the genetic modification methods, purification procedure and material properties of the VLP sensing receptors. Based on a thorough understanding of the VLP characteristics, the VLPs were integrated in electrochemical sensors for TNT explosive sensing, and in impedimetric sensors for antibody sensing through immunoassay process (ELISA). The capabilities of VLPs as universal and versatile receptor-displaying vehicles for the integration into sensors with different transduction principles, and for the detection of targets with different scales have been validated through experiments. A microsystem platform with capillary microfluidics and impedance sensors was further developed to leverage the self-assembly capability and biological affinity of VLPs. The system achieved controlled, accelerated VLP sensor functionalization and sensitivity-enhanced antibody sensing (Figure 6-1). Overall, this work combined the fundamental research of the material properties of an emerging biological receptor, the development of bio-nano-receptor integration methodology, and the microsystem solution for accelerated receptor integration and enhanced sensing performances.

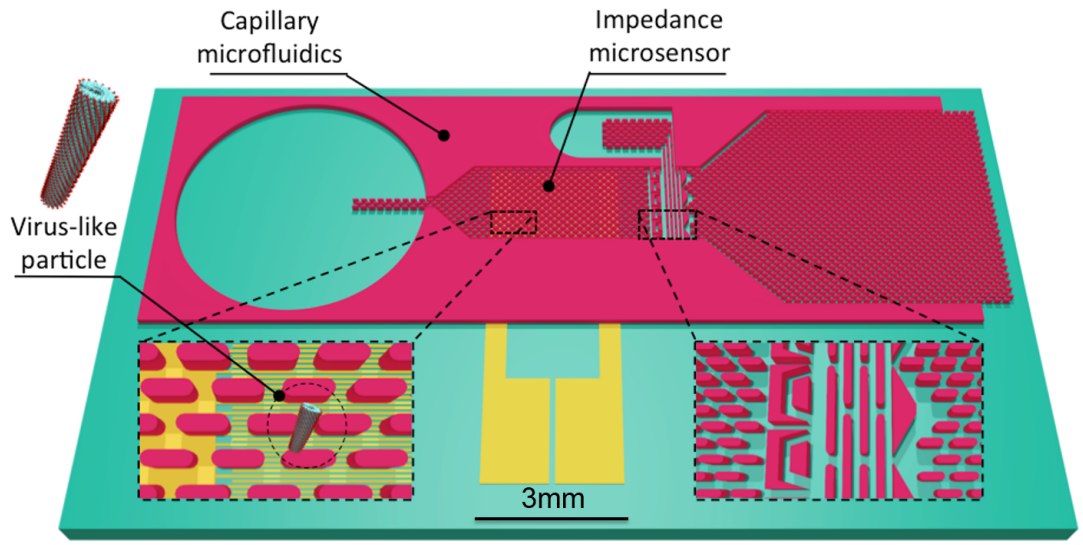

Figure 6-1 Schematic of the capillary microfluidic system with integrated impedance sensor for rapid VLP assembly and label-free sensing

The TMV VLP molecular structure, genetic modification, surface attachment onto substrates, and biological binding efficacy and stability were first studied. By the multiple genetic modifications of the TMV coat proteins produced in the *E. coli* bacteria hosts, thousands of identical coat proteins were able to be self-assembled into nano-rod structures with genetically engineered binding affinity on the outer surfaces of the nanorods. The two different constructs of VLPs with either a TNT binding peptide or a FLAG-tag peptide on each of the coat protein C-terminal end were successfully developed. With the cysteine residue on the TMV coat protein N-terminal end, all the TMV VLP constructs can be self-assembled on to a variety of material surfaces without chemical treatment. The morphology of a VLP-assembled surface can be controlled by VLP concentration, flow and evaporation conditions (Figure 6-2). The biological binding efficacy of the VLPs was validated using

colorimetric ELISA. The genetically modified VLPs showed good stability in a wide temperature and pH ranges.

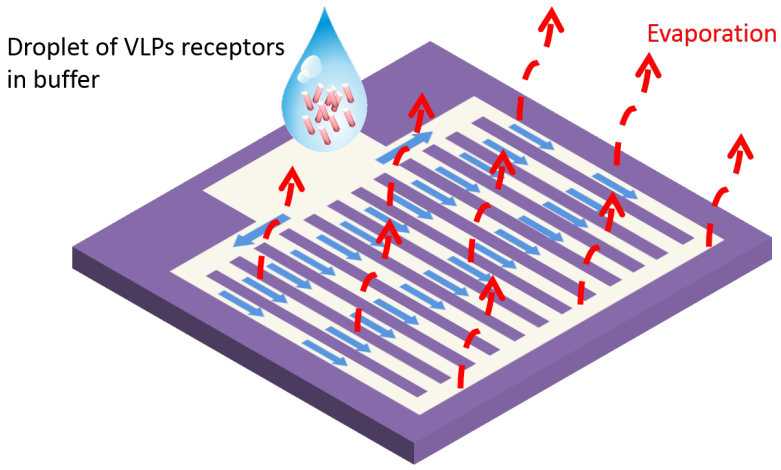

Figure 6-2 Schematic of the evaporation-based VLP assembly process

The genetically modified VLPs were utilized as sensing elements in both miniaturized chemical and biological sensors for TNT chemical explosive and antibody sensing. The TNT sensor operated based on the diffusion modulation from the TNT and receptor VLP binding which selectively changed the TNT electrochemical characteristics in a voltammetric microsensors. Due to the distinct size difference between the VLP-TNT binding agent and target TNT molecule, binding of TNT onto the VLP binding agent can greatly lower its diffusion coefficient, selectively inducing a quantifiable decrease in the TNT characteristic redox current peak. By comparing with the control experiment, the differential current was utilized to quantify the concentration of the target TNT molecules. This method leveraged the high TNT binding affinity of the genetically modified VLPs and added selectivity to the traditional electrochemical sensing method. Since the differential current only relied on

the presence of both target TNT and binding agent VLP, the clean environmental sample and background signal analysis are no longer necessary, making the VLP-based TNT sensor suitable for direct sample analysis.

The integration of VLPs as receptors in biological sensors for medical applications was also studied. The VLP receptors carrying FLAG-tag peptides on the coat proteins were integrated in impedance microsensors for antibody sensing. The VLPs assembled onto interdigitated electrode surfaces through self-assembly, formed a functional nano-receptor layer on the impedance sensor surface. The real-time impedance evolution during the VLP assembly process revealed the VLP self-assembly dynamics, which indicated the saturation on the surface within 3 hours. The subsequent sandwiched immunoassays validated the efficacy of the assembled VLPs as selective receptors in the impedance sensor. The VLP-FLAG assembled impedance sensor was able to quantify the concentration of the target anti-FLAG IgG using immunoassay on-chip. Meanwhile, by increasing VLP concentration during sensing functionalization process, sensitivity of the sensor can be greatly improved.

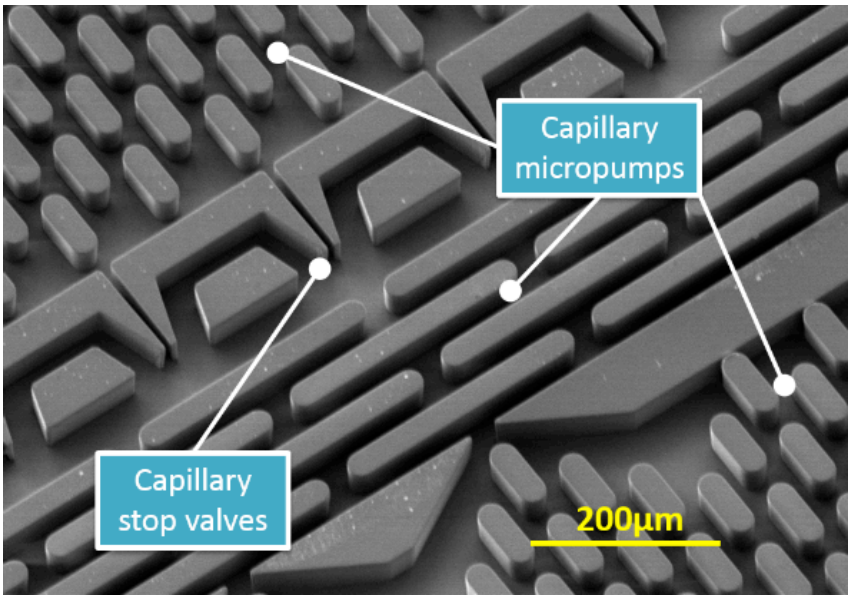

Figure 6-3 SEM image of microfabricated open-channel capillary microfluidics for rapid VLP assembly and biosensing

Based on the fundamental understanding of VLP material characteristics and the self-assembly limitation in sensors, a microsystem comprising capillary microfluidics and impedance microsensors was developed to further enable accelerated VLP assembly and rapid biosensing. The open channel capillary microfluidic components included capillary micropumps and stop valves were developed for controlled and accelerated assembly of VLP receptors on impedance sensor surface (Figure 6-3). The capillary micropumps autonomously delivered the VLP-containing solution into the sensor microsystem using capillary driving forces in the microfluidic channel surface. Evaporation of the VLP solution from the capillary micropump surface resulted in an accelerated VLP assembly within 6 minutes, a significant reduction in time compared to the existing 3-18 hours of VLP self-assembly process. Owing to the dense VLP receptor assembled closely on the impedance sensor electrode surface, the sensor was able to perform label-free antibody sensing within 5

minutes after sensor functionalization, and achieved a detection limit of 55 pM for anti-FLAG IgG sensing. This microsystem platform greatly enhanced the VLP assembly process in terms of time, density and morphology. It was also an integrated sensor microsystem capable of controlled sensor functionalization and rapid target molecule quantification for on-demand biosensing applications. This is the first time that capillary microfluidics is utilized for enhanced sensor functionalization.

6.2 Future work

Based on the fundamental understanding of TMV VLP characteristics and its biosensing capabilities, the potential future directions of the VLP-based sensing research include multiplexed sensing, multi-functional VLP sensing probes assembly, and three-dimensional (3D) VLP-based sensor architecture for improved sensitivity.

Multiplexed sensing enabled by microfluidics:

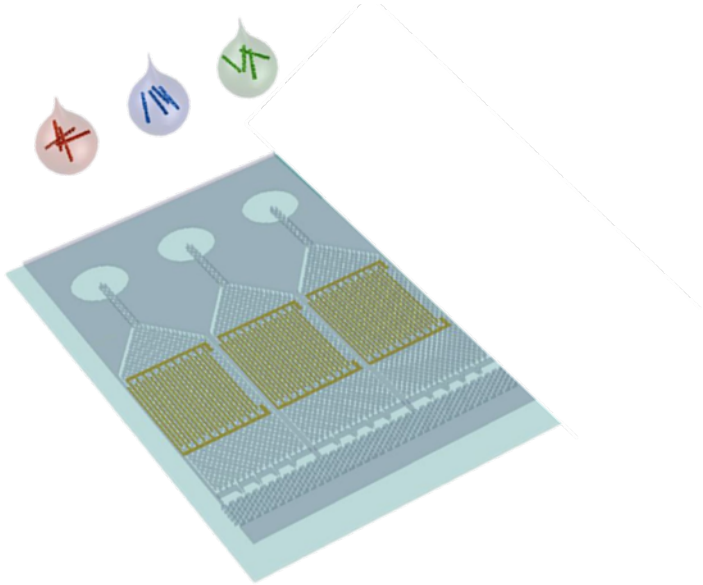

Figure 6-4 Schematic showing the multiplexed VLP-based sensor platform concept enabled by microfluidics

The joint operation of passive capillary micropumps and stop valves has demonstrated the possibility of controlling the VLP assembly location in a microsensor. This provides chances to sequentially pattern multiple kinds of VLP constructs genetically modified with different receptor peptides on separate sensors and form a sensor array. After the sensor array functionalization, the test sample that containing mixed analytes in solution can flow through the sensor array. By monitoring the impedance changes from each sensor, the composition of the test sample can be analysed. Thus, multiplexed sensing can be achieved that reduces the time and cost for biological sample analysis.

Alternatively, different VLP constructs can also be delivered simultaneously onto single impedance microsensor by multiple capillary micropumps. If these VLP constructs all express cysteine residues on their coat protein and are suspended at the same concentration, the evaporation-based VLP assembly will create a "composite" VLP functional layer on an impedance microsensor surface, enabling multiplexed biosensing affinity. Compared to the aforementioned method, this alternative method can reduce the cost of microelectrode fabrication and lower the variations from VLP assembly quality on different sensors.

Two VLP constructs have been demonstrated as bioreceptors in chemical and biological sensing model systems. These model systems can be directly translated to detect other target molecules with similar electrochemical

characteristics or dielectric constants. In the next step, more real-life application-relevant VLP receptors will be genetically engineered, and aimed at molecules such as cancer biomarkers, cardiac biomarkers and toxins.

Multi-functional VLP receptor assembled from sub-units:

Rather than creating multiple sensors, a different route to achieve the multiplexed sensing is creating multi-target sensing receptor or probe on the molecular level. Working toward this goal requires the assembly of a single VLP from sub-units carrying different receptor peptide on the sub-units' coat proteins. Preliminary experimental results have shown that the assembly of multi-functional VLP rods can be realized by programmed complimentary affinity between coat proteins and the pH response of VLPs.

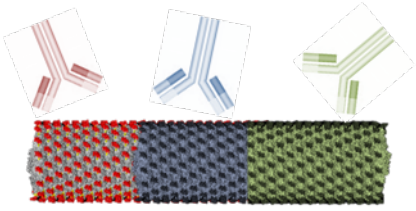

Figure 6-5 VLP receptors with multi-target sensing sub-units

The first step toward this goal is to further study the controllability of VLP assembly and disassembly using pH levels in the solution. Microfluidics provides unique opportunities to efficiently study the pH responses from VLP. For example, two capillary microfluidic pumps can deliver VLP-containing buffer solutions at two extreme pH levels, pH=3 and pH=9, to the same area on-chip. Once the two fluids mix in the center, a natural pH gradient will form with the pH ranging from 3 to 9. The length of VLPs at each pH level can then

be efficiently studied. Very importantly, the VLPs assembled at different pH condition should hold geometric integrity once the environment is restored to neural pH=7, a usual condition in which most biomarkers are tested.

The next step is to validate that VLPs assembled in different pH level can maintain similar biosensing efficacy. This step is extremely critical because part of the affinity of a binding peptide to its target molecule is due to charge preference. Florescence or colorimetric ELISA can be utilized in this validation.

Three-dimensional VLP-coated sensor electrodes:

In the current research, the impedance sensor electrodes use a planar setup which is compatible with the conventional photolithography process. However, the efficiency for target molecule capturing is not optimized: a large amount of target molecules flow through the bulk microfluidic channel without effectively touching the VLP-functionalized electrodes on the substrate. To further increase the target molecule capture efficacy, it is necessary to create three dimensional sensor electrodes, and microfluidic channel with similar dimensions compared to the sensor.

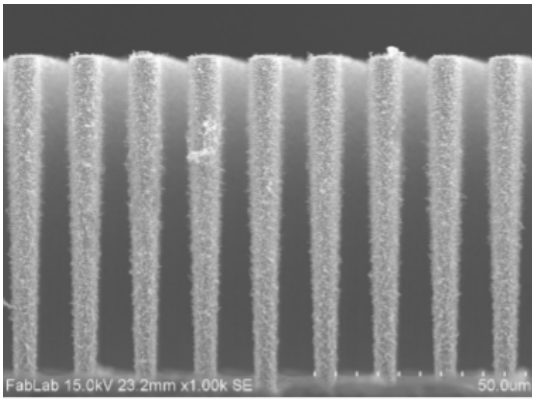

Figure 6-6 SEM image showing TMV 3D coating on gold-coated silicon pillars. [180] (Reprinted with permission from S. Chu, K. Gerasopoulos, and R. Ghodssi, Journal of Physics: Conference Series, 2015, p. 012046. Copyright 2015, IOP Publishing Ltd.)

In the future work, possible three-dimensional sensor electrodes can be fabricated using the emerging 3D printing process. This can further improve the surface area and optimized the utilization of the limited footprint of a microsensor resulting in an enhanced sensitivity. A resin-based interdigitated 3D structure can be printed on the substrate. By metal deposition with a shadow mask, the 3D structures can be metalized into interdigitated electrodes for impedance sensing. Also, interdigitated electrodes may not be the ideal feature in 3D to achieve the highest surface area. A parallel study can be done to investigate the most efficient electrode geometric for the largest surface-to-volume ratio. This will result in improved VLP coating for sensitivity biosensing.

6.3 Conclusion

Chemical hazards and biological pathogens are threatening our lives in both public and personal levels. Rapid, selective and sensitive detection of these invisible pathogenic molecules are crucial for tailing the control and treatment strategies. This dissertation addressed these needs through the integration of *Tobacco mosaic* virus-like particles (VLP) macromolecular receptors in miniaturized biosensors. These genetically modified and nanostructured receptors greatly enhanced both the selectivity and sensitivity of chemical and biological microsensors. The VLP-based explosive electrochemical microsensor worked on unique diffusion modulation

mechanism, which was able to quantify the concentration of the target TNT molecules in solution without being influenced by interfering species. The integration of VLPs in impedance microsensors through both self-assembly and evaporation-enhanced assembly processes have created affinity-based biosensors for antibody detection. The highly integrated sensor microsystem comprising VLP receptors, capillary microfluidics and impedance sensor showed experimental results of rapid sensor functionalization, label-free sensing, programmability and portability; thus, it is a promising microsystem for on-demand and on-site biological sensing. The fundamental research of VLP assembly protocols and the rapid system-level solution for VLP integration in sensors provided foundations for developing next generation portable and versatile biosensing microsystems.

Appendices

Appendix I – Matlab codes for capillary force calculation

Calculating the relations between capillary force and contact angle of microfluidic sidewall (with a constant substrate contact angle of 50^{o}).

```
d=60*10^-6; % channel depth 60 micron
p1=1;% 1/aspect ratio=1
p=0.25;% 1/aspect ratio=2
p2=2;% 1/aspect ratio=0.5
tension=72.8*10^-3;
viscosity=0.89*10^-3;
theta_substrate=50/180*pi;
theta_sidewall=0/180*pi:1/180*pi:180/180*pi;
theta_sidewall_angle=theta_sidewall/pi*180
t=0:1e-3:10;
f_capillary=d*(2*cos(theta_sidewall)*tension-p*tension*(1-
cos(theta_substrate)));
f_capillary_1=d*(2*cos(theta_sidewall)*tension-p1*tension*(1-
cos(theta_substrate)));
f_capillary_2=d*(2*cos(theta_sidewall)*tension-p2*tension*(1-
cos(theta_substrate)));
plot(theta_sidewall_angle,f_capillary_2,theta_sidewall_angle,f_capil
lary_1,theta_sidewall_angle,f_capillary);
xlabel('Contact angle \theta of sidewall (deg)');
ylabel('Capillary force (N)');
legend('Aspect ratio (depth/width)=0.5','Aspect ratio
(depth/width)=1','Aspect ratio (depth/width)=2');
```

Calculating the relations between capillary force and contact angle of substrate (with a constant sidewall contact angle of 40^{o}).

```
d=60*10^-6; % channel depth 60 micron
p=0.5;% aspect ratio=2
p1=1; % aspect ratio=1
tension=72.8*10^-3;
viscosity=0.89*10^-3;
theta_substrate=0/180*pi:1/180*pi:180/180*pi;
theta_substrate_angle=theta_substrate/pi*180;
theta_sidewall=40/180*pi;
theta_sidewall_angle=theta_sidewall/pi*180
f_capillary=d*(2*cos(theta_sidewall)*tension-p*tension*(1-
cos(theta_substrate)));
f_capillary_1=d*(2*cos(theta_sidewall)*tension-p1*tension*(1-
cos(theta_substrate)));
plot(theta_substrate_angle,f_capillary_1,theta_substrate_angle,f_cap
illary);
xlabel('Contact angle \theta of substrate (deg)');
ylabel('Capillary force (N)');
legend('Aspect ratio (depth/width)=1','Aspect ratio (depth/width)=2')
```

Calculating the relations between capillary force and microfluidic channel aspect ratio.

```
d=60*10^-6;
p=0.1:0.1:10;% aspect ratio
tension=72.8*10^-3;
viscosity=0.89*10^-3;
theta_substrate=60/180*pi;
theta_sidewall=6/180*pi;
theta_sidewall_angle=theta_sidewall/pi*180
a=cos(60/180*pi);
f_capillary=d*(2*cos(theta_sidewall)*tension-p*tension*(1-
cos(theta_substrate)));
plot(1./p, f_capillary);
xlabel('Channel aspect ratio (depth/width)');
ylabel('Capillary force (N)');
```

References

[1] A. Mangili and M. A. Gendreau, "Transmission of infectious diseases during commercial air travel," *Lancet,* vol. 365, pp. 989-996, Mar 12 2005.

[2] J. K. Taubenberger and D. M. Morens, "The pathology of influenza virus infections," *Annual Review of Pathology-Mechanisms of Disease,* vol. 3, pp. 499-522, 2008.

[3] V. Colizza, A. Barrat, M. Barthelemy, and A. Vespignani, "The role of the airline transportation network in the prediction and predictability of global epidemics," *Proceedings of the National Academy of Sciences of the United States of America,* vol. 103, pp. 2015-2020, Feb 14 2006.

[4] F. S. R. R. Teles, "Biosensors and rapid diagnostic tests on the frontier between analytical and clinical chemistry for biomolecular diagnosis of dengue disease: A review," *Analytica Chimica Acta,* vol. 687, pp. 28-42, Feb 14 2011.

[5] G. Urban, G. Jobst, F. Kohl, A. Jachimowicz, F. Olcaytug, O. Tilado, P. Goiser, G. Nauer, F. Pittner, T. Schalkhammer, and E. Mannbuxbaum, "Miniaturized Thin-Film Biosensors Using Covalently Immobilized Glucose-Oxidase," *Biosensors & Bioelectronics,* vol. 6, pp. 555-562, 1991.

[6] S. Belkin, "Microbial whole-cell sensing systems of environmental pollutants," *Current Opinion in Microbiology,* vol. 6, pp. 206-212, Jun 2003.

[7] J. Wang, "Amperometric biosensors for clinical and therapeutic drug monitoring: a review," *Journal of Pharmaceutical and Biomedical Analysis,* vol. 19, pp. 47-53, Feb 1999.

[8] C. D. Chin, V. Linder, and S. K. Sia, "Lab-on-a-chip devices for global health: Past studies and future opportunities," *Lab on a Chip,* vol. 7, pp. 41-57, 2007.

[9] L. A. Su, W. Z. Jia, C. J. Hou, and Y. Lei, "Microbial biosensors: A review," *Biosensors & Bioelectronics,* vol. 26, pp. 1788-1799, Jan 15 2011.

[10] Y. Lei, W. Chen, and A. Mulchandani, "Microbial biosensors," *Analytica Chimica Acta,* vol. 568, pp. 200-210, May 24 2006.

[11] L. G. Carrascosa, M. Moreno, M. Alvarez, and L. M. Lechuga, "Nanomechanical biosensors: a new sensing tool," *Trac-Trends in Analytical Chemistry,* vol. 25, pp. 196-206, Mar 2006.

[12] N. V. Lavrik, M. J. Sepaniak, and P. G. Datskos, "Cantilever transducers as a platform for chemical and biological sensors," *Review of Scientific Instruments,* vol. 75, pp. 2229-2253, Jul 2004.

[13] R. McKendry, J. Y. Zhang, Y. Arntz, T. Strunz, M. Hegner, H. P. Lang, M. K. Baller, U. Certa, E. Meyer, H. J. Guntherodt, and C. Gerber, "Multiple label-free biodetection and quantitative DNA-binding assays on a nanomechanical cantilever array," *Proceedings of the National Academy of Sciences of the United States of America,* vol. 99, pp. 9783-9788, Jul 23 2002.

[14] Y. Arntz, J. D. Seelig, H. P. Lang, J. Zhang, P. Hunziker, J. P. Ramseyer, E. Meyer, M. Hegner, and C. Gerber, "Label-free protein assay based on a nanomechanical cantilever array," *Nanotechnology,* vol. 14, pp. 86-90, Jan 2003.

[15] X. J. Bai, H. Hou, B. L. Zhang, and J. L. Tang, "Label-free detection of kanamycin using aptamer-based cantilever array sensor," *Biosensors & Bioelectronics,* vol. 56, pp. 112-116, Jun 15 2014.

[16] J. Zhang, H. P. Lang, F. Huber, A. Bietsch, W. Grange, U. Certa, R. McKendry, H. J. Guntgerodt, M. Hegner, and C. Gerber, "Rapid and label-free nanomechanical detection of biomarker transcripts in human RNA," *Nature Nanotechnology,* vol. 1, pp. 214-220, Dec 2006.

[17] S. L. Biswal, D. Raorane, A. Chaiken, H. Birecki, and A. Majumdar, "Nanomechanical detection of DNA melting on microcantilever surfaces," *Analytical Chemistry,* vol. 78, pp. 7104-7109, Oct 15 2006.

[18] C. Ziegler, "Cantilever-based biosensors," *Analytical and Bioanalytical Chemistry,* vol. 379, pp. 946-959, Aug 2004.

[19] K. Gruber, T. Horlacher, R. Castelli, A. Mader, P. H. Seeberger, and B. A. Hermann, "Cantilever Array Sensors Detect Specific Carbohydrate-Protein Interactions with Picomolar Sensitivity," *Acs Nano,* vol. 5, pp. 3670-3678, May 2011.

[20] M. Yue, J. C. Stachowiak, H. Lin, R. Datar, R. Cote, and A. Majumdar, "Label-free protein recognition two-dimensional array using nanomechanical sensors," *Nano Letters,* vol. 8, pp. 520-524, Feb 2008.

[21] H. Hou, X. J. Bai, C. Y. Xing, N. Y. Gu, B. L. Zhang, and J. L. Tang, "Aptamer-Based Cantilever Array Sensors for Oxytetracycline Detection," *Analytical Chemistry,* vol. 85, pp. 2010-2014, Feb 19 2013.

[22] C. R. Suri, J. Kaur, S. Gandhi, and G. S. Shekhawat, "Label-free ultra-sensitive detection of atrazine based on nanomechanics," *Nanotechnology,* vol. 19, Jun 11 2008.

[23] X. Huang, M. F. Li, X. H. Xu, H. J. Chen, H. F. Ji, and S. F. Zhu, "Microcantilevers modified by specific peptide for selective detection of trimethylamine," *Biosensors & Bioelectronics,* vol. 30, pp. 140-144, Dec 15 2011.

[24] C. Ricciardi, R. Castagna, I. Ferrante, F. Frascella, S. L. Marasso, A. Ricci, G. Canavese, A. Lore, A. Prelle, M. L. Gullino, and D. Spadaro, "Development of a microcantilever-based immunosensing method for mycotoxin detection," *Biosensors & Bioelectronics,* vol. 40, pp. 233-239, Feb 15 2013.

[25] K. W. Wee, G. Y. Kang, J. Park, J. Y. Kang, D. S. Yoon, J. H. Park, and T. S. Kim, "Novel electrical detection of label-free disease marker proteins using piezoresistive self-sensing micro-cantilevers," *Biosensors & Bioelectronics,* vol. 20, pp. 1932-1938, Apr 15 2005.

[26] C. M. Dominguez, P. M. Kosaka, A. Sotillo, J. Mingorance, J. Tamayo, and M. Calleja, "Label-Free DNA-Based Detection of Mycobacterium tuberculosis and Rifampicin Resistance through Hydration Induced Stress in Microcantilevers," *Analytical Chemistry,* vol. 87, pp. 1494-1498, Feb 3 2015.

[27] M. Rodahl, F. Hook, and B. Kasemo, "QCM operation in liquids: An explanation of measured variations in frequency and Q factor with liquid conductivity," *Analytical Chemistry,* vol. 68, pp. 2219-2227, Jul 1 1996.

[28] R. L. Caygill, G. E. Blair, and P. A. Millner, "A review on viral biosensors to detect human pathogens," *Analytica Chimica Acta,* vol. 681, pp. 8-15, Nov 29 2010.

[29] J. L. Arlett, E. B. Myers, and M. L. Roukes, "Comparative advantages of mechanical biosensors," *Nature Nanotechnology,* vol. 6, pp. 203-215, Apr 2011.

[30] N. Kim, D. K. Kim, and Y. J. Cho, "Development of indirect-competitive quartz crystal microbalance immunosensor for C-reactive protein," *Sensors and Actuators B-Chemical,* vol. 143, pp. 444-448, Dec 4 2009.

[31] S. Kurosawa, M. Nakamura, J. W. Park, H. Aizawa, K. Yamada, and M. Hirata, "Evaluation of a high-affinity QCM immunosensor using antibody fragmentation and 2-methacryloyloxyethyl phosphorylcholine (MPC) polymer," *Biosensors & Bioelectronics,* vol. 20, pp. 1134-1139, Dec 15 2004.

[32] G. Wingqvist, "AlN-based sputter-deposited shear mode thin film bulk acoustic resonator (FBAR) for biosensor applications - A review," *Surface & Coatings Technology,* vol. 205, pp. 1279-1286, Nov 25 2010.

[33] K. Lange, B. E. Rapp, and M. Rapp, "Surface acoustic wave biosensors: a review," *Analytical and Bioanalytical Chemistry,* vol. 391, pp. 1509-1519, Jul 2008.

[34] Y. Q. Fu, J. K. Luo, X. Y. Du, A. J. Flewitt, Y. Li, G. H. Markx, A. J. Walton, and W. I. Milne, "Recent developments on ZnO films for acoustic wave based bio-sensing and microfluidic applications: a review," *Sensors and Actuators B-Chemical,* vol. 143, pp. 606-619, Jan 7 2010.

[35] E. Gizeli, N. J. Goddard, C. R. Lowe, and A. C. Stevenson, "A Love Plate Biosensor Utilizing a Polymer Layer," *Sensors and Actuators B-Chemical,* vol. 6, pp. 131-137, Jan 1992.

[36] X. W. Guo, "Surface plasmon resonance based biosensor technique: A review," *Journal of Biophotonics,* vol. 5, pp. 483-501, Jul 2012.

[37] M. Piliarik, H. Vaisocherová, and J. Homola, "Surface plasmon resonance biosensing," in *Biosensors and Biodetection*, ed: Springer, 2009, pp. 65-88.

[38] F. Vollmer and S. Arnold, "Whispering-gallery-mode biosensing: label-free detection down to single molecules," *Nature Methods,* vol. 5, pp. 591-596, Jul 2008.

[39] J. S. Daniels and N. Pourmand, "Label-free impedance biosensors: Opportunities and challenges," *Electroanalysis,* vol. 19, pp. 1239-1257, Jun 2007.

[40] D. R. Thevenot, K. Toth, R. A. Durst, and G. S. Wilson, "Electrochemical biosensors: recommended definitions and classification," *Biosensors & Bioelectronics,* vol. 16, pp. 121-131, Jan 2001.

[41] T. G. Drummond, M. G. Hill, and J. K. Barton, "Electrochemical DNA sensors," *Nature Biotechnology,* vol. 21, pp. 1192-1199, Oct 2003.

[42] E. Bakker, "Electrochemical sensors," *Analytical Chemistry,* vol. 76, pp. 3285-3298, Jun 15 2004.

[43] L. C. Clark and C. Lyons, "Electrode Systems for Continuous Monitoring in Cardiovascular Surgery," *Annals of the New York Academy of Sciences,* vol. 102, pp. 29-&, 1962.

[44] J. Wang, "Electrochemical glucose biosensors," *Chemical Reviews,* vol. 108, pp. 814-825, Feb 2008.

[45] F. Palmisano, P. G. Zambonin, D. Centonze, and M. Quinto, "A disposable, reagentless, third-generation glucose biosensor based on overoxidized poly(pyrrole)/tetrathiafulvalene-tetracyanopuinodimethane composite," *Analytical Chemistry,* vol. 74, pp. 5913-5918, Dec 1 2002.

[46] W. Jing and Q. Yang, "Mediator-free amperometric determination of glucose based on direct electron transfer between glucose oxidase and an oxidized boron-doped diamond electrode," *Analytical and Bioanalytical Chemistry,* vol. 385, pp. 1330-1335, Aug 2006.

[47] J. Wang, F. Lu, D. MacDonald, J. M. Lu, M. E. S. Ozsoz, and K. R. Rogers, "Screen-printed voltammetric sensor for TNT," *Talanta,* vol. 46, pp. 1405-1412, Aug 1998.

[48] A. H. Liu, M. D. Wei, I. Honma, and H. S. Zhou, "Biosensing properties of titanate-nanotube films: Selective detection of dopamine in the presence of ascorbate and uric acid," *Advanced Functional Materials,* vol. 16, pp. 371-376, Feb 3 2006.

[49] A. A. Ensafi, B. Rezaei, M. Amini, and E. Heydari-Bafrooei, "A novel sensitive DNA-biosensor for detection of a carcinogen, Sudan II, using electrochemically treated pencil graphite electrode by voltammetric methods," *Talanta,* vol. 88, pp. 244-251, Jan 15 2012.

[50] V. K. Gupta, A. K. Jain, and S. K. Shoora, "Multiwall carbon nanotube modified glassy carbon electrode as voltammetric sensor for the simultaneous determination of ascorbic acid and caffeine," *Electrochimica Acta,* vol. 93, pp. 248-253, Mar 30 2013.

[51] M.-I. Mohammed and M. P. Desmulliez, "Lab-on-a-chip based immunosensor principles and technologies for the detection of cardiac biomarkers: a review," *Lab on a Chip,* vol. 11, pp. 569-595, 2011.

[52] M. Varshney, Y. B. Li, B. Srinivasan, and S. Tung, "A label-free, microfluidics and interdigitated array microelectrode-based impedance biosensor in combination with nanoparticles immunoseparation for detection of Escherichia coli O157 : H7 in food samples," *Sensors and Actuators B-Chemical,* vol. 128, pp. 99-107, Dec 12 2007.

[53] L. Yang and R. Bashir, "Electrical/electrochemical impedance for rapid detection of foodborne pathogenic bacteria," *Biotechnology Advances,* vol. 26, pp. 135-150, Mar-Apr 2008.

[54] J. R. Macdonald, "Impedance spectroscopy: emphasizing solid materials and systems," *Applied Optics,* vol. 28, p. 1083, 1989.

[55] K. Besteman, J. O. Lee, F. G. M. Wiertz, H. A. Heering, and C. Dekker, "Enzyme-coated carbon nanotubes as single-molecule biosensors," *Nano Letters,* vol. 3, pp. 727-730, Jun 2003.

[56] M. J. Schoning and A. Poghossian, "Bio FEDs (Field-Effect devices): State-of-the-art and new directions," *Electroanalysis,* vol. 18, pp. 1893-1900, Oct 2006.

[57] N. Backmann, C. Zahnd, F. Huber, A. Bietsch, A. Pluckthun, H. P. Lang, H. J. Guntherodt, M. Hegner, and C. Gerber, "A label-free immunosensor array using single-chain antibody fragments," *Proceedings of the National Academy of Sciences of the United States of America,* vol. 102, pp. 14587-14592, Oct 11 2005.

[58] G. H. Wu, R. H. Datar, K. M. Hansen, T. Thundat, R. J. Cote, and A. Majumdar, "Bioassay of prostate-specific antigen (PSA) using microcantilevers," *Nature Biotechnology,* vol. 19, pp. 856-860, Sep 2001.

[59] M. G. von Muhlen, N. D. Brault, S. M. Knudsen, S. Y. Jiang, and S. R. Manalis, "Label-Free Biomarker Sensing in Undiluted Serum with Suspended Microchannel Resonators," *Analytical Chemistry,* vol. 82, pp. 1905-1910, Mar 1 2010.

[60] P. S. Waggoner, M. Varshney, and H. G. Craighead, "Detection of prostate specific antigen with nanomechanical resonators," *Lab on a Chip,* vol. 9, pp. 3095-3099, 2009.

[61] L. Pinnaduwage, A. Gehl, D. Hedden, G. Muralidharan, T. Thundat, R. Lareau, T. Sulchek, L. Manning, B. Rogers, and M. Jones, "Explosives: A microsensor for trinitrotoluene vapour," *Nature,* vol. 425, pp. 474-474, 2003.

[62] Y. Weizmann, F. Patolsky, and I. Willner, "Amplified detection of DNA and analysis of single-base mismatches by the catalyzed deposition of gold on Au-nanoparticles," *Analyst,* vol. 126, pp. 1502-1504, Sep 2001.

[63] D. Dell'Atti, M. Zavaglia, S. Tombelli, G. Bertacca, A. O. Cavazzana, G. Bevilacqua, M. Minunni, and M. Mascini, "Development of combined DNA-based piezoelectric biosensors for the simultaneous detection and genotyping of high risk Human Papilloma Virus strains," *Clinica Chimica Acta,* vol. 383, pp. 140-146, Aug 2007.

[64] J. Weber, W. M. Albers, J. Tuppurainen, M. Link, R. Gabl, W. Wersing, and M. Schreiter, "Shear mode FBARs as highly sensitive liquid biosensors," *Sensors and Actuators a-Physical,* vol. 128, pp. 84-88, Mar 31 2006.

[65] D. Chen, J. J. Wang, Y. Xu, W. H. Liu, and P. Wang, "Film bulk acoustic biosensor for detection of trace pesticide residues in agricultural products," *Electronics Letters,* vol. 49, pp. 924-+, Jul 18 2013.

[66] J. T. Baca, V. Severns, D. Lovato, D. W. Branch, and R. S. Larson, "Rapid Detection of Ebola Virus with a Reagent-Free, Point-of-Care Biosensor," *Sensors,* vol. 15, pp. 8605-8614, Apr 2015.

[67] N. Atar, T. Eren, and M. L. Yola, "A molecular imprinted SPR biosensor for sensitive determination of citrinin in red yeast rice," *Food Chemistry,* vol. 184, pp. 7-11, Oct 1 2015.

[68] H. Zhang, Y. Sun, J. Wang, J. Zhang, H. Q. Zhang, H. Zhou, and D. Q. Song, "Preparation and application of novel nanocomposites of magnetic-Au nanorod in SPR biosensor," *Biosensors & Bioelectronics,* vol. 34, pp. 137-143, Apr 15 2012.

[69] A. L. Washburn, M. S. Luchansky, A. L. Bowman, and R. C. Bailey, "Quantitative, Label-Free Detection of Five Protein Biomarkers Using Multiplexed Arrays of Silicon Photonic Microring Resonators," *Analytical Chemistry,* vol. 82, pp. 69-72, Jan 1 2010.

[70] M. S. Luchansky and R. C. Bailey, "Silicon Photonic Microring Resonators for Quantitative Cytokine Detection and T-Cell Secretion Analysis," *Analytical Chemistry,* vol. 82, pp. 1975-1981, Mar 1 2010.

[71] Y. Qu, M. Ma, Z. G. Wang, G. Q. Zhan, B. H. Li, X. Wang, H. F. Fang, H. J. Zhang, and C. Y. Li, "Sensitive amperometric biosensor for phenolic compounds based on graphene-silk peptide/tyrosinase composite nanointerface," *Biosensors & Bioelectronics,* vol. 44, pp. 85-88, Jun 15 2013.

[72] P. J. Lamas-Ardisana, O. A. Loaiza, L. Anorga, E. Jubete, M. Borghei, V. Ruiz, E. Ochoteco, G. Cabanero, and H. J. Grande, "Disposable amperometric biosensor based on lactate oxidase immobilised on platinum nanoparticle-decorated carbon nanofiber and poly(diallyldimethylammonium chloride) films," *Biosensors & Bioelectronics,* vol. 56, pp. 345-351, Jun 15 2014.

[73] J. S. Caygill, S. D. Collyer, J. L. Holmes, F. Davis, and S. P. J. Higson, "Disposable screen-printed sensors for the electrochemical detection of TNT and DNT," *Analyst,* vol. 138, pp. 346-352, 2013.

[74] M. Shamsipur, M. A. Tabrizi, M. Mahkam, and J. Aboudi, "A High Sensitive TNT Sensor Based on Electrochemically Reduced Graphene Oxide-Poly(amidoamine) Modified Electrode," *Electroanalysis,* vol. 27, pp. 1466-1472, Jun 2015.

[75] W. Su, M. Lin, H. Lee, M. Cho, W. S. Choe, and Y. Lee, "Determination of endotoxin through an aptamer-based impedance biosensor," *Biosensors & Bioelectronics,* vol. 32, pp. 32-36, Feb 15 2012.

[76] R. B. Queiros, N. de-los-santos-Alvarez, J. P. Noronha, and M. G. F. Sales, "A label-free DNA aptamer-based impedance biosensor for the detection of E. coli outer membrane proteins," *Sensors and Actuators B-Chemical,* vol. 181, pp. 766-772, May 2013.

[77] Z. Y. Lin, L. F. Chen, G. Y. Zhang, Q. D. Liu, B. Qiu, Z. W. Cai, and G. N. Chen, "Label-free aptamer-based electrochemical impedance biosensor for 17 beta-estradiol," *Analyst,* vol. 137, pp. 819-822, 2012.

[78] T. T. N. Binh, A. E. K. Peh, C. Y. L. Chee, K. Fink, V. T. K. Chow, M. M. L. Ng, and C. S. Toh, "Electrochemical impedance spectroscopy characterization of nanoporous alumina dengue virus biosensor," *Bioelectrochemistry,* vol. 88, pp. 15-21, Dec 2012.

[79] Y. Z. Fu, R. Yuan, L. Xu, Y. Q. Chai, Y. Liu, D. P. Tang, and Y. Zhang, "Electrochemical impedance behavior of DNA biosensor based on colloidal Ag and bilayer two-dimensional sol-gel as matrices," *Journal of Biochemical and Biophysical Methods,* vol. 62, pp. 163-174, Feb 28 2005.

[80] C. Tlili, H. Korri-Youssoufi, L. Ponsonnet, C. Martelet, and N. Jaffrezic-Renault, "Label-free detection of DNA hybridization with EIS measurements," *Transducers '05, Digest of Technical Papers, Vols 1 and 2,* pp. 1600-1603, 2005.

[81] O. A. Sadik, H. Xu, E. Gheorghiu, D. Andreescu, C. Balut, M. Gheorghiu, and D. Bratu, "Differential impedance Spectroscopy for monitoring protein immobilization and antibody-antigen reactions," *Analytical Chemistry,* vol. 74, pp. 3142-3150, Jul 1 2002.

[82] G. F. Zheng, X. P. A. Gao, and C. M. Lieber, "Frequency Domain Detection of Biomolecules Using Silicon Nanowire Biosensors," *Nano Letters,* vol. 10, pp. 3179-3183, Aug 2010.

[83] E. Stern, A. Vacic, N. K. Rajan, J. M. Criscione, J. Park, B. R. Ilic, D. J. Mooney, M. A. Reed, and T. M. Fahmy, "Label-free biomarker detection from whole blood," *Nature Nanotechnology,* vol. 5, pp. 138-142, Feb 2010.

[84] R. Daw and J. Finkelstein, "Lab on a chip," *Nature,* vol. 442, pp. 367-367, 2006.

[85] C. A. Emrich, H. Tian, I. L. Medintz, and R. A. Mathies, "Microfabricated 384-lane capillary array electrophoresis bioanalyzer for ultrahigh-throughput genetic analysis," *Analytical Chemistry,* vol. 74, pp. 5076-5083, 2002.

[86] R. Pal, M. Yang, R. Lin, B. Johnson, N. Srivastava, S. Razzacki, K. Chomistek, D. Heldsinger, R. Haque, and V. Ugaz, "An integrated microfluidic device for influenza and other genetic analyses," *Lab on a Chip,* vol. 5, pp. 1024-1032, 2005.

[87] N. Bontoux, L. Dauphinot, T. Vitalis, V. Studer, Y. Chen, J. Rossier, and M. Potier, "Integrating whole transcriptome assays on a lab-on-a-chip for single cell gene profiling," *Lab on a Chip,* vol. 8, pp. 443-450, 2008.

[88] G. Medoro, N. Manaresi, A. Leonardi, L. Altomare, M. Tartagni, and R. Guerrieri, "A lab-on-a-chip for cell detection and manipulation," *Sensors Journal, IEEE,* vol. 3, pp. 317-325, 2003.

[89] X. Chen, D. F. Cui, C. C. Liu, and H. Li, "Microfluidic chip for blood cell separation and collection based on crossflow filtration," *Sensors and Actuators B: Chemical,* vol. 130, pp. 216-221, 2008.

[90] B. H. Weigl, R. L. Bardell, and C. R. Cabrera, "Lab-on-a-chip for drug development," *Advanced drug delivery reviews,* vol. 55, pp. 349-377, 2003.

[91] P. Neuži, S. Giselbrecht, K. Länge, T. J. Huang, and A. Manz, "Revisiting lab-on-a-chip technology for drug discovery," *Nature Reviews Drug Discovery,* vol. 11, pp. 620-632, 2012.

[92] C. H. Ahn, J.-W. Choi, G. Beaucage, J. H. Nevin, J.-B. Lee, A. Puntambekar, and J. Y. Lee, "Disposable smart lab on a chip for point-of-care clinical diagnostics," *Proceedings of the IEEE,* vol. 92, pp. 154-173, 2004.

[93] J. Do and C. H. Ahn, "A polymer lab-on-a-chip for magnetic immunoassay with on-chip sampling and detection capabilities," *Lab on a Chip,* vol. 8, pp. 542-549, 2008.

[94] L. XuanáQuang, G. HunáSeong, and K. JunáDo, "A portable surface-enhanced Raman scattering sensor integrated with a lab-on-a-chip for field analysis," *Lab on a Chip,* vol. 8, pp. 2214-2219, 2008.

[95] G. Suárez, Y.-H. Jin, J. Auerswald, S. Berchtold, H. F. Knapp, J.-M. Diserens, Y. Leterrier, J.-A. E. Månson, and G. Voirin, "Lab-on-a-chip for multiplexed biosensing of residual antibiotics in milk," *Lab on a Chip,* vol. 9, pp. 1625-1630, 2009.

[96] Z. Zou, J. Kai, M. J. Rust, J. Han, and C. H. Ahn, "Functionalized nano interdigitated electrodes arrays on polymer with integrated microfluidics for direct bio-affinity sensing using impedimetric measurement," *Sensors and Actuators A: Physical,* vol. 136, pp. 518-526, 2007.

[97] L. Gervais and E. Delamarche, "Toward one-step point-of-care immunodiagnostics using capillary-driven microfluidics and PDMS substrates," *Lab on a Chip,* vol. 9, pp. 3330-3337, 2009.

[98] A. Duval, F. Bardin, A. Aide, A. Bellemain, J. Moreau, and M. Canva, "Anisotropic surface-plasmon-resonance imaging biosensor."

[99] K. S. Kim, H.-S. Lee, J.-A. Yang, M.-H. Jo, and S. K. Hahn, "The fabrication, characterization and application of aptamer-functionalized Si-nanowire FET biosensors," *Nanotechnology,* vol. 20, p. 235501, 2009.

[100] J. Wang, "Survey and summary from DNA biosensors to gene chips," *Nucleic Acids Research,* vol. 28, pp. 3011-3016, 2000.

[101] J. H. Lee, K. H. Yoon, K. S. Hwang, J. Park, S. Ahn, and T. S. Kim, "Label free novel electrical detection using micromachined PZT monolithic thin film

cantilever for the detection of C-reactive protein," *Biosensors & Bioelectronics,* vol. 20, pp. 269-275, Sep 15 2004.

[102] M. I. Rocha-Gaso, C. March-Iborra, A. Montoya-Baides, and A. Arnau-Vives, "Surface Generated Acoustic Wave Biosensors for the Detection of Pathogens: A Review," *Sensors,* vol. 9, pp. 5740-5769, Jul 2009.

[103] S. Haeberle and R. Zengerle, "Microfluidic platforms for lab-on-a-chip applications," *Lab on a Chip,* vol. 7, pp. 1094-1110, 2007.

[104] J. K. Luo, Y. Q. Fu, Y. Li, X. Y. Du, A. J. Flewitt, A. J. Walton, and W. I. Milne, "Moving-part-free microfluidic systems for lab-on-a-chip," *Journal of Micromechanics and Microengineering,* vol. 19, May 2009.

[105] C. D. Chin, V. Linder, and S. K. Sia, "Commercialization of microfluidic point-of-care diagnostic devices," *Lab on a Chip,* vol. 12, pp. 2118-2134, 2012.

[106] P. Abgrall and A. M. Gue, "Lab-on-chip technologies: making a microfluidic network and coupling it into a complete microsystem - a review," *Journal of Micromechanics and Microengineering,* vol. 17, pp. R15-R49, May 2007.

[107] A. Arora, G. Simone, G. B. Salieb-Beugelaar, J. T. Kim, and A. Manz, "Latest Developments in Micro Total Analysis Systems," *Analytical Chemistry,* vol. 82, pp. 4830-4847, Jun 15 2010.

[108] G. B. Salieb-Beugelaar, G. Simone, A. Arora, A. Philippi, and A. Manz, "Latest Developments in Microfluidic Cell Biology and Analysis Systems," *Analytical Chemistry,* vol. 82, pp. 4848-4864, Jun 15 2010.

[109] F. H. Hou, Q. Zhang, J. P. Yang, X. C. Li, X. J. Yang, S. P. Wang, and Z. Y. Cheng, "Development of a microplate reader compatible microfluidic chip for ELISA," *Biomedical Microdevices,* vol. 14, pp. 729-737, Aug 2012.

[110] L. Zhu, Y. Y. Feng, X. Y. Ye, J. Y. Feng, Y. B. Wu, and Z. Y. Zhou, "An ELISA Chip Based on an EWOD Microfluidic Platform," *Journal of Adhesion Science and Technology,* vol. 26, pp. 2113-2124, 2012.

[111] A. Rasooly, H. A. Bruck, and Y. Kostov, "An ELISA lab-on-a-chip (ELISA-LOC)," in *Microfluidic Diagnostics*, ed: Springer, 2013, pp. 451-471.

[112] S. Sun, M. H. Yang, Y. Kostov, and A. Rasooly, "ELISA-LOC: lab-on-a-chip for enzyme-linked immunodetection," *Lab on a Chip,* vol. 10, pp. 2093-2100, 2010.

[113] M. Herrmann, E. Roy, T. Veres, and M. Tabrizian, "Microfluidic ELISA on non-passivated PDMS chip using magnetic bead transfer inside dual networks of channels," *Lab on a Chip,* vol. 7, pp. 1546-1552, 2007.

[114] A. W. Martinez, "Microfluidic paper-based analytical devices: from POCKET to paper-based ELISA," *Bioanalysis,* vol. 3, pp. 2589-2592, Dec 2011.

[115] N. Yanagisawa, J. O. Mecham, R. C. Corcoran, and D. Dutta, "Multiplex ELISA in a single microfluidic channel," *Analytical and Bioanalytical Chemistry,* vol. 401, pp. 1173-1181, Sep 2011.

[116] Y. W. Lin, M. J. Huang, and H. T. Chang, "Analysis of double-stranded DNA by microchip capillary electrophoresis using polymer solutions containing gold nanoparticles," *Journal of Chromatography A,* vol. 1014, pp. 47-55, Oct 3 2003.

[117] K. D. Dorfman, "DNA electrophoresis in microfluidic post arrays under moderate electric fields (vol 73, art no 061922, 2006)," *Physical Review E,* vol. 77, Jan 2008.

[118] A. J. Hopwood, C. Hurth, J. N. Yang, Z. Cai, N. Moran, J. G. Lee-Edghill, A. Nordquist, R. Lenigk, M. D. Estes, J. P. Haley, C. R. McAlister, X. Chen, C. Brooks, S. Smith, K. Elliott, P. Koumi, F. Zenhausern, and G. Tully, "Integrated Microfluidic System for Rapid Forensic DNA Analysis: Sample Collection to DNA Profile," *Analytical Chemistry,* vol. 82, pp. 6991-6999, Aug 15 2010.

[119] M. Javanmard and R. W. Davis, "A microfluidic platform for electrical detection of DNA hybridization," *Sensors and Actuators B-Chemical,* vol. 154, pp. 22-27, May 20 2011.

[120] R. T. Kelly and A. T. Woolley, "Microfluidic systems for integrated, high-throughput DNA analysis.," *Analytical Chemistry,* vol. 77, pp. 96a-102a, Mar 1 2005.

[121] V. M. Ugaz, "PCR in integrated microfluidic systems," in *Integrated Biochips for DNA Analysis*, ed: Springer, 2007, pp. 90-106.

[122] M. Pumera, "Nanomaterials meet microfluidics," *Chemical Communications,* vol. 47, pp. 5671-5680, 2011.

[123] M. Pumera and A. Escarpa, "Nanomaterials as electrochemical detectors in microfluidics and CE: Fundamentals, designs, and applications," *Electrophoresis,* vol. 30, pp. 3315-3323, Oct 2009.

[124] D. Tang, R. Yuan, and Y. Chai, "Magnetic control of an electrochemical microfluidic device with an arrayed immunosensor for simultaneous multiple immunoassays," *Clinical Chemistry,* vol. 53, pp. 1323-1329, Jul 2007.

[125] S. P. Chen, X. D. Yu, J. J. Xu, and H. Y. Chen, "Gold nanoparticles-coated magnetic microspheres as affinity matrix for detection of hemoglobin Al c in blood by microfluidic immunoassay," *Biosensors & Bioelectronics,* vol. 26, pp. 4779-4784, Aug 15 2011.

[126] W. Wang, L. Zhao, J. R. Zhang, X. M. Wang, J. J. Zhu, and H. Y. Chen, "Modification of poly (dimethylsiloxane) microfluidic channels with silica nanoparticles based on layer-by-layer assembly technique," *Journal of Chromatography A,* vol. 1136, pp. 111-117, Dec 8 2006.

[127] A. J. Wang, J. J. Xu, Q. Zhang, and H. Y. Chen, "The use of poly(dimethylsiloxane) surface modification with gold nanoparticles for the microchip electrophoresis," *Talanta,* vol. 69, pp. 210-215, Mar 15 2006.

[128] K. B. Kim, J. H. Han, H. Choi, H. C. Kim, and T. D. Chung, "Dynamic Preconcentration of Gold Nanoparticles for Surface-Enhanced Raman Scattering in a Microfluidic System," *Small,* vol. 8, pp. 378-383, Feb 6 2012.

[129] M. Hu, Y. He, S. P. Song, J. A. Yan, H. T. Lu, L. X. Weng, L. H. Wang, and C. H. Fan, "DNA-bridged bioconjugation of fluorescent quantum dots for highly sensitive microfluidic protein chips," *Chemical Communications,* vol. 46, pp. 6126-6128, 2010.

[130] H. Zhang, T. Xu, C. W. Li, and M. S. Yang, "A microfluidic device with microbead array for sensitive virus detection and genotyping using quantum dots as fluorescence labels," *Biosensors & Bioelectronics,* vol. 25, pp. 2402-2407, Jul 15 2010.

[131] E. Piccin, R. Laocharoensuk, J. Burdick, E. Carrilho, and J. Wang, "Adaptive nanowires for switchable microchip devices," *Analytical Chemistry,* vol. 79, pp. 4720-4723, Jun 15 2007.

[132] A. G. Crevillen, M. Avila, M. Pumera, M. C. Gonzalez, and A. Escarpa, "Food analysis on microfluidic devices using ultrasensitive carbon nanotubes detectors," *Analytical Chemistry,* vol. 79, pp. 7408-7415, Oct 1 2007.

[133] V. Krivitsky, L. C. Hsiung, A. Lichtenstein, B. Brudnik, R. Kantaev, R. Elnathan, A. Pevzner, A. Khatchtourints, and F. Patolsky, "Si Nanowires Forest-Based On-Chip Biomolecular Filtering, Separation and Preconcentration Devices: Nanowires Do it All," *Nano Letters,* vol. 12, pp. 4748-4756, Sep 2012.

[134] M. C. McAlpine, H. D. Agnew, R. D. Rohde, M. Blanco, H. Ahmad, A. D. Stuparu, W. A. Goddard, and J. R. Heath, "Peptide-nanowire hybrid materials for selective sensing of small molecules," *Journal of the American Chemical Society,* vol. 130, pp. 9583-9589, Jul 23 2008.

[135] F. Patolsky, B. P. Timko, G. F. Zheng, and C. M. Lieber, "Nanowire-based nanoelectronic devices in the life sciences," *Mrs Bulletin,* vol. 32, pp. 142-149, Feb 2007.

[136] F. Patolsky, G. Zheng, and C. M. Lieber, "Nanowire sensors for medicine and the life sciences," *Nanomedicine,* vol. 1, pp. 51-65, Jun 2006.

[137] G. F. Zheng, F. Patolsky, Y. Cui, W. U. Wang, and C. M. Lieber, "Multiplexed electrical detection of cancer markers with nanowire sensor arrays," *Nature Biotechnology,* vol. 23, pp. 1294-1301, Oct 2005.

[138] P. K. Ang, A. Li, M. Jaiswal, Y. Wang, H. W. Hou, J. T. L. Thong, C. T. Lim, and K. P. Loh, "Flow Sensing of Single Cell by Graphene Transistor in a Microfluidic Channel," *Nano Letters,* vol. 11, pp. 5240-5246, Dec 2011.

[139] Y. Cui, S. N. Kim, S. E. Jones, L. L. Wissler, R. R. Naik, and M. C. McAlpine, "Chemical Functionalization of Graphene Enabled by Phage Displayed Peptides," *Nano Letters,* vol. 10, pp. 4559-4565, Nov 2010.

[140] Y. Cui, S. N. Kim, R. R. Naik, and M. C. Mcalpine, "Biomimetic Peptide Nanosensors," *Accounts of Chemical Research,* vol. 45, pp. 696-704, May 2012.

[141] H. M. Yi, S. Nisar, S. Y. Lee, M. A. Powers, W. E. Bentley, G. F. Payne, R. Ghodssi, G. W. Rubloff, M. T. Harris, and J. N. Culver, "Patterned assembly of genetically modified viral nanotemplates via nucleic acid hybridization," *Nano Letters,* vol. 5, pp. 1931-1936, Oct 2005.

[142] W. S. Tan, C. L. Lewis, N. E. Horelik, D. C. Pregibon, P. S. Doyle, and H. M. Yi, "Hierarchical Assembly of Viral Nanotemplates with Encoded Microparticles via Nucleic Acid Hybridization," *Langmuir,* vol. 24, pp. 12483-12488, Nov 4 2008.

[143] H. Yi, G. W. Rubloff, and J. N. Culver, "TMV microarrays: Hybridization-based assembly of DNA-programmed viral nanotemplates," *Langmuir,* vol. 23, pp. 2663-2667, Feb 27 2007.

[144] M. A. Bruckman, J. Liu, G. Koley, Y. Li, B. Benicewicz, Z. W. Niu, and Q. A. Wang, "Tobacco mosaic virus based thin film sensor for detection of volatile organic compounds," *Journal of Materials Chemistry,* vol. 20, pp. 5715-5719, 2010.

[145] K. Srinivasan, "Nanomaterial sensing layer based surface acoustic wave hydrogen sensors," University of South Florida, 2005.

[146] L. M. C. Yang, J. E. Diaz, T. M. McIntire, G. A. Weiss, and R. M. Penner, "Covalent virus layer for mass-based biosensing," *Analytical Chemistry,* vol. 80, pp. 933-943, Feb 15 2008.

[147] C. S. Jeon, I. Hwang, and T. D. Chung, "Virus-Tethered Magnetic Gold Microspheres with Biomimetic Architectures for Enhanced Immunoassays," *Advanced Functional Materials,* vol. 23, pp. 1484-1489, Mar 25 2013.

[148] J. A. Arter, D. K. Taggart, T. M. McIntire, R. M. Penner, and G. A. Weiss, "Virus-PEDOT Nanowires for Biosensing," *Nano Letters,* vol. 10, pp. 4858-4862, Dec 2010.

[149] J. H. Lee and J. N. Cha, "Amplified Protein Detection through Visible Plasmon Shifts in Gold Nanocrystal Solutions from Bacteriophage Platforms," *Analytical Chemistry,* vol. 83, pp. 3516-3519, May 1 2011.

[150] H. Jin, N. Won, B. Ahn, J. Kwag, K. Heo, J. W. Oh, Y. T. Sun, S. G. Cho, S. W. Lee, and S. Kim, "Quantum dot-engineered M13 virus layer-by-layer composite films for highly selective and sensitive turn-on TNT sensors," *Chemical Communications,* vol. 49, pp. 6045-6047, 2013.

[151] D. W. Domaille, J. H. Lee, and J. N. Cha, "High density DNA loading on the M13 bacteriophage provides access to colorimetric and fluorescent protein

microarray biosensors," *Chemical Communications,* vol. 49, pp. 1759-1761, 2013.

[152] J. H. Lee, D. W. Domaille, and J. N. Cha, "Amplified Protein Detection and Identification through DNA-Conjugated M13 Bacteriophage," *Acs Nano,* vol. 6, pp. 5621-5626, Jun 2012.

[153] X. Z. Fan, E. Pomerantseva, M. Gnerlich, A. Brown, K. Gerasopoulos, M. McCarthy, J. Culver, and R. Ghodssi, "Tobacco mosaic virus: A biological building block for micro/nano/bio systems," *Journal of Vacuum Science & Technology A,* vol. 31, Sep 2013.

[154] A. D. Brown, L. Naves, X. Wang, R. Ghodssi, and J. N. Culver, "Carboxylate-Directed In Vivo Assembly of Virus-like Nanorods and Tubes for the Display of Functional Peptides and Residues," *Biomacromolecules,* vol. 14, pp. 3123-3129, Sep 2013.

[155] J. N. Culver, A. D. Brown, F. Zang, M. Gnerlich, K. Gerasopoulos, and R. Ghodssi, "Plant virus directed fabrication of nanoscale materials and devices," *Virology,* vol. 479, pp. 200-212, 2015.

[156] J. W. Jaworski, D. Raorane, J. H. Huh, A. Majumdar, and S.-W. Lee, "Evolutionary screening of biomimetic coatings for selective detection of explosives," *Langmuir,* vol. 24, pp. 4938-4943, 2008.

[157] F. Zang, K. Gerasopoulos, X. Z. Fan, A. D. Brown, J. N. Culver, and R. Ghodssi, "Real-time monitoring of macromolecular biosensing probe self-assembly and on-chip ELISA using impedimetric microsensors," *Biosensors and Bioelectronics,* vol. 81, pp. 401-407, 2016.

[158] K. Bratin, P. Kissinger, R. C. Briner, and C. S. Bruntlett, "Determination of nitro aromatic, nitramine, and nitrate ester explosive compounds in explosive mixtures and gunshot residue by liquid chromatography and reductive electrochemical detection," *Analytica Chimica Acta,* vol. 130, pp. 295-311, 1981.

[159] L. Feng, H. Li, Y. Qu, and C. Lü, "Detection of TNT based on conjugated polymer encapsulated in mesoporous silica nanoparticles through FRET," *Chemical Communications,* vol. 48, pp. 4633-4635, 2012.

[160] S. Z. Nergiz, N. Gandra, M. E. Farrell, L. Tian, P. M. Pellegrino, and S. Singamaneni, "Biomimetic SERS substrate: peptide recognition elements for highly selective chemical detection in chemically complex media," *Journal of Materials Chemistry A,* vol. 1, pp. 6543-6549, 2013.

[161] J. L. Pablos, M. Trigo-López, F. Serna, F. C. García, and J. M. García, "Water-soluble polymers, solid polymer membranes, and coated fibres as smart sensory materials for the naked eye detection and quantification of TNT in aqueous media," *Chemical Communications,* vol. 50, pp. 2484-2487, 2014.

[162] T. H. Kim, B. Y. Lee, J. Jaworski, K. Yokoyama, W.-J. Chung, E. Wang, S. Hong, A. Majumdar, and S.-W. Lee, "Selective and sensitive TNT sensors

using biomimetic polydiacetylene-coated CNT-FETs," *Acs Nano,* vol. 5, pp. 2824-2830, 2011.

[163] J. Yinon, *Toxicity and metabolism of explosives*: CRC press, 1990.

[164] E. R. Travis, N. K. Hannink, C. J. Van Der Gast, I. P. Thompson, S. J. Rosser, and N. C. Bruce, "Impact of transgenic tobacco on trinitrotoluene (TNT) contaminated soil community," *Environmental science & technology,* vol. 41, pp. 5854-5861, 2007.

[165] J. Wang, "Nanoparticle-based electrochemical bioassays of proteins," *Electroanalysis,* vol. 19, pp. 769-776, Apr 2007.

[166] F. Zang, K. Gerasopoulos, X. Z. Fan, A. D. Brown, J. N. Culver, and R. Ghodssi, "An electrochemical sensor for selective TNT sensing based on Tobacco mosaic virus-like particle binding agents," *Chemical Communications,* vol. 50, pp. 12977-12980, 2014.

[167] K. Gerasopoulos, E. Pomerantseva, M. McCarthy, A. Brown, C. S. Wang, J. Culver, and R. Ghodssi, "Hierarchical Three-Dimensional Microbattery Electrodes Combining Bottom-Up Self-Assembly and Top-Down Micromachining," *Acs Nano,* vol. 6, pp. 6422-6432, Jul 2012.

[168] S. P. Wargacki, B. Pate, and R. A. Vaia, "Fabrication of 2D ordered films of tobacco mosaic virus (TMV): processing morphology correlations for convective assembly," *Langmuir,* vol. 24, pp. 5439-5444, 2008.

[169] F. Zang, X. Z. Fan, K. D. Gerasopoulos, H. Ben-Yoav, A. D. Brown, J. N. Culver, and R. Ghodssi, "Scale-down effects: Towards miniaturization of an electrochemical sensor using biomolecules," in *SENSORS, 2013 IEEE*, Baltimore, USA, 2013, pp. 1-4.

[170] P. Mandal, A. Biswas, K. Choi, and U. Pal, "Methods for rapid detection of foodborne pathogens: an overview," *American Journal Of Food Technology,* vol. 6, pp. 87-102, 2011.

[171] A. Bratov, J. Ramon-Azcon, N. Abramova, A. Merlos, J. Adrian, F. Sanchez-Baeza, M. P. Marco, and C. Dominguez, "Three-dimensional interdigitated electrode array as a transducer for label-free biosensors," *Biosensors & Bioelectronics,* vol. 24, pp. 729-735, Dec 1 2008.

[172] P. Van Gerwen, W. Laureyn, W. Laureys, G. Huyberechts, M. O. De Beeck, K. Baert, J. Suls, W. Sansen, P. Jacobs, L. Hermans, and R. Mertens, "Nanoscaled interdigitated electrode arrays for biochemical sensors," *Sensors and Actuators B-Chemical,* vol. 49, pp. 73-80, Jun 25 1998.

[173] J. Hong, D. S. Yoon, S. K. Kim, T. S. Kim, S. Kim, E. Y. Pak, and K. No, "AC frequency characteristics of coplanar impedance sensors as design parameters," *Lab on a Chip,* vol. 5, pp. 270-279, 2005.

[174] P. Dak, A. Ebrahimi, and M. A. Alam, "Non-faradaic impedance characterization of an evaporating droplet for microfluidic and biosensing applications," *Lab on a Chip,* vol. 14, pp. 2469-2479, 2014.

[175] M. Ibrahim, J. Claudel, D. Kourtiche, and M. Nadi, "Geometric parameters optimization of planar interdigitated electrodes for bioimpedance spectroscopy," *Journal of Electrical Bioimpedance,* vol. 4, pp. 13-22, 2013.

[176] F. Walther, P. Davydovskaya, S. Zucher, M. Kaiser, H. Herberg, A. M. Gigler, and R. W. Stark, "Stability of the hydrophilic behavior of oxygen plasma activated SU-8," *Journal of Micromechanics and Microengineering,* vol. 17, pp. 524-531, Mar 2007.

[177] M. Nordstrom, R. Marie, M. Calleja, and A. Boisen, "Rendering SU-8 hydrophilic to facilitate use in micro channel fabrication," *Journal of Micromechanics and Microengineering,* vol. 14, pp. 1614-1617, Dec 2004.

[178] M. D. Abràmoff, P. J. Magalhães, and S. J. Ram, "Image processing with ImageJ," *Biophotonics international,* vol. 11, pp. 36-42, 2004.

[179] T. Ferreira and W. Rasb, *ImageJ user guide*, 2012.

[180] S. Chu, K. Gerasopoulos, and R. Ghodssi, "Bio-nanotextured high aspect ratio micropillar arrays for high surface area energy storage devices," in *Journal of Physics: Conference Series*, 2015, p. 012046.